UNIVERSITY OF SOUTHAMPTON

Deconstructed Models at the Tree and Loop Level

by

Philip John Membry

A thesis submitted for the degree of

Doctor of Philosophy

School of Physics and Astronomy

September 2006

To the many people who tirelessly and patiently supported me through Bipolar Disorder, Dyslexia and SPD. Some things are never achieved alone.

This thesis was submitted for examination in 2006. It does not necessarily represent the final form of the thesis as deposited in the University after examination.

UNIVERSITY OF SOUTHAMPTON

ABSTRACT

FACULTY OF SCIENCE

SCHOOL OF PHYSICS AND ASTRONOMY

Doctor of Philosophy

DECONSTRUCTED MODELS AT THE TREE AND LOOP LEVEL

Philip John Membry

Deconstructed Models of the Electroweak sector are investigated. A tree level analysis of the phenomenology in these models is shown to be Higgsless at the energy scales the LHC can probe and with new gauge bosons observable as the signature particles. Loop level calculations are performed for N=1 Deconstructed models. The loop level contributions to the S parameter are shown to be of order the experimental constraints or larger.

Contents

List of Figures

Preface

The work described in this thesis was carried out with Dr. Nick Evans.

- Chapter 3 N. Evans and P. J. Membry arXiv:hep-ph/0406285

No claims of original work are made for Chapters 1, 2 and 4. The original work in this thesis is found within Chapters 3 and 5.

Acknowledgements

I'd like to thank my supervisor Dr. Nick Evans for giving me such an interesting project and patiently supporting me through my PhD. Olly Eyton Williams, Jon Shock and Dr. Jonathan Flynn for answering my many questions through my difficult first year and beyond. Martin Wiebusch, Martin Nolten, Dr. Stefano Morretti and Prof. Doug Ross for their invaluable input on phenomenology, that has been so useful. Iain Peddie for his helpful answering of computer questions, as well as physics.

I'd also like to thank Prof. Tim Morris, Prof. Peter de Groot and the Southampton Physics Department for facilitating the funding of my university fees these past four years. My Granny and late Grandpa for showing such vision and generosity in investing so early in my education so I could afford to cover my living expenses during this PhD.

It has been a wonderful four years here at Southampton, which I will remember fondly. Many thanks to Prof. Ken Barnes for founding such a friendly research group that has been a joy to be a part of. I've made many friends here at SHEP and will miss those of you who have left, or are leaving, to various parts of the world, it's been good.

Finally I'd like to thank my family who have kept me together these past years and long before. I know how lucky I am to have your support.

Chapter 1

Introduction

1.1 The Standard Model

The modern understanding of the fundamental principles, that are at the root of how the universe works, is through quantum particles. There are four forces in nature, the Strong Nuclear Force, the Weak Nuclear Force, the Electromagnetic Force and Gravity. Due to the relatively weak strength of gravity over short distances, and for small masses, its understanding is largely separate from the other three forces of nature. Today Gravity is well described by General Relativity [1] and does not impinge on any physics at the atomic scale within current experiments. The remaining three forces of nature have been successfully described for the past thirty years by what is called the Standard Model.

The Standard Model has had a remarkable degree of success meeting experimental tests for the past three decades. It breaks down into two parts: Electroweak Theory [2, 3, 4], a theory which incorporates the Weak Nuclear Force with Quantum Electrodynamics (QED) [5] that describes the Electromagnetic Force. The Electromagnetic Force describes how charged particles are attracted or repelled by the interchange of

photons. The Weak Nuclear Force is responsible for radioactive β-decay within the nuclei of atoms. The second part of the Standard Model is Quantum Chromodynamics (QCD)[6, 7, 8, 9, 10, 11, 12], which describes the Strong Nuclear Force that binds proton's and neutron's, and more specifically the quarks that make these composite particles, together via the exchange of particles called gluons.

The guiding principle in the construction of theories of the forces is gauge invariance with the prototype theory QED. QED has a U(1) local gauge symmetry [13] - that is the phase of the charged quantum fields can be rotated by a space-time dependent phase without the physics of the theory changing. The photon naturally emerges from this theory - it communicates the different phase conventions in different regions of space.

The Standard Model can be described as possessing the internal wave function symmetries $SU(3) \times SU(2) \times U(1)_Y$. The $SU(3)$ symmetry corresponds to the symmetry over the interchange of the three so called colour charges of quarks, red, green and blue, where the symmetry is upheld by the passage of colour charge through the gluons. The gluons are as such the force carriers for the Strong Nuclear Force in QCD. The Weak Nuclear Force is described by the symmetry $SU(2) \times U(1)_Y$ which is upheld at high energies, but spontaneously broken at lower energy scales into the $U(1)$ symmetry of electromagnetism. The $SU(2)$ symmetry describes the approximate symmetry over weak isospin, the symmetry between 'up' and 'down' quarks preserved by three massless particles called gauge bosons. The $U(1)_Y$ or hypercharge gauge symmetry of $SU(2) \times U(1)_Y$ also has a massless gauge boson similar to the photon. After the $SU(2) \times U(1)_Y$ symmetry is broken three gauge bosons gain a mass and become the particles known as the W^+, W^- and Z^0 bosons. The symmetry is lost and the 'up' and 'down' quarks become distinguishable as a result. However, one gauge boson remains massless and

becomes the photon of electromagnetism. As such, it is said that the high energy symmetry $SU(2) \times U(1)_Y$ has broken down to $U(1)$ electromagnetism.

The standard description of how this symmetry is broken is the so called Higgs Mechanism, which also generates the Higgs boson. However, the Higgs Mechanism remains unproven by experiments, and as we shall see in Chapter 2 there are other alternative explanations of how this symmetry breaking may occur. In the next 12 months a new particle accelerator is due to come on line named the Large Hadron Collider. This new experiment will probe fully the energies at which spontaneous symmetry breaking must occur. In this experiment it is hoped the Higgs boson will be discovered as a signature verifying the Higgs Mechanism, or alternatively other new particles will be found establishing alternative explanations of Electroweak Symmetry breaking.

1.2 Introduction to Thesis Research

In this section we will present an overview of the research in this thesis and how it fits into the broader field. It is not intended that the reader should follow the details in this section, but instead get a general feel for the structure of what will follow and its place in the wider subject. We will hold off until Chapter 2 before introducing Deconstruction in full from the beginning.

The need to restore unitarity in high energy WW scattering has long been cited as evidence that there must be a Higgs boson with mass below of order 1 TeV [14]. The Higgs may be a strongly bound fermion composite such as in technicolor [15] or top condensate models [16] but the presence of an effective scalar is still needed at the 1 TeV scale. An alternative suggestion has been that the loss of unitarity is a signal of non-perturbative WW physics [17] - it is possible a non-perturbative resolution of the

problem might exist.

Recently though it has been realized that unitarity can also be restored by a Kaluza Klein (KK) like tower of massive W-bosons without a Higgs [19, 20, 21, 22]. These models [21, 23] are variants on the idea that there is a fifth dimension that is a discrete interval. The gauge group is broken by boundary conditions at the ends of the interval rather than by a Higgs mechanism. In the four dimensional theory at long distance scales there are only the W, Z fields and their KK towers, yet the theory is unitary.

Such a model must though meet the stringent experimental constraints on the masses of extra W bosons, and on the precision data for $\sin\theta_W$ and $\delta\rho$ (or equivalently the parameters S and T). Some of the above models in which the extra dimension is warped have made progress in meeting these constraints. However a five dimensional theory is naively ill defined in the UV where it becomes strongly coupled - one might expect the strong coupling to bind the constituent particles into bound states and there would be no sense in which a weak coupling regime existed at lower energies (one could imagine some strong coupled fixed point that might allow such a scenario but such physics is not understood). We expect in five dimensional models that some UV completion would be needed before strong coupling is reached. One must be careful not to make use of spacetime curvature on scales where the theory is strongly coupled - the AdS metric used in [22] with an exponential warp factor may for example be hard to support. Also the analysis of [24], which uses the models we study below, explicitly works in the strong coupling limit.

To keep track of the gauge coupling strength it is useful to have a fully defined theory with an explicit UV completion. Deconstruction [25, 26] provides such a realization with the fifth dimension manually constructed by the reproduction of the Kaluza Klein tower in a renormalizable four dimensional theory. The extra fifth dimension is first thought of

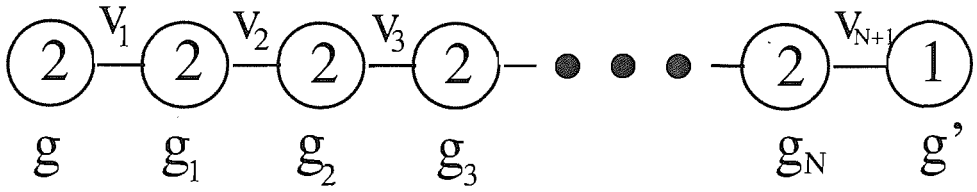

Figure 1.1: The moose model under consideration - numbered circles represent SU(N) gauge groups and links bi-fundamental Higgs fields.

as a lattice where a separate copy of the four dimensional gauge group lives at each site. The sites are then linked by Goldstone fields transforming in the $(N, \bar{N})$ representation of the two neighbouring site gauge groups. The resulting gauge boson mass spectrum, in the purely four dimensional model, then mimics a KK tower at scales well below the symmetry breaking scale. A fully renormalizable gauge theory can be found by promoting the Goldstone fields to a full Higgs multiplet. WW unitarity is restored by the Kaluza Klein tower at low energies and finally at the very high fundamental symmetry breaking scale by the Higgs bosons [19]. These models therefore are only Higgsless in the sense that the Higgs mass rises relative to that of the Standard Model and phenomenology may appear Higgsless at the LHC.

The simplest Deconstruction extension of the Standard Model has been suggested by a number of authors [24, 27, 28, 29]. It consists of multiple repeats of the SU(2) gauge group as shown in the moose diagram notation [30, 31] of Figure 1.1, an explanation of moose diagram notation will be presented in section 2.4. There are $N+1$ copies of SU(2) each potentially with a unique coupling g_i. The gauge bosons are coupled by bi-fundamental Higgs with vevs v_i linking $\mathrm{SU}(2)_i$ and $\mathrm{SU}(2)_{i+1}$. Finally the $(N+1)$th SU(2) is coupled by the $(N+1)$th Higgs to a $\mathrm{U}(1)_Y$ hypercharge group. This final symmetry breaking pattern ensures that there is a massless photon.

The low energy dynamics is described by a non-linear realization of the Goldstone

fields [32]

$$\mathcal{L} = \sum_i \frac{v_i^2}{4} Tr D^\mu U_i^\dagger D_\mu U_i + \text{higher derivative} \tag{1.1}$$

where as usual $U_i = exp(2i\pi_i^a T^a / v_i)$ with π_i^a the Goldstone fields associated with the broken generators T^a. The gauge fields enter the covariant derivatives with generators acting on U_i from the left or right depending upon their coupling to the left or right in the moose diagram.

The tree level W and Z mass matrices may be read off as

$$M^2_{W\,ij} = \begin{pmatrix} g^2 v_1^2 & -g g_1 v_1^2 & 0 & 0 & \dots & 0 & 0 & 0 \\ -g g_1 v_1^2 & g_1^2(v_1^2+v_2^2) & -g_1 g_2 v_2^2 & 0 & \dots & 0 & 0 & 0 \\ 0 & -g_1 g_2 v_2^2 & -g_2^2(v_2^2+v_3^2) & -g_2 g_3 v_3^2 & \dots & 0 & 0 & 0 \\ . & . & . & . & \dots & . & . & . \\ . & . & . & . & \dots & . & . & . \\ 0 & 0 & 0 & 0 & \dots & 0 & -g_{N-1} g_N v_{N-1}^2 & g_N^2(v_{N-1}^2+v_N^2) \end{pmatrix} \tag{1.2}$$

$$M^2_{Z\,ij} = \begin{pmatrix} g^2 v_1^2 & -g g_1 v_1^2 & 0 & 0 & \dots & 0 & 0 & 0 & 0 \\ -g g_1 v_1^2 & g_1^2(v_1^2+v_2^2) & -g_1 g_2 v_2^2 & 0 & \dots & 0 & 0 & 0 & 0 \\ 0 & -g_1 g_2 v_2^2 & -g_2^2(v_2^2+v_3^2) & -g_2 g_3 v_3^2 & \dots & 0 & 0 & 0 & 0 \\ . & . & . & . & \dots & . & . & . & . \\ . & . & . & . & \dots & . & . & . & . \\ 0 & 0 & 0 & 0 & \dots & 0 & -g_{N-1} g_N v_{N-1}^2 & g_N^2(v_{N-1}^2+v_N^2) & g_N g' v_N^2 \\ 0 & 0 & 0 & 0 & \dots & 0 & 0 & g_N g' v_N^2 & g'^2 v_N^2 \end{pmatrix} \tag{1.3}$$

Note that in the limit where $N = 0$ this description of the Goldstone modes of the model is simply the Standard Model. In fact to completely recover the Standard Model the Higgs in the UV completion must also be made real.

For larger N when the couplings and vevs are all equal the W mass matrix has

eigenvalues [21]

$$M_W^k = gv \sin\left[\frac{(2k-1)\pi}{4N-2}\right] \tag{1.4}$$

which for large N and $k < N$ reproduces a KK like tower of W states. Note that the W tower masses are suppressed relative to v by a factor of N. This is the mechanism by which we will remove the Higgs from the low energy spectrum. In fact the couplings g grow as $\sqrt{N}$ to keep the low energy coupling invariant so the gain in Higgs mass is only $\sqrt{N}$ too. In a simple Higgs model the Higgs mass is given by $\sqrt{\lambda}v$ with λ the quartic coupling in the Higgs potential. Thus as the Higgs vev increases by a factor of $\sqrt{N}$ so does its mass. In fact in the UV completion the scalar potential could be considerably more complicated with renormalizable terms of the form $|h_i|^2|h_j|^2$ affecting the masses, but it is only our intention here to study the dependence of the vev on N which is indicative of the Higgs mass scale. Unitarity in W scattering must still be maintained at scales of order the lightest W mass - as discussed in [19] the KK tower acts as the restoring mechanism.

This simple set up will not make for good phenomenology since the first KK partner of the W is very light (the direct experimental bound is of order 500 GeV). We must therefore look at limits where the KK modes are starting to become more massive and decouple. There are two obvious limits of this form. Firstly we can raise the vevs $v_1 - v_N$; in the limit where they are infinite the low energy theory just becomes the Standard Model. This limit seems promising since precision parameters will naturally tend to the Standard Model values in this limit too (we will see soon how well the new physics decouples). However, the lightest Higgs is becoming Standard Model like too in this limit and hence light. The second limit, explored in [24], is to take the couplings

$g_1 - g_N$ to be large - this makes the KK modes heavy but does not precisely return the Standard Model even in the infinite coupling limit. Varying the vevs and couplings along the chain corresponds at the five dimensional level to warping the geometry [33] so we might hope to find the same successes seen in such models. We will explore both of these limits in Chapter 3.

To present results that can be compared to experimental data we will numerically solve for the eigenvalues of the matrices (1.2,1.3). Within Chapter 3 we will work at tree level and search for a theory compatible with the data at this level. We must also couple the Standard Model matter fields into the model. We will follow [24] and allow the fermions to couple to the end two gauge groups in the moose chain. This choice ensures that $T = U = 0$ [24] when the central SU(2) groups' couplings are taken large. We have also explored other assignments but found little benefit from them. As usual we will fix our model to the measured values of M_Z the electric charge e and the Fermi constant G_F since these are the best measured experimental results.

Having presented results at tree level we will then move on to perform loop level calculations with specific attention to the S parameter ($T = U = 0$ [24]). Where a small S parameter correction at the loop level implies minimal corrections to the tree level phenomenology and establishes perturbativity. In Chapter 4 we will perform these loop level S parameter calculations within the Standard Model. This detailed analysis will provide insight into how the loop level calculation should be generalized in Deconstruction. In Chapter 5 we will present the evaluated results for the S parameter for a Deconstructed Model with one additional gauge group.

Chapter 2

Introduction to Deconstruction

In this chapter we will introduce Deconstruction and the idea of Higgsless models of electroweak symmetry breaking. First though let us review the Higgs and gauge sectors of the Standard Model.

2.1 The Standard Model Higgs Mechanism

The Standard Model Lagrangian for a non-abelian gauge theory coupling to the Higgs scalar Σ is shown in equation 2.1.

$$\mathcal{L} = -\tfrac{1}{4}B^{\mu\nu}B_{\mu\nu} - \tfrac{1}{4}W^{a\mu\nu}W_{a\mu\nu} + \frac{1}{4}tr\left[D^{\mu}\Sigma(D_{\mu}\Sigma)^{\dagger}\right] - V(\Sigma) \tag{2.1}$$

Where the potential is,

$$V(\Sigma) = -\mu^2\Sigma^*\Sigma + \frac{\lambda}{2}(\Sigma^*\Sigma)^2 \tag{2.2}$$

And the gauge boson tensors are of the form,

$$F^a_{\mu\nu} \equiv \partial_\mu A^a_\nu - \partial_\nu A^a_\mu + g f^{abc} A^b_\mu A^c_\nu \tag{2.3}$$

from which it is possible to generate the mass matrices and in turn the masses for the W boson, Z boson and photon. These mass matrices form from the covariant derivative part of the Lagrangian,

$$D_\mu \Sigma = \partial_\mu \Sigma - ig' I B_\mu \Sigma + ig \Sigma T^a W_\mu^a \tag{2.4}$$

Where Σ is the Higgs field which generates the masses of the W and Z bosons through the Higgs Mechanism.

$$\Sigma = \begin{pmatrix} \phi^+ - i\phi^- \ , \ v + (h + i\chi) \end{pmatrix} \tag{2.5}$$

This field contains the Goldstone fields ϕ^-, ϕ^-, χ which are absorbed in the generation of the W and Z masses. It also contains the Higgs boson field h and the Higgs vacuum expectation value (vev), v.

The presence of the Goldstone fields, the physical Higgs boson and the gauge boson masses can be understood by observation of the Higgs potential for the spontaneously broken symmetry $V(\Sigma)$ shown in Figure 2.1. The shape of this potential follows from the form in equation 2.2, where the explicit minus sign on the μ^2 term results in the circular minimum away from zero value of the field. The fact that the minimum of the Higgs potential is shifted from the centre where everything is symmetric to phase changes of the field Σ, to a position where this is no longer an explicit symmetry, is the breaking of the $O(N)$ rotation symmetry. It is natural to rewrite the Higgs field in a manner that centres things around the minimum of the potential. This results in the vacuum expectation value v with a new field, called the Higgs field, directed along the radial direction and an additional field χ which is a Goldstone boson field directed

along the trough in the potential. The $\phi^+, i\phi^-$ fields are directed along the trough of the potential in the dimensions not shown in the diagram, and like the χ field the fact that they see flat potentials makes them massless particles.

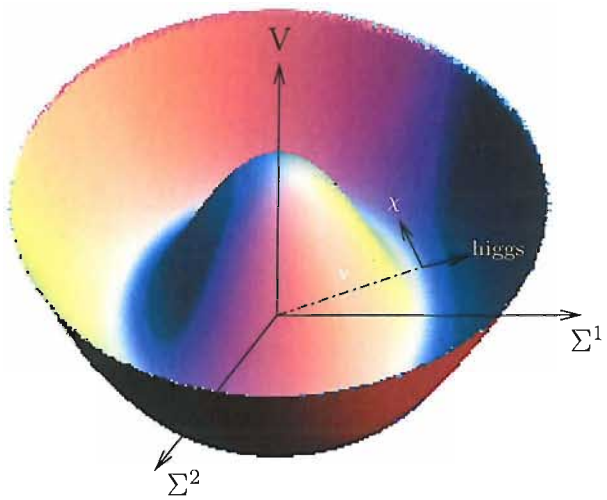

Figure 2.1: Two dimensional representation of the Higgs potential for spontaneous breaking of a continuous $O(N)$ rotation symmetry, showing Higgs vev v, Higgs boson h and Goldstone boson χ. The Goldstone bosons ϕ^-, ϕ^+ appear in the two suppressed dimensions of the four dimension Higgs field.

When we rewrite the Higgs potential centred upon the minimum value of the field there are terms in the Lagrangian that contain the gauge boson fields coupled to the Higgs vev coming from the four point interactions of the unbroken theory. Since the Higgs vev is a constant, not a fluctuating field, this term in the Lagrangian becomes a two point vertex with a coefficient of the Higgs vev squared, this in effect is a mass squared term and the gauge boson field has gained a mass. These mass terms in the Lagrangian are for the W^+, W^- bosons and Z boson.

The Goldstone fields can be said to be absorbed in the generation of the W/Z masses. This can be seen most easily in Unitary gauge where the Goldstones are

explicitly removed by a gauge transformation. This removal of the Goldstone fields corresponds to a removal of degrees of freedom from the Lagrangian, however the additional longitudinal degrees of freedom required for gauge bosons to have a mass exactly compensates, in effect the Goldstone's degrees of freedom have been absorbed into the the generation of gauge boson masses.

In this thesis we will follow the trend in the research literature and work in the Feynman-t'Hooft gauge. Unlike the Unitary gauge the Goldstone bosons do not get removed from the Lagrangian through the gauge choice, instead they remain consistent with the Unitary gauge in asserting the unphysical nature of the Goldstone bosons through their cancellation within the S matrix [34, 35]. In Feynman-'t Hooft gauge the Goldstone bosons have masses equal to that of their corresponding gauge bosons, $\phi^+, i\phi^-$ having the W boson mass and χ having the Z boson mass. These shared masses tie in neatly with the principle that such unphysical Goldstone bosons should ultimately be absorbed into their respective massive gauge bosons.

The gauge fixing Lagrangian in 't Hooft gauge is [36],

$$\mathcal{L} = -\frac{1}{2\zeta}(\partial_\mu A^{a\mu} - \zeta g \phi^a i T^a v)^2 \tag{2.6}$$

Where Unitary gauge corresponds to $\zeta = \infty$, while Feynman-'t Hooft gauge corresponds to $\zeta = 1$. It can be seen that in Feynman-'t Hooft gauge the charged Goldstone fields have a mass $m_\phi = gv$, which we will see later is equal to the mass of the W boson. There is also a term for the hypercharge component of the gauge fixing Lagrangian which analogously produces $m_\chi = v\sqrt{(g^2 + g'^2)}$, equivalent to the Z boson mass.

Expanding the covariant derivative part of the Lagrangian with attention to the

Higgs vev forms the mass matrices for the gauge bosons.

$$tr\left[D^{\mu}\Sigma(D_{\mu}\Sigma)^{\dagger}\right] = \begin{pmatrix} 0 & v \end{pmatrix}(\partial_{\mu} - ig'IB_{\mu} + igT^{a}W_{\mu}^{a}) \times(\partial_{\mu} - ig'IB_{\mu} + igT^{a}W_{\mu}^{a})^{\dagger}\begin{pmatrix} 0 \\ v \end{pmatrix} \tag{2.7}$$

This yields

$$\begin{pmatrix} W_{\mu}^{3} & B_{\mu} \end{pmatrix} v^{2} \begin{pmatrix} g^{2} & -gg' \\ -gg' & g'^{2} \end{pmatrix} \begin{pmatrix} W_{\mu}^{3} \\ B_{\mu} \end{pmatrix} + \begin{pmatrix} W_{\mu}^{1} & W_{\mu}^{2} \end{pmatrix} g^{2}v^{2} \begin{pmatrix} W_{\mu}^{1} \\ W_{\mu}^{2} \end{pmatrix} \tag{2.8}$$

We can diagonalise the mass matrices to explicitly display the eigenvalues. These eigenvalues correspond to the masses of the gauge bosons.

$$\begin{pmatrix} A & Z \end{pmatrix} v^{2} \begin{pmatrix} 0 & \\ & (g^{2}+g'^{2}) \end{pmatrix} \begin{pmatrix} A \\ Z \end{pmatrix} + \begin{pmatrix} W^{+} & W^{-} \end{pmatrix} g^{2}v^{2} \begin{pmatrix} W^{+} \\ W^{-} \end{pmatrix} \tag{2.9}$$

Hence the Photon mass is zero, $M_A = 0$, the Z mass is $M_Z = v\sqrt{(g^2+g'^2)}$ and the W mass is $M_W = vg$.

The relationships between the unbroken gauge fields and their broken counterparts are shown in equations 2.10,2.11. Where the coefficients are formed from components of the eigenvectors of the mass matrix. It is conventional to describe the neutral current matrix, equation 2.11, in terms of a single parameter known as the weak mixing angle θ_W, matrices of this form are therefore referred to as the mixing angle matrices.

$$W_{\mu}^{\pm} = \frac{1}{\sqrt{2}}\left(W_{\mu}^{1} \mp iW_{\mu}^{2}\right) \tag{2.10}$$

$$\begin{pmatrix} Z_\mu \\ A_\mu \end{pmatrix} = \begin{pmatrix} \cos\theta_W & -\sin\theta_W \\ \sin\theta_W & \cos\theta_W \end{pmatrix} \begin{pmatrix} W_\mu^3 \\ B_\mu \end{pmatrix} \tag{2.11}$$

The physics of gauge boson masses is also often described in terms of an additional parameter ρ. The ρ-parameter is equal to one at tree level in the Standard Model and deviates from one both at the loop level in the Standard Model and at tree level for certain beyond the Standard Model theories (In Chapter 3 we shall see that Deconstruction is such a theory).

$$\rho_{tree} = \frac{M_W^2}{M_Z^2 \cos^2\theta_W} \equiv 1 \tag{2.12}$$

The experimental value for the ρ-parameter is updated within the particle data book [37], and recorded in terms of the parameter $\delta\rho$ the deviation from the ρ-parameter's tree level value of one.

$$\delta\rho = \frac{M_W^2}{M_Z^2 \cos^2\theta_W} - 1 \tag{2.13}$$

We can input the experimental values of M_W, M_Z and $\cos\theta_W$ (we use the renormalization scheme of [61]). The value of $\delta\rho$ is 0.0009 with 1σ errors 0.0027. In Chapter 3 we will present graphs of the parameter $\delta\rho$ which must remain within these experimental bounds. Given the accuracy with which the Z boson mass is experimentally constrained, the ρ-parameter bounds are essentially degenerate with the W boson mass bounds and so we will say little about $\delta\rho$ in Chapter 3, but include the plots for completeness.

The covariant derivative,

$$D_\mu = \partial_\mu - ig' I B_\mu + igT^a W_\mu^a \tag{2.14}$$

transforms after symmetry breaking into the form,

$$\begin{aligned} D_\mu = \quad & \partial_\mu - i\tfrac{g}{\sqrt{2}}(W_\mu^+ T^+ + W_\mu^- T^-) - i\tfrac{1}{\sqrt{g^2+g'^2}} Z_\mu (g^2 T^3 - g'^2 Y) \\ & -i\tfrac{gg'}{\sqrt{g^2+g'^2}} A_\mu (T^3 + Y) \end{aligned} \tag{2.15}$$

where $T\pm = T^1 \pm iT^2$. By observing the photon term in the covariant derivative and making the association $Q = T^3 + Y$, we can clearly see that the electron coupling e, that couples the electron to photons, is defined as follows.

$$e \equiv \frac{gg'}{\sqrt{g^2 + g'^2}} \tag{2.16}$$

The photon part of the covariant derivative is now,

$$\Delta D_\mu = -ieQA_\mu \tag{2.17}$$

With Q representing electric charge.

There is an alternative formulation to the Higgs mechanism for describing symmetry breaking in which the Goldstones are inserted by hand [38]. In this method the Higgs boson is not assumed and there is no attempt to describe how the theory remains renormalizable at the scale of the Higgs mass and above. The symmetry is not spontaneously broken, as through the Higgs mechanism, but broken explicitly through the mentioned introduction of Goldstone fields. This formalism does have the advantage of being consistent with experimental data (the non-renormalizable operators in the theory can be chosen to reproduce the observed data - see [65]) , without introducing any physics that has yet to be verified experimentally.

Mathematically the alternative formulation can be described by the Goldstone field

below,

$$U = e^{i\pi^a T^a/f} \tag{2.18}$$

where T^a is the generator of the symmetry for the individual Goldstone boson fields π^a, with a symmetry breaking vev f [39]. U enters the Lagrangian as,

$$\mathcal{L} = \frac{v^2}{4} Tr D^\mu U^\dagger D_\mu U \ + \ \text{higher derivative} \tag{2.19}$$

where $SU(2)_L$ transformations act on U from the left and $SU(2)_R$ transformations from the right.

2.2 Unitarity Problem

One of the major open questions in modern high energy physics is how to resolve the so called Unitarity Problem. There have been numerous theories and models proposed to fix this anomaly that presents itself in W boson scattering in the Electroweak Field Theory.

The Unitarity Problem explicitly presents itself in the cross sections for gauge boson scatterings at high energy. This cross section grows at high energies until the probability of the interaction grows greater than one, which is clearly unphysical. The relevant Feynman diagrams are shown in Figure 2.2. The energies at which the Unitarity Problem appears have yet to be probed fully by experiments, but will be thoroughly explored by the Large Hadron Collider (LHC) when it comes online in the near future. It is hoped that the accelerator will detect evidence of whatever theory is ultimately responsible for recovering unitarity. It is a very relevant time to be expanding options,

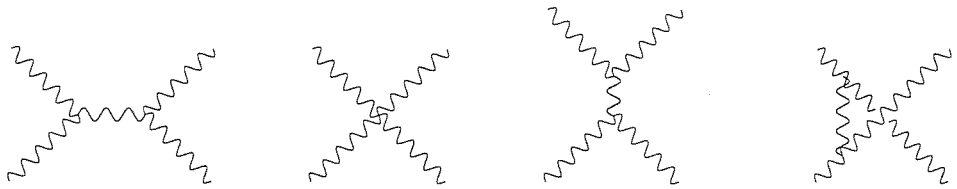

Figure 2.2: Feynman diagrams for gauge boson scattering

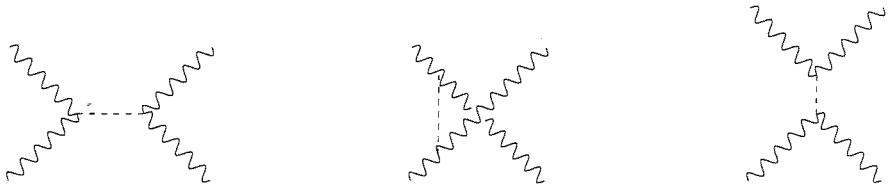

Figure 2.3: Additional Feynman diagrams contributing to the gauge boson scattering through the presence of the Higgs field

with theories to resolve the Unitarity Problem.

The simplest known solution to this unphysical probability is the Higgs Mechanism, proposed in 1964 by Peter Higgs [40, 41, 42]. The Higgs Mechanism of the Standard Model includes a symmetry breaking Higgs field. The Higgs field produces a new particle known as the Higgs boson that represents the calling card by which the mechanism might be detected at the LHC.

The presence of the Higgs field introduces additional Feynman diagrams, as shown in Figure 2.3, which must be accounted for in gauge boson scattering. The corrections due to these new diagrams resolve the Unitarity Problem by reducing the cross section probability of such scatterings occurring, to less than one [43, 44, 45, 46, 47].

Given the necessity of a unitarity correcting mechanism within Quantum Field Theory at higher energies, and the naturalness and relative simplicity of the Higgs Mechanism it has been adopted as an accepted part of the Standard Model. We will follow the convention of referring to the Higgs Mechanism as implicit in the term 'Standard Model' throughout this thesis. (Unless we are describing the Higgs Mechanism itself explicitly, where the break with this convention should be apparent to the reader). Models that extend the Standard Model without using a conventional Higgs Mechanism

will be categorised as Beyond the Standard Model.

However, in spite of the attractiveness of the Higgs Mechanism in the Standard Model, there remains no proof that it is in fact the reality in Nature. Alternatives, to prepare for the eventuality that the Higgs is not observed at the LHC, are thus highly relevant. Two leading rival descriptions of how unitarity might be maintained at high energy will be presented in this introduction, namely Kaluza-Klein Theory and Deconstruction. It is the second of these that will be the subject of this thesis.

2.3 Unitarity Through Kaluza-Klein Theory and Deconstruction

Since the Higgs hasn't been found yet, it is appropriate to look for alternate solutions to the unitarity problem. Kaluza-Klein Theory and Deconstruction are such alternatives. Here we will briefly introduce the principles involved. We will go into more detail of the mechanism of Deconstruction in section 2.5.

2.3.1 Resolving Unitarity Through Kaluza-Klein Theory

Kaluza-Klein Theory [18] was first introduced as an extra dimensional description of Electromagnetism in the 1920's in a hope of unifying Electromagnetism with General Relativity. However, the form of Kaluza-Klein Theory that we present in this thesis is the modern revival of such extra dimensional methods to describe Electroweak symmetry breaking [48, 49, 50, 51, 52, 53].

In straightforward terms Kaluza-Klein Theory is a theory in which a compactified fifth dimension is introduced in addition to the four dimensions of the Standard Model (Standard Model refers to existing physics exclusive of the Higgs mechanism in this

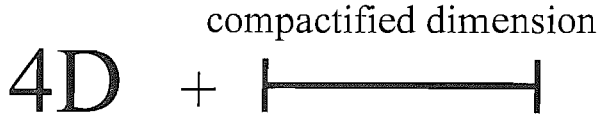

Figure 2.4: Pictorial description of Kaluza Klein Theory as a combination of a four dimensional bulk and a compactified fifth dimension

section). This is presented pictorially in Figure 2.4, where we note that the gauge bosons W,Z,γ are present in the four dimensional bulk as the lowest energy excitations of their respective fields in the compactified dimension. In fact Kaluza-Klein Theories can be generalized to any number of additional compactified dimensions, but the principle remains essentially unchanged.

In Kaluza-Klein theory additional compactified dimensions (Figure 2.5) are introduced with periodic boundary conditions to resolve the unitarity problem without the need for a Higgs field.

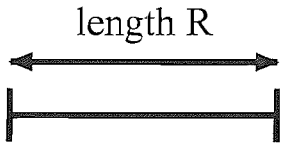

Figure 2.5: Pictorial display of a compactified dimension with periodic boundary condition

Fields from the standard four-dimensional bulk must also propagate within the compactified dimension, in effect forming waves on the compactified dimension. The lowest excited states, the ground states, correspond to the familiar Standard Model gauge bosons (where our attention here is on the Electroweak sector only). The excited states become copies of the these bosons with greater masses, which are known as the W' bosons and Z' bosons.

Periodic boundary conditions require a periodic wavefunction. If we describe the waves of the fields on the compactified dimension in terms of exponentials we can follow the following path. As we move once around the compact dimension a free wave soluton

will change as

$$e^{ipx} \Rightarrow e^{ip(x+2\pi R)} \tag{2.20}$$

The wave must return to itself so we require $e^{ip(2\pi R)} = 1$. We learn that pR is an integer n, so that $p = \frac{n}{R}$

On shell a particle satisfies $p^2 = m^2$ so we have

$$m = \frac{n}{R} \tag{2.21}$$

This describes a set of masses known as a Kaluza-Klein tower. The Kaluza-Klein towers for W bosons due to the presence of an additional compactified dimension is shown in Figure 2.6

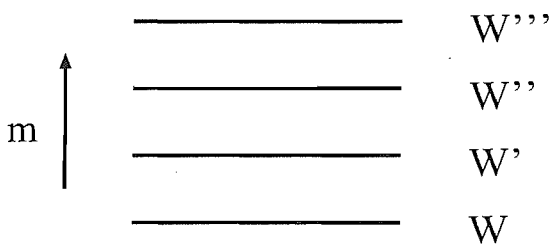

Figure 2.6: Pictorial display of the Kaluza Klein tower of additional massive W' bosons from a compactified dimension.

The excitation from the ground state in the compactified dimension of the W,Z, and γ bosons forms a tower of more massive equivalents: $W', W''...$, $Z', Z''...$,$\gamma', \gamma''...$ The presence of these additional bosons, at the higher energies required for their production, adds an array of Feynman diagrams into the gauge boson scattering cross section. These new diagrams, presented pictorially in figure 2.7, correct the cross section for gauge boson scattering so that it remains less than one in an analogous way to that of the

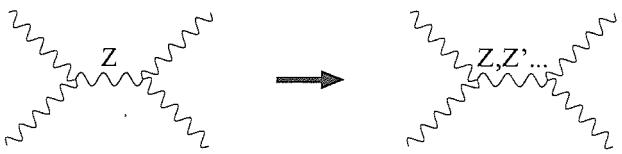

Figure 2.7: Example of the additional scattering diagrams entering from Kaluza Klein theory at higher energy scales to correct unitarity

diagrams in figure 2.3, and thus resolve the unitarity problem [19, 20, 54, 55, 56, 57, 21].

One distinction of note between the resolution of unitarity in the Higgs mechanism and that of Kaluza-Klein Theory, is that there are a finite number of additional diagrams in the Higgs mechanism. Kaluza-Klein theory, however, has an ever increasing number of additional Feynman diagrams as the energy scale rises, due to the presence of extra excited gauge bosons emerging from the additional energy states available within the compactified dimension. In effect the new gauge bosons formed at each energy level maintain unitarity for their respective energies, much as the W/Z bosons do in the Standard Model at low energy.

It is, of course, key to the merits of Kaluza-Klein Theory that it solves the unitarity problem without a Higgs field or the Higgs mechanism. It is, as such, a Higgsless model.

It is appealing that Kaluza-Klein theory solves unitarity in a manner fundamentally distinct from the Higgs mechanism. However, it has several key difficulties. Firstly it is strongly coupled in the ultra violet and so potentially non-perturbative at high scales. Secondly, in its most basic form, it predicts additional massive gauge bosons with masses excluded by searches performed at existing accelerators.

2.3.2 Resolving Unitarity Through Deconstruction

The new model of Deconstruction can extend the four dimensional Standard Model to imitate Kaluza-Klein Theory, without requiring extra dimensions, and their inherent

problems. This model proposed by Arkani-Hamed, Cohen and Georgi in 2001 [25] was devised to recreate the interesting phenomenology of Kaluza-Klein Theory, while avoiding the problems of having additional dimensions.

Deconstruction was born out of considering the compactified dimensions of Kaluza-Klein Theory as a lattice of gauge groups. By latticising the model it then became possible to reconsider the compactified dimension, not as a dimension at all, but instead as an array of new gauge groups coupled together by Higgs fields. It then became reasonable to reduce the number of gauge groups, which is equivalent to increasing the lattice spacing, until the chain of gauge groups no longer resembled a realistic extra dimension. In effect the additional dimension, 'constructed' out of a lattice of gauge groups, has been 'deconstructed' - from which the name Deconstruction derives.

The new model is explicitly four dimensional but will reproduce the phenomenology of Kaluza-Klein Theory, inclusive of its unitarity correcting additional gauge bosons, up to an energy level at which the lattice spacing becomes overt. Deconstruction ultimately is an effective five (or more) dimensional model described within four dimensions. The pay-off, for having the best of both worlds in effect, is that at a certain energy scale the imitated additional dimensionality breaks down and the model displays the chain of Higgs fields that go into its construction. This means that at a certain scale the model ceases to be Higgsless like Kaluza-Klein Theory, but instead continues to maintain unitarity through a generalisation of the Higgs mechanism.

In summary Deconstruction could be seen as a middle ground between Kaluza-Klein Theory and the Higgs Mechanism. It resolves unitarity as both do, but offers potentially Higgsless phenomenology within future experiments without the complications of additional dimensions. On the other hand it is by its very make-up an extension of the Standard Model Higgs Mechanism. In fact the minimal limiting case of a Decon-

structed lattice chain containing just two gauge groups, an $SU(2)$ and a $U(1)$ coupled together by a single Higgs field, is precisely the Standard Model.

2.4 Moose Diagrams

Deconstructed models are typically described using a convenient diagrammatic form known as Moose Diagrams. Figure 2.8 shows the general appearance of a moose diagram, with the Higgs fields that correspond to lines and the gauge groups that correspond to circles labelled. The Higgs fields in Deconstructed models are all in the $(N, \bar{N})$ representation. Figure 2.8 shows an N=1 moose, where N stands for the number of additional gauge groups beyond the Standard Model.

The reader should note that in the original Deconstruction paper the lines within the diagrams refer to Goldstone fields and the theory may not contain a Higgs. Such models may perform the symmetry breaking in some other manner, or are simply effective theories up to the symmetry breaking scale. They are as such, only renormalizable up to the symmetry breaking scale. Our models will always contain a Higgs vacuum expectation value as indicated in Figure 2.8, and are consequently fully renormalizable.

A good example of the principle by which moose diagrams describe Deconstructed models, is to look at the limiting case of an N=0 moose diagram as shown in Figure 2.9. This diagram is precisely the Standard Model Electroweak $SU(2) \times U(1)$ written in moose notation. Deconstruction is then diagrammatically seen to be an extension of the same principles that operate in the formation of the Standard Model Higgs Mechanism.

Here moose diagram notation displays diagrammatically the useful fact that the Standard Model can be replicated as a limiting case of a Deconstructed Model. This fact can be used as a check on the correctness of Deconstructed Models by establishing they can replicate the Standard Model for N=0. It also provides a limiting case guaranteeing

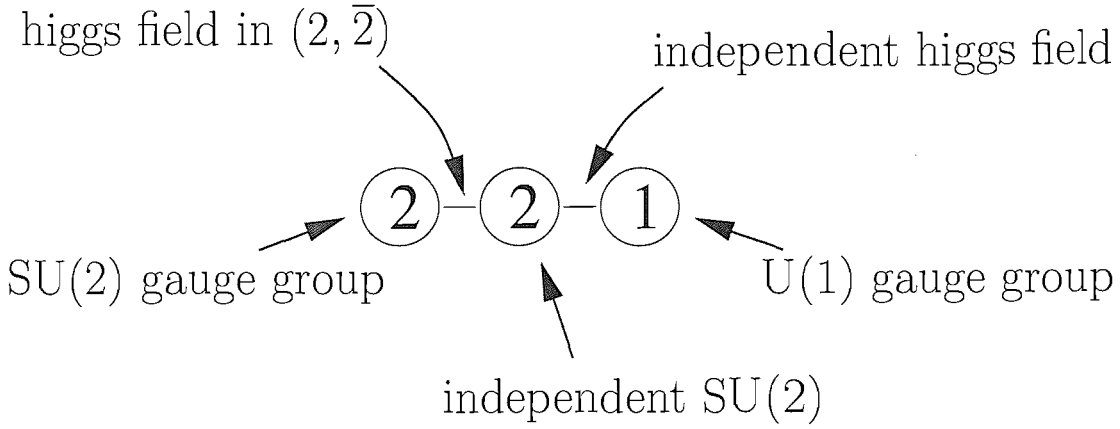

Figure 2.8: Labelled moose diagram for an N=1 Deconstructed model

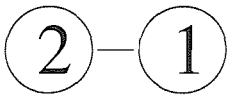

Figure 2.9: Labelled moose diagram for an N=0 Deconstructed model, which corresponds to the Electroweak Standard Model

experimental consistency, that can be used as a solid base from which to expand towards Deconstructed models that yield fresh phenomenology without violating experimental bounds.

2.5 Deconstruction

If we use the analogy between Deconstruction and the Standard model shown diagrammatically in Figure 2.10, it is easier to see how Deconstructed models can be described mathematically by the extension of the principles of section 2.1.

Consider just the simplest form of a Deconstructed model, that of an N=1 $U(1) \times$

Figure 2.10: Schematic description using moose diagram notation of the analogy between the Electroweak Standard Model and generalised Deconstructed models of single chain form

$SU(2)_1 \times SU(2)_2$ [24]. The Lagrangian Density for this N=1 Deconstructed model is,

$$\mathcal{L} = -\tfrac{1}{4}B^{\mu\nu}B_{\mu\nu} - \tfrac{1}{4}W_1^{a\ \mu\nu}W_{1\ \mu\nu}^a - \tfrac{1}{4}W_2^{a\ \mu\nu}W_{2\ \mu\nu}^a + \tfrac{1}{4}tr\left[D^\mu\Sigma_1(D_\mu\Sigma_1)^\dagger\right] + \tfrac{1}{4}tr\left[D^\mu\Sigma_2(D_\mu\Sigma_2)^\dagger\right] \quad (2.22)$$

Where Σ_1, Σ_2 are the two Higgs doublets within the N=1 Deconstructed model.

$$\Sigma_1 = \begin{pmatrix} \Phi_1^+ - i\Phi_1^- \ , \ v_1 + (h_1 + i\chi_1) \end{pmatrix} \quad (2.23)$$

$$\Sigma_2 = \begin{pmatrix} \Phi_2^+ - i\Phi_2^- \ , \ v_2 + (h_2 + i\chi_2) \end{pmatrix} \quad (2.24)$$

The two covariant derivatives in the $(N, \tilde{N})$ representation are as follows,

$$D_\mu\Sigma_1 = \partial_\mu\Sigma_1 - ig'IB_\mu\Sigma_1 + i\tilde{g}\Sigma_1 T^a W_{1\mu}^a \quad (2.25)$$

$$D_\mu\Sigma_2 = \partial_\mu\Sigma_2 - i\tilde{g}T^a W_{1\mu}^a\Sigma_2 + ig\Sigma_2 T^a W_{2\mu}^a \quad (2.26)$$

Giving the Lagrangian mass terms:

$$\mathcal{L} = (W_1^{a\mu}, W_2^{a\mu})v^2 \begin{pmatrix} g^2 & -g\tilde{g} \\ -\tilde{g}g & \tilde{g}^2 \end{pmatrix} \begin{pmatrix} W_{\mu 1}^a \\ W_{\mu 2}^a \end{pmatrix} + (W_1^{3\mu}, W_2^{3\mu}, B^\mu)v^2 \begin{pmatrix} g^2 & -g\tilde{g} & 0 \\ -\tilde{g}g & \tilde{g}^2 & -\tilde{g}g' \\ 0 & -\tilde{g}g' & g'^2 \end{pmatrix} \begin{pmatrix} W_{\mu 1}^3 \\ W_{\mu 2}^3 \\ B_\mu \end{pmatrix} \quad (2.27)$$

More generally for an arbitrary N model the terms take the form

$$\mathcal{L} = (W_1^{a\mu}, W_2^{a\mu}, ...)v^2 \begin{pmatrix} g^2 & -g^2 & & \\ -g^2 & 2g^2 & & \\ & & \ddots & \\ & & & g^2 \end{pmatrix} \begin{pmatrix} W^a_{\mu 1} \\ W^a_{\mu 2} \\ .. \end{pmatrix}$$
$$+ (W_1^{3\mu}, W_2^{3\mu}, ..., B^\mu)v^2 \begin{pmatrix} g^2 & -g\tilde{g} & & & \\ -g\tilde{g} & 2\tilde{g}^2 & & & \\ & & \ddots & & \\ & & & 2\tilde{g}^2 & -\tilde{g}g' \\ & & & -\tilde{g}g' & g'^2 \end{pmatrix} \begin{pmatrix} W^3_{\mu 1} \\ W^3_{\mu 2} \\ .. \\ B_\mu \end{pmatrix} \quad (2.28)$$

The eigenvalues of these matrices are the physical masses of multiple excited W/Z bosons as well as the W boson, Z boson and massless photon.

2.6 Connection Between Kaluza-Klein Theory and Deconstruction

In subsection 2.3.2 we described how Deconstruction originated as a way of describing Kaluza-Klein theory on a four dimensional lattice. In this section we will now go into the details of that process.

In Figure 2.11 we show pictorially the idea of a compactified extra dimension described in terms of moose diagram notation. The gauge groups are represented here by the lattice points. The lines linking sites correspond to the Higgs fields. In order to replicate an extra dimension there must be an infinite number of gauge groups linked by an infinite number of bi-fundamental Higgs fields.

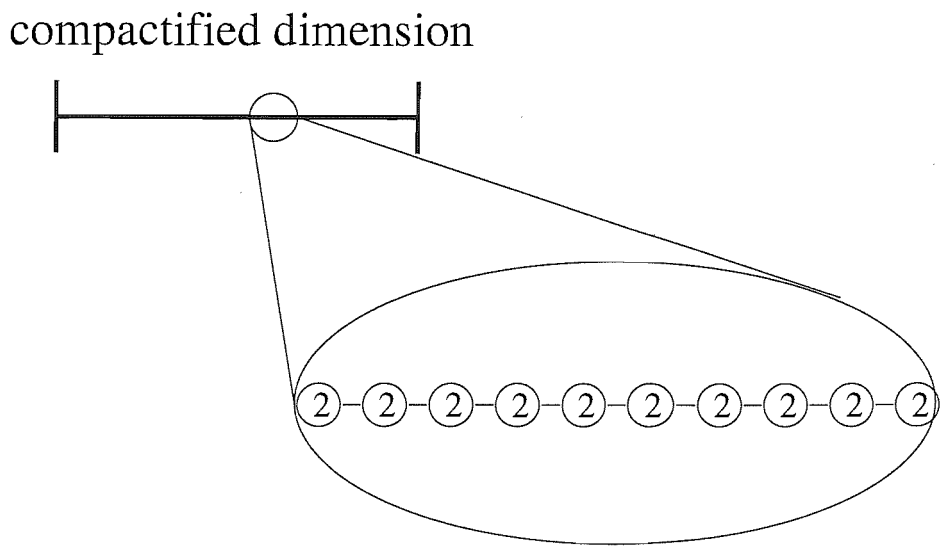

Figure 2.11: Pictorial display of a Kaluza Klein compactified dimension as a moose diagram from a Deconstructed model with an arbitrarily large number of SU(2) gauge groups, and one boundary U(1) group.

The mass matrix of such a moose diagram has the same structure as a coupled harmonic oscillator. If all the couplings to the gauge groups are equal and we take equal Higgs vevs on each link, as in a conventional lattice where all points are treated as equivalent, then the mass matrix and associated eigenvectors take the form of equation 2.29.

$$g^2v^2\begin{pmatrix} \ddots & & & & & \\ -1 & 2 & -1 & & & \\ & -1 & 2 & -1 & & \\ & & -1 & 2 & -1 & \\ & & & & \ddots \end{pmatrix}\begin{pmatrix} \vdots \\ e^{\frac{i\pi}{N}(\frac{N}{2}-1)n} \\ e^{\frac{i\pi}{N}\frac{N}{2}n} \\ e^{\frac{i\pi}{N}(\frac{N}{2}+1)n} \\ \vdots \end{pmatrix} = \lambda\begin{pmatrix} \vdots \\ e^{\frac{i\pi}{N}(\frac{N}{2}-1)n} \\ e^{\frac{i\pi}{N}\frac{N}{2}n} \\ e^{\frac{i\pi}{N}(\frac{N}{2}+1)n} \\ \vdots \end{pmatrix} \tag{2.29}$$

With eigenvalues,

$$\lambda = M^2 = 4g^2v^2\sin^2\left(\frac{\pi n}{N}\right) \tag{2.30}$$

The lightest gauge bosons ($n \ll N$) then generate a Kaluza-Klein tower of masses as

in equation 2.31.

$$M = 2gv\pi\frac{n}{N} \tag{2.31}$$

Here we can see that the lattice of gauge groups of our Deconstructed moose model does indeed replicate the phenomenology of Kaluza-Klein theory.

By reducing the number of gauge groups in a Deconstructed model we can replicate some of the physics of Kaluza-Klein theory, while working with models that are explicitly only four dimensional. Such models resolve unitarity at low energy scales through the formation of a tower of excited W/Z bosons, analogous to Kaluza-Klein Theory, while at much higher energies a very massive Higgs corrects unitarity, analogously to the Standard Model.

It is of particular interest that these manifestly four dimensional models, can be seen as Higgsless effective theories up to an arbitrarily high scale where the Higgs resides.

2.7 Fermion Couplings in Deconstructed Models

In Deconstruction the electron couples to the gauge groups in analogy to how they do in the Standard Model. In this thesis we will impose that the fermions couple to the end two gauge groups of the moose chain, ie one SU(2) and one U(1) (this ensures there is a custodial symmetry in the model). We must generate the same value for the electron coupling as found from experiment and this requirement will place a constraint upon the values of the couplings in the moose model.

The electron coupling can be established from the Lagrangian through the evalua-

tion of the neutral current coupling to the electron

$$\mathcal{L} = \bar{e}\gamma^{\mu} D_{\mu} e, \qquad D^{\mu} = \partial^{\mu} - igW^{a}_{N+1\mu} - ig'B^{\mu} \tag{2.32}$$

We must re-write the gauge fields in terms of their physical mass eigenstates. We will generically write the mixing angle matrix for the neutral currents in Deconstruction as,

$$A = b_{00}B + b_{10}W^{3}_{1} + ... + b_{(N+1)0}W^{3}_{N+1} \tag{2.33}$$

$$Z' = b_{01}B + b_{11}W^{3}_{1} + ... + b_{(N+1)1}W^{3}_{N+1} \tag{2.34}$$

$$Z'' = b_{02}B + b_{12}W^{3}_{1} + ... + b_{(N+1)2}W^{3}_{N+1} \tag{2.35}$$

$$\vdots$$

$$Z = b_{0(N+1)}B + b_{1(N+1)}W^{3}_{1} + ... + b_{(N+1)(N+1)}W^{3}_{N+1} \tag{2.36}$$

The choice of ordering for the coefficients follows that of reference [24], for consistency with the existing research literature.

The Z boson vertex contributions are

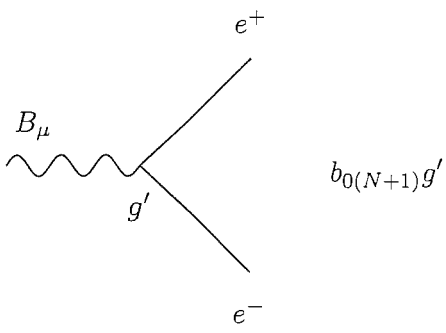

summed with,

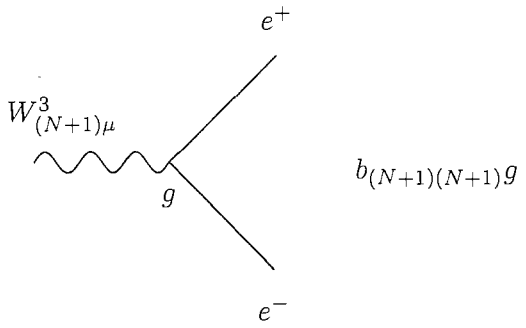

Where the coefficients $b_{0(N+1)}$,$b_{(N+1)(N+1)}$ are elements from the mixing angle matrix which transforms the unbroken fields $W^3_{(N+1)\mu}$,B_μ into their broken counterparts the Z boson and photon.

Similarly the photon vertex contributions are:

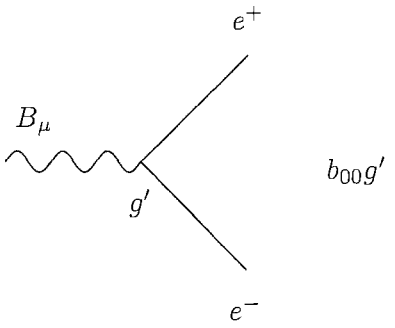

summed with,

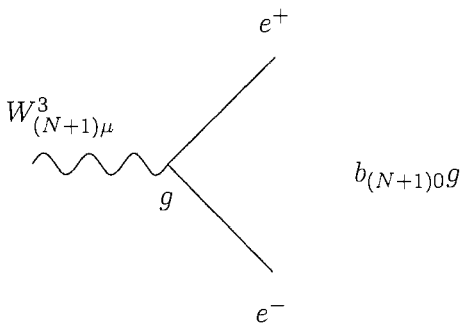

From which we get the neutral current parts of the covariant derivative;

$$D_\mu^{NC} = Z_\mu(b_{(N+1)(N+1)}gT^3 + b_{0(N+1)}g'Y) + A_\mu(b_{(N+1)0}gT^3 + b_{00}g'Y) \tag{2.37}$$

We define the charge Q to be the coupling between photons and fermions. By requiring that the electric charge be a coefficient of a single electron coupling and using the relation $Q = T^3 + Y$ as in the standard model, the mixing angle matrix elements need to be re-expressed in terms of a single coupling e as follows,

$$b_{00} = \frac{e}{g'}, \qquad b_{(N+1)0} = \frac{e}{g} \tag{2.38}$$

Therefore,

$$D_\mu^{NC} = Z_\mu(b_{(N+1)(N+1)}gT^3 + b_{0(N+1)}g'Y) + A_\mu(eT^3 + eY) \tag{2.39}$$

$$= Z_\mu(b_{(N+1)(N+1)}gT^3 + b_{0(N+1)}g'Y) + A_\mu eQ \tag{2.40}$$

The coupling e is now clearly the electron coupling with a coefficient of electric charge Q, which couples the photon field A_μ to fermions. The mixing angle matrices are now linked by a common factor of the electron coupling that is very precisely constrained by experimental data [37], removing a degree of freedom from the model.

The Fermi constant G_F is an additional strong constraint from experimental data [37] on the values of the couplings in the Deconstructed model. It is defined as below,

$$\frac{G_F}{\sqrt{2}} = \frac{g^2}{8m_W^2} \tag{2.41}$$

Finally the Z boson mass is very accurately measured compared to the W boson mass and so we will treat the Z boson mass as a constant. We now have three constraints on the parameters of our Deconstructed models, that can be used to establish the values of the couplings g,g' and the Higgs vev v.

Chapter 3

Tree Level Plots

Having introduced Deconstructed models we will now present our own numerical analysis of various such models at the tree level, undertaken in order to find out what interesting phenomenology is predicted. We are particularly interested in whether such models can present effective Higgsless phenomenology at scales probable at the Large Hadron Collider (LHC). This would provide alternative physics consistent with resolving unitarity and renormalizability if the LHC failed to find a Higgs.

3.1 N=50 One U(1) Group

In this section we will present the first of a string of models covered through this Chapter as we investigate the array of possible models that may present effective Higgsless phenomenology at LHC energy scales.

Increasing the size of the mass matrix creates additional W/Z bosons, making it possible for the Higgs mass to be greater. Consequently we chose to begin our investigations by numerically analysing a model with a large number of gauge groups.

We construct an example of a large mass matrix, with fifty SU(2) gauge groups. This is shown in moose diagram form in Figure 3.1. The SU(2) couplings are all set to

be equal. The U(1) coupling is set to its Standard Model value and the SU(2) groups are all given the Standard Model value multiplied by the number of these gauge groups, in this case fifty. This choice recovers the standard coupling to the electron.

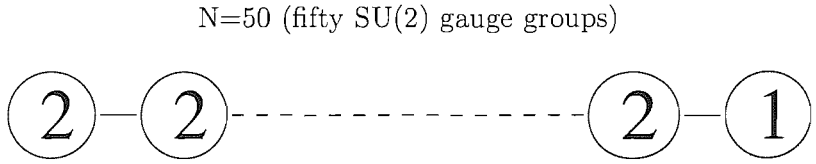

Figure 3.1: Moose diagram for a Deconstructed model with fifty SU(2) gauge groups and one U(1) group

We fix the first non-zero eigenvalue and set it to the Z mass (~90GeV). This fixes our Higgs vacuum expectation value (vev) which in this case is 1.2 TeV and the Z' masses. We use the same normalisation to determine the predicted masses for the W mass matrix, fixing the W mass and the W' masses.

If we set all the Higgs vevs to be of equal value we yield the Kaluza-Klein tower of massive gauge bosons shown in Figures 3.2 and 3.3

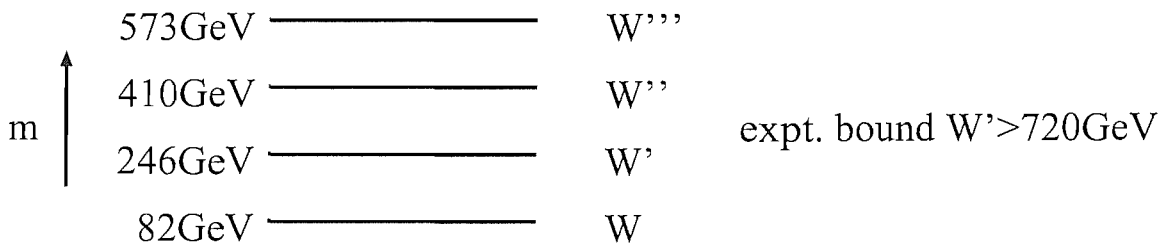

Figure 3.2: Kaluza-Klein tower of W' bosons for a Deconstructed model with fifty SU(2) gauge groups and one U(1) group

We would like throughout this chapter to have some measure of success in raising the Higgs mass relative to the Standard Model. In fact each line in the moose diagrams corresponds to a Higgs field generating three Goldstone bosons that are eaten and one physical Higgs boson - in this case we will assume that all of these fields have the same

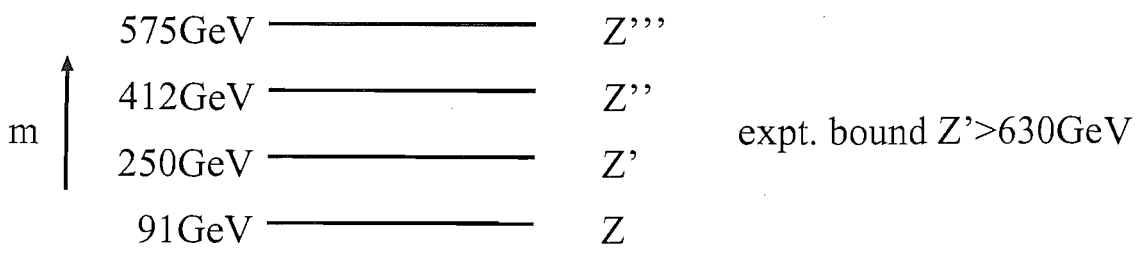

Figure 3.3: Kaluza Klein tower of Z' bosons for a Deconstructed model with fifty SU(2) gauge groups and one U(1) group

potential. The Higgs mass is given by a product of the four point self coupling and the vev. Since we have increased the Higgs vev relative to the Standard Model here, the Higgs is naturally heavier. In the Standard Model one normally assumes that the Higgs mass lies below about 1 TeV - if this is not the case the four point self coupling is so large as to become non-perturbative - there is a Landau pole in its running very close by [58, 59]. Naively if the coupling is strong at the 1 TeV scale one would expect bound states and so forth at that scale so 1 TeV is still the scale at which the Higgs physics would be found. We will therefore plot the largest possible Higgs mass in these models as

$$m_{H\ \mathrm{Decon}} = \frac{v_{\mathrm{Decon}}}{v_{SM}} \times 1\mathrm{TeV} \tag{3.1}$$

Using this estimate here the Higgs mass upper limit is driven up to 4700GeV. This is clearly Higgsless at energies that can be probed at the Large Hadron Collider (LHC). This Higgs mass increases with the number of additional gauge groups up to an infinite value, where it decouples from physics, in the Kaluza-Klein emulating limiting case of Deconstruction $N \to \infty$.

It is reassuring that we have managed to emulate the Kaluza-Klein theory phenomenology from our Deconstructed model with a large number of gauge groups. While fifty additional gauge groups is still far from the continuum limit we nevertheless see

aspects of Kaluza-Klein phenomenology.

Recreating the Kaluza-Klein tower is to be expected, however standard Kaluza-Klein models predict W' boson masses and Z' boson masses that are far below the lower bounds set by experimental searches for these bosons [37]. Only more exotic Kaluza-Klein models meet such experimental bounds [22], where the lightest additional W boson should be at least 720GeV and the lightest additional Z boson should be heavier than 630GeV. Our interest in recreating such Kaluza-Klein like phenomenology is therefore restricted only to establishing that our calculations are showing valid behaviour.

Perhaps more concerning is the fact that the W mass fails to meet its quite tight experimental bounds, we hope to correct this by exploring more relevant models.

3.2 Exploring The Space of Deconstruction Models

We have seen that a Deconstructed model with many additional gauge groups beyond the Standard Model can generate a Kaluza-Klein like tower of gauge bosons and push the mass of the Higgs bosons in the model beyond the range of the LHC. Our task now is to try to find a model with these benefits but which is also compatible with precision experimental constraints. We have many free parameters we can vary - the number of extra gauge groups, the vevs of the individual Higgs fields and the couplings of each additional SU(2) group. Let us see what benefit we can gain from each of these changes.

3.3 N=50 One U(1) Group, Adjusting the Last Higgs Vev

We'll first explore varying the last Higgs vev in the moose chain, the one coupling the U(1) group to an SU(2) group. This case is of particular interest as setting this Higgs vev small decouples the additional gauge groups, in a sense, to recreate the Standard Model when this Higgs vev is infinitesimal relative to the other Higgs vevs. This is of course identical to making the other Higgs vevs very big so they generate huge gauge boson masses - the additional SU(2) groups decouple at low energy leaving the Standard Model.

The results of this analysis are shown in Figures 3.4, 3.5 and 3.6. The Higgs mass shown in these plots is that given by (3.1) with the smallest Higgs vev of the moose chain inserted - this will be the lightest Higgs in the model. Here we are able to confirm that we can emulate Standard Model phenomenology by using the limit of a small final Higgs vev. The Standard Model W mass is reproduced in this limit and the masses of the additional W' bosons and Z' bosons rise to an infinite scale, removing themselves from the model. This is a good test of the reliability of our calculations.

By moving away from this limit we can maintain a degree of consistency with the Standard Model while introducing new phenomenology. Here we are able to see from Figure 3.6 that the W mass remains within its 2σ experimental bounds with the varied Higgs vev as large as a tenth of the value of the other Higgs vevs. For this value of the Higgs vev we can see the W' bosons and Z' bosons in Figures 3.4, 3.5 are well within the detectable range at the Large Hadron Collider (LHC). They are however too light, and are ruled out by the bounds set by experimental searches for these particles. Unfortunately the lightest Higgs mass in the model is not appreciably larger than that in the Standard Model even as we move away from the Standard Model limit. The

Higgs mechanism is still playing a large role in correcting unitarity at the lowest energy scales.

Nonetheless, we have formed a model consistent with experimental data on the W bounds, which predicts new physics. The model also displays in Figures 3.4 and 3.5 both Standard Model behaviour on the left hand side of the plot and a Kaluza-Klein tower of states emulating Kaluza-Klein theory on the right hand side of the plot. We have as such been able to recreate the characteristic features expected of a Deconstructed model. This is a sound basis for venturing out to explore new models with new parameters in hope of finding experimentally consistent physics with interesting new physics.

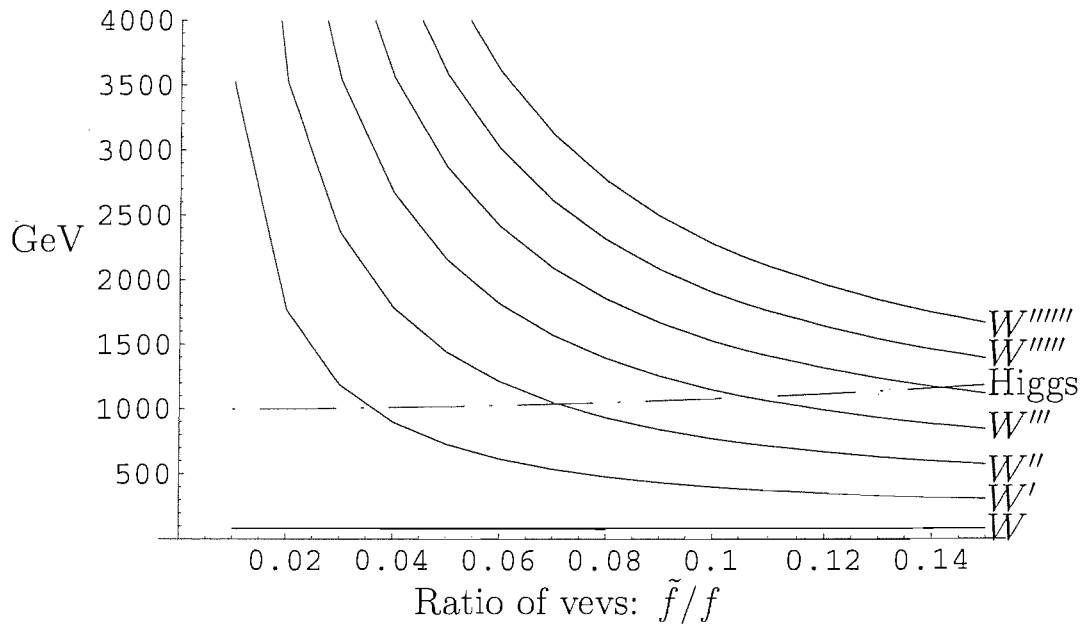

Figure 3.4: Plot of the ratio between Higgs vevs, against W' boson masses and Higgs mass for a Deconstructed model with fifty SU(2) gauge groups and one U(1) group and one variable Higgs vev

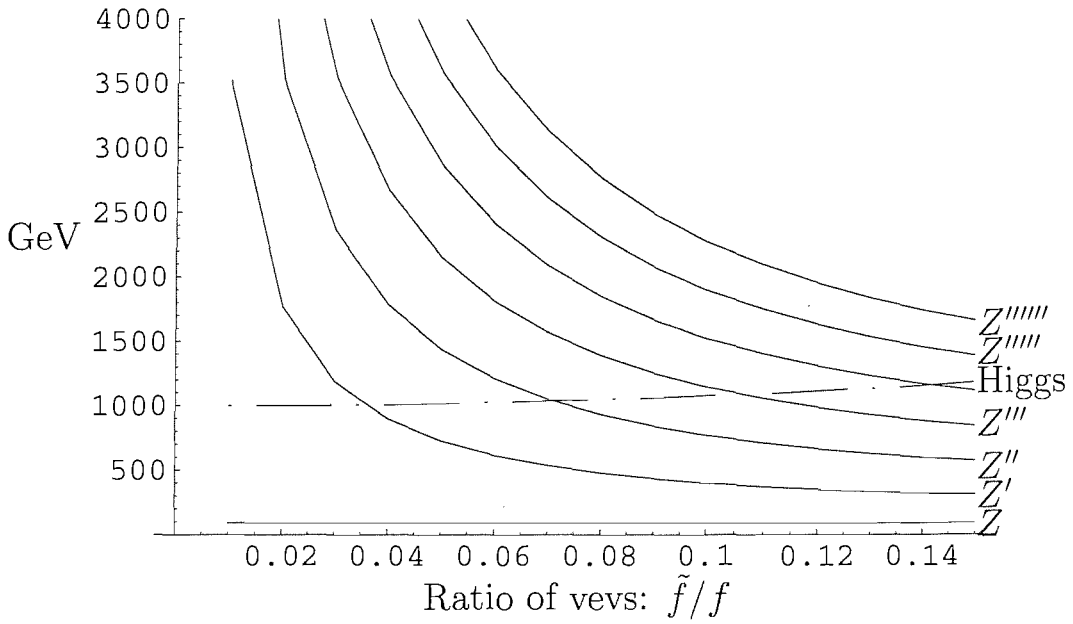

Figure 3.5: Plot of the ratio between Higgs vevs, against Z' boson masses and Higgs mass for a Deconstructed model with fifty SU(2) gauge groups and one U(1) group and one variable Higgs vev

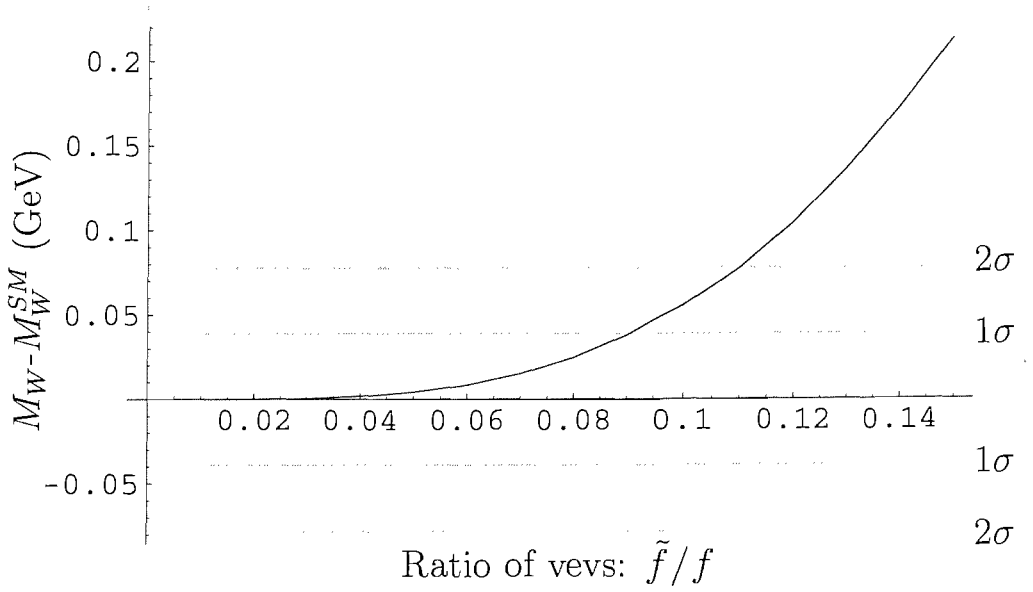

Figure 3.6: Plot of the ratio between Higgs vevs, against the W boson mass less the W mass in the Standard Model, for a Deconstructed model with fifty SU(2) gauge groups and one U(1) group and one variable Higgs vev

3.4 Varying Multiple Vevs

We note here that we have performed a considerable search of the parameter space of these types of models including varying the full range of vevs in a number of Deconstructed models. For example we tried varying two Higgs vevs instead of one. The result of this investigation yielded both heavier Higgs masses and larger W' boson and Z' boson masses. However, there was no great difference in the pattern of Higgs and gauge boson masses from that seen by varying a single vev. We then proceeded to take the approach of varying multiple vevs further, by even varying all vevs within a model. Included in this investigation was a look at exponentially varying Higgs vevs in an attempt to recreate the models in the paper by [22]. The results of this analysis again failed to throw up any radically new results though. We do not therefore provide plots for these cases. Inevitably however, there are an unlimited number of ways of exploring such parameters so we cannot conclude that this path is fruitless, but we satisfied ourselves that it was probably a dead end.

3.5 Varying Couplings

Having explored the benefits of having a large number of additional gauge groups, and managed to confirm to our satisfaction that the expected Kaluza Klein emulating behaviour was apparent we now explore slightly smaller moose models with only ten SU(2) groups. The purpose of this is partly the flexibility of being able to generate results with speed and convenience in order to investigate a large range of parameter choices.

Having made only limited progress by varying the vevs, we now turn our attention to the other obvious set of parameters at our disposal to vary, that of the couplings.

By increasing the strength of the extra gauge bosons' couplings, we hoped that the tower of bosons would make a greater contribution to the unitarity of the lightest W scattering. This might then free the Higgs boson to become heavier since it is no longer needed to be light for unitarity. This is a direct way of targeting the Higgs mass, in order to increase it as we hope to do in order to find an existence proof of a Higgsless model at the Large Hadron Collider.

As a first example, we will adopt an approach from [24]. In these models only the end two gauge groups couple to fermions. The remaining gauge groups have identical couplings, which are set by hand.

In the original paper by Schmidt et al the central gauge boson couplings were given values far larger than the gauge boson couplings at each end. In this limit it was possible to calculate physical parameters analytically. However we had concerns that the presence of such strong couplings in the theory might result in the model being non-perturbative. As such models of this kind in such a limit would have large loop level corrections, rendering the tree level results invalid.

The phenomenology obtained by Schmidt et al in their paper [24] was however very promising - they found that in the limit where the new gauge groups couplings go to infinity deviations from the Standard Model predictions in precision measurements are small (as we will see). We considered it worthwhile to explore these models using our numerical methods, outside of the strong coupling limit, to see if the interesting results could be preserved. As shall be shown in the following sections, we performed these calculations over a range of coupling strengths and variable Higgs vev values for different sizes moose chains.

3.6 Deconstructed Models with Varying Additional Couplings $\tilde{g}$

Let us explore the Deconstructed model with $N = 10$ in the limit proposed by Schmidt et al. We first explore the effect of varying the coupling strengths $\tilde{g}$ of the central gauge groups. We do this with all the Higgs vevs set to equal values. Pictorially we have:

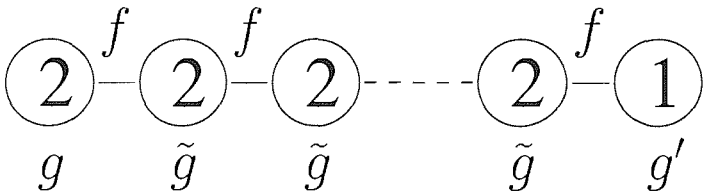

The N=10 model is both strongly Deconstructed but clearly distinct from the Kaluza-Klein equivalent limit.

Our results are displayed in Figures 3.7 to 3.10. Here we can observe the more massive partners to the W boson already forming an approximate Kaluza-Klein tower of states. We have only plotted the first six additional W like bosons, but it can be seen that the differences between their masses are decreasing as we go up the tower. The presence of a Higgs boson is, of course, distinct from any Kaluza-Klein limit. As such the properties unique to Deconstructed models are becoming apparent.

The raised level of the Higgs mass is clearly preserved outside the strong additional coupling limit employed by Schmidt et al. This is promising, as is the reduction in the masses of the additional W like bosons - which would become more evident at LHC energy scales. Unfortunately the W mass diverges from its experimental bounds as the coupling reduces away from the strong coupling limit. It appears that these models lose some of their consistency with experiments for perturbative values of $\tilde{g}$. However, we can still explore other choices of parameters to see if they might be consistent with experimental bounds.

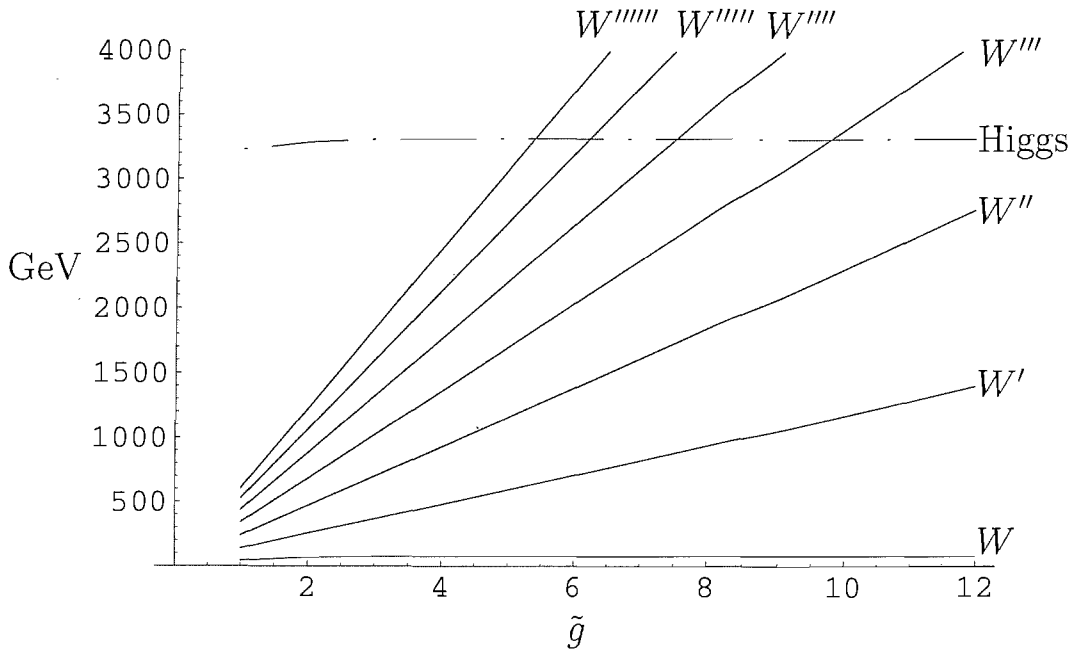

Figure 3.7: Plot of the coupling strength of the additional gauge groups ($\tilde{g}$), against W' boson masses and Higgs mass for a Deconstructed model with ten additional SU(2) gauge groups and one U(1) group

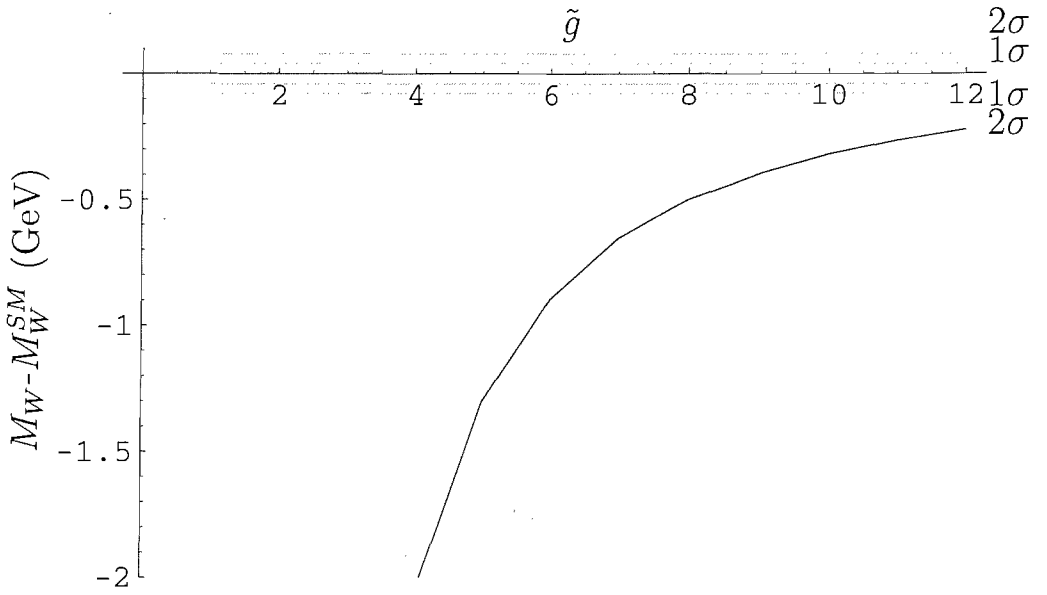

Figure 3.8: Plot of the coupling strength of the additional gauge groups ($\tilde{g}$), against the W boson mass less its Standard Model value for a Deconstructed model with ten additional SU(2) gauge groups and one U(1) group

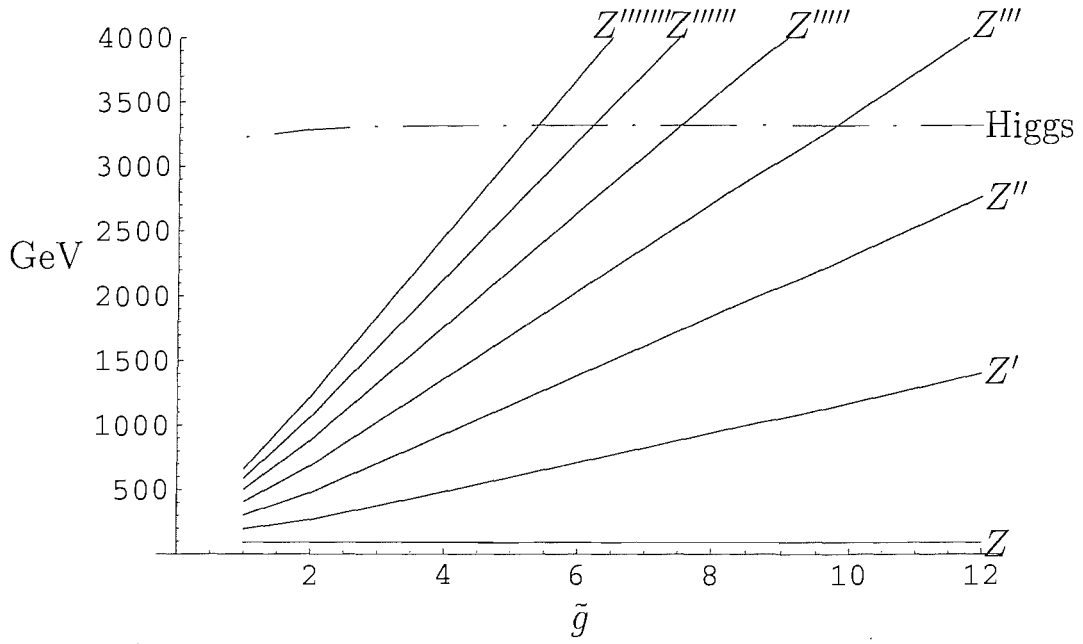

Figure 3.9: Plot of the coupling strength of the additional gauge groups ($\tilde{g}$), against Z' boson masses and Higgs mass for a Deconstructed model with ten additional SU(2) gauge groups and one U(1) group

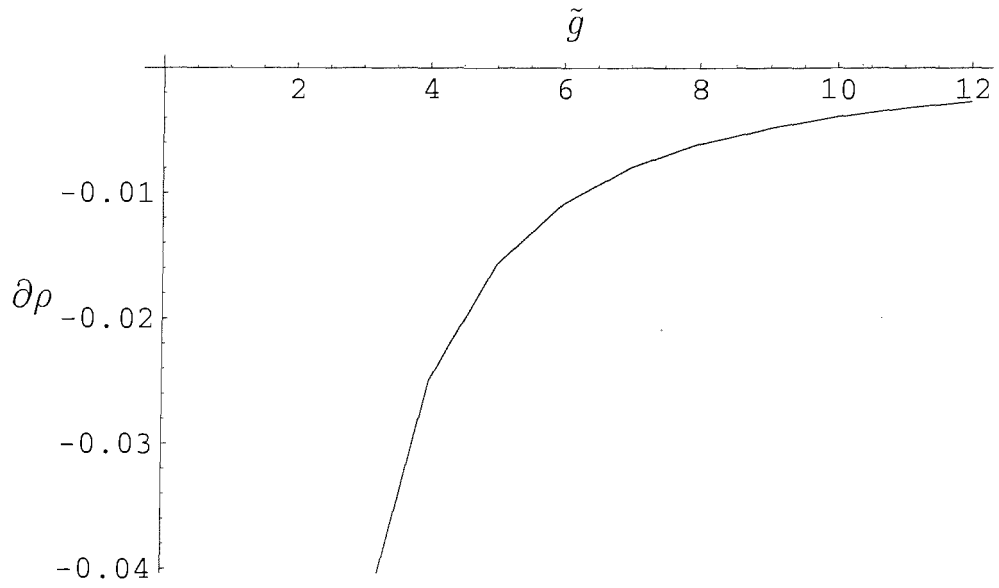

Figure 3.10: Plot of the coupling strength of the additional gauge groups ($\tilde{g}$), against the ρ parameter for a Deconstructed model with ten additional SU(2) gauge groups and one U(1) group

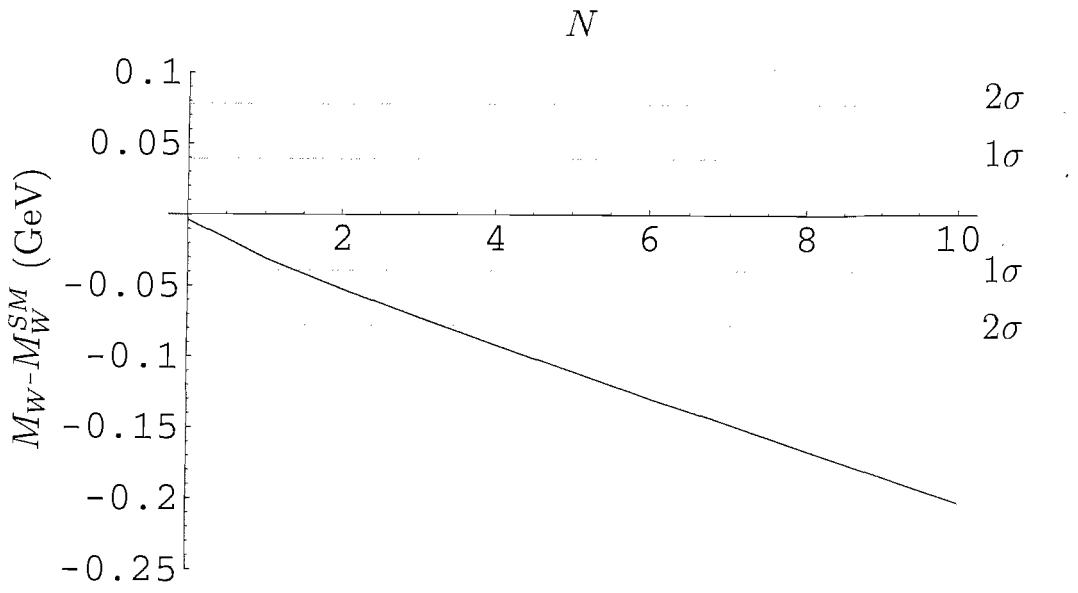

Figure 3.11: Plot of the number of additional gauge groups (N), against the W boson mass less its Standard Model value for a Deconstructed model with one additional SU(2) gauge group and one U(1) group, with additional coupling strengths $\tilde{g} = 4\pi$

3.7 Deconstructed Models with Variable Numbers of Gauge Groups.

Having found that the W mass is inconsistent with experimental bounds for an N=10 model, we consider varying the number of additional gauge groups to see if this offers any improvement.

We plot in Figure 3.11 the W mass against number of additional gauge groups N. We do this for $\tilde{g} = 4\pi$, the naive maximum value for a theory to be perturbative. This is an upper bound on perturbative correctness, it is of course far too high to be perturbative in any practical sense. This limiting case will be used simply to place an upper limit on what our best case scenario might be.

The plot shows that consistency with W mass bounds can be more easily met for

smaller numbers of additional gauge groups. This result confirms what intuition would suggest, that the closer we go towards the Standard Model case of no additional gauge groups the more consistent we become with experiment. The Standard Model is in fact represented on this plot at N=0, with the standard model mass as would be, of course, required.

Clearly it is worth exploring Deconstructed models with fewer gauge groups.

3.8 Deconstructed Models with Varying Additional Couplings' $\tilde{g}$ Continued for Smaller Moose Chains

3.8.1 N=1

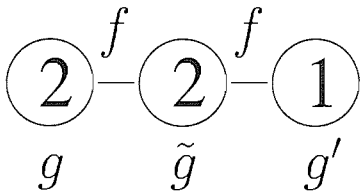

Based on the indications of section 3.7 we explore the moose model with the minimum additional gauge groups N=1, in order to understand how the experimental consistency for the W mass improves. As can be seen in Figures 3.12-3.15 the W mass remains within experimental bounds up to 3σ for additional coupling strengths as small as 6. A coupling strength of 6 is perturbative, although the size of the perturbations would be prohibitively high. However, for the purposes of pursuing an existence proof it is informative simply to have results that are perturbative in principle.

Here we have a model that is technically perturbative, is consistent with the experimental bounds on the W mass and has one additional W' boson as light as 1.5 TeV. This W' boson is comfortably both above the limit on searches for massive bosons of around 5-7 TeV [37] and clearly within the range of the LHC to detect. As such we

have a model, that at tree level, presents new physics visible at future experiments and consistent with current experimental bounds.

Unfortunately, although this model offers valid new physics, it only increases the Higgs mass up to a maximum of 1.4 TeV. Consequently it falls short of our goal of an existence proof of a model without a Higgs visible at the LHC. Without a heavier Higgs these models offer little of phenomenological use to justify their added complexity.

Nonetheless, these N=1 moose diagram models have demonstrated that the indication of section 3.7, that smaller moose diagrams can make the W mass more consistent with experiment. It is therefore worth exploring slightly larger moose diagram models to see if a compromise can be found between experimental consistency and a heavy Higgs.

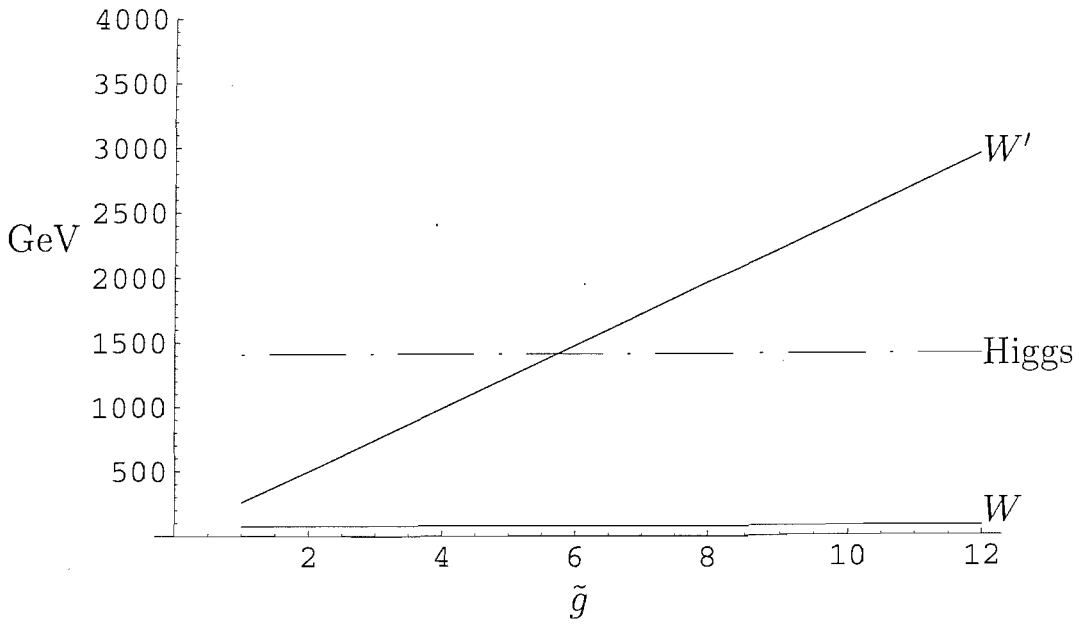

Figure 3.12: Plot of the coupling strength of the additional gauge group ($\tilde{g}$), against W' boson masses and Higgs mass for a Deconstructed model with one additional SU(2) gauge group and one U(1) group

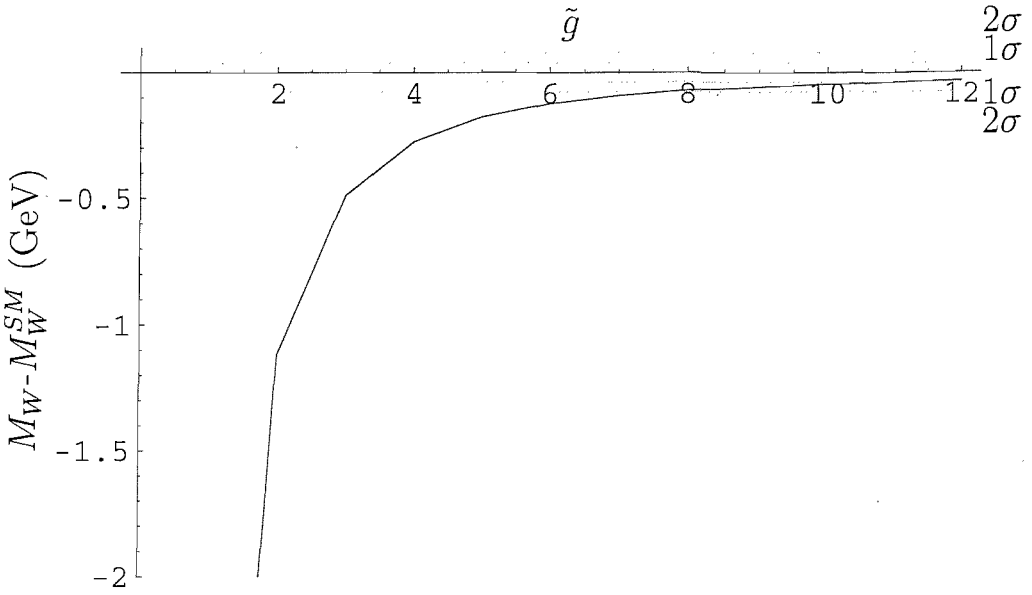

Figure 3.13: Plot of the coupling strength of the additional gauge group ($\tilde{g}$), against the W boson mass less its Standard Model value for a Deconstructed model with one additional SU(2) gauge group and one U(1) group

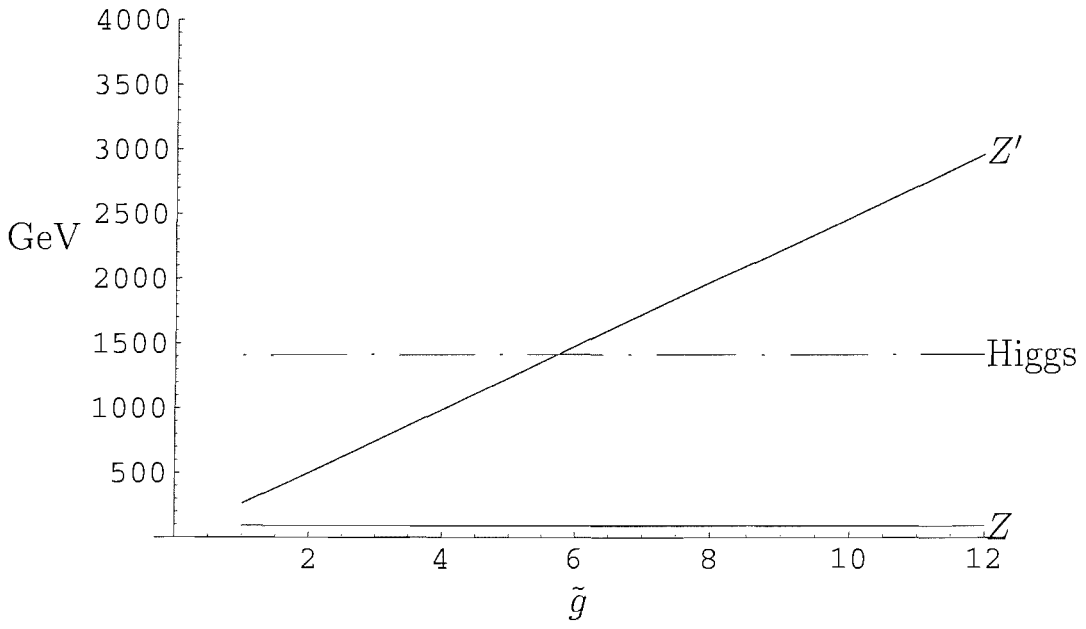

Figure 3.14: Plot of the coupling strength of the additional gauge group ($\tilde{g}$), against Z' boson masses and Higgs mass for a Deconstructed model with one additional SU(2) gauge group and one U(1) group

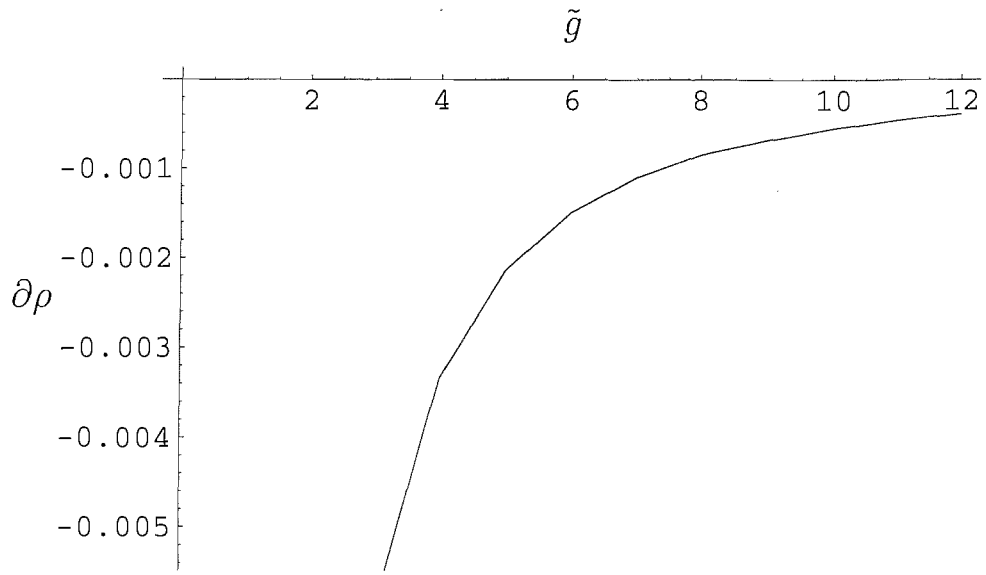

Figure 3.15: Plot of the coupling strength of the additional gauge group ($\tilde{g}$), against the ρ parameter for a Deconstructed model with one additional SU(2) gauge group and one U(1) group

3.8.2 N=3

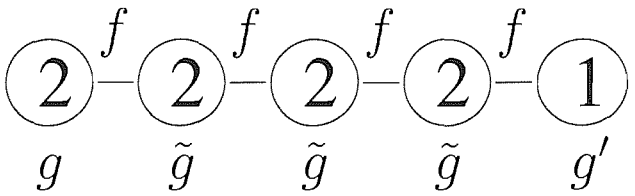

Having found regions of consistency with the experimental bounds on the W mass for an N=1 moose model, we now look to increase the number of additional gauge groups. We find the best balance at N=3.

As can be seen in Figures 3.16-3.19 the W mass is within the experimental bounds below the strict cut-off for perturbativity. For additional coupling strengths $\tilde{g}$ of about 10 the W' boson mass is marginally lower than the Higgs mass, while the W mass remains correct to within 3σ accuracy. The Higgs mass itself is slightly above 2 TeV and as such is at the limits of what might be seen at the LHC.

This N=3 model represents a very borderline example of a model which is experi-

mentally consistent at tree level. But also, describes potentially 'Higgsless' phenomenology at energies accessible by the LHC, with the very marginal possibility of a signature W' boson being observed. The above N=3 moose diagram model could be said to fulfil the objective of an existence proof of a verifiably Deconstructed model without a Higgs at the LHC.

However, this existence proof has numerous caveats and achieves its goals in only the most borderline sense. It represents evidence of the potential of such Deconstructed models to provide interesting phenomenology at LHC energy scales. We feel this is a step forward, although the borderline perturbativity renders the model merely an indicator and not a truly computable alternative to a Standard Model Higgs scenario.

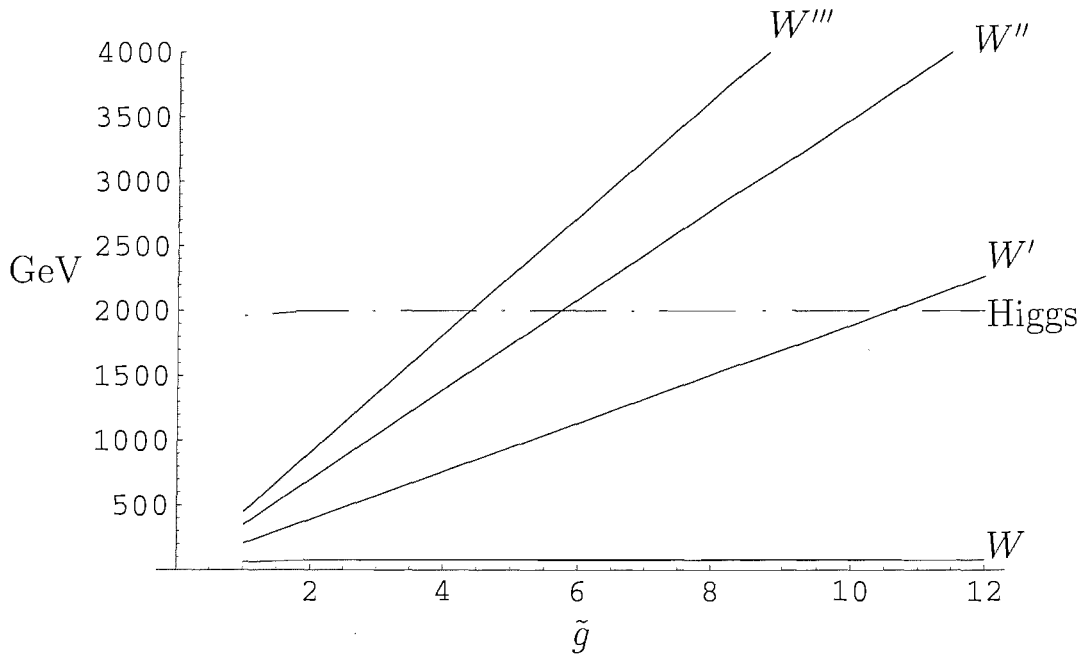

Figure 3.16: Plot of the coupling strength of the additional gauge groups ($\tilde{g}$), against W' boson masses and Higgs mass for a Deconstructed model with three additional SU(2) gauge groups and one U(1) group

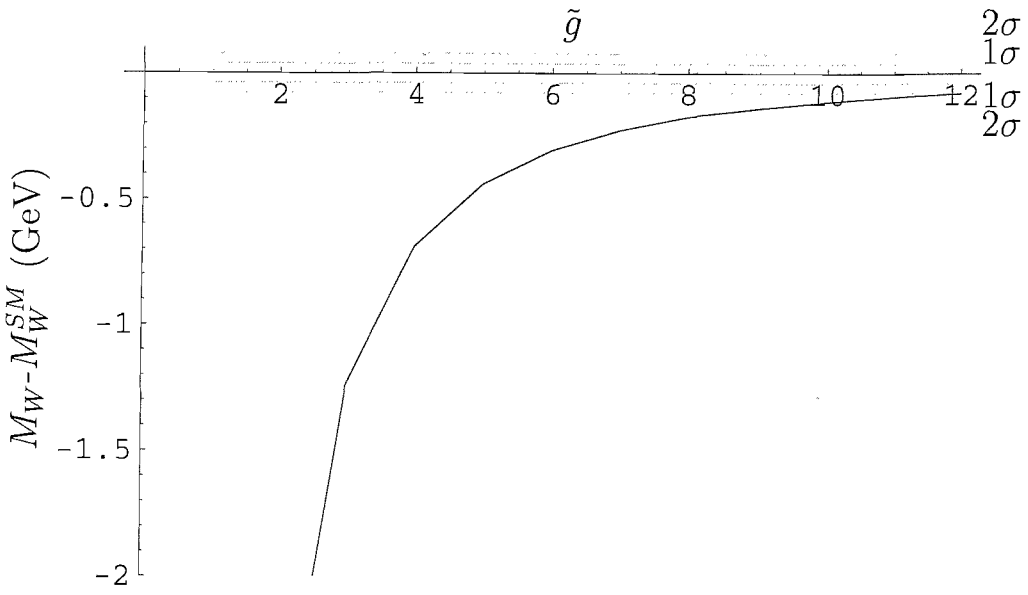

Figure 3.17: Plot of the coupling strength of the additional gauge groups ($\tilde{g}$), against the W boson mass less its Standard Model value for a Deconstructed model with three additional SU(2) gauge groups and one U(1) group

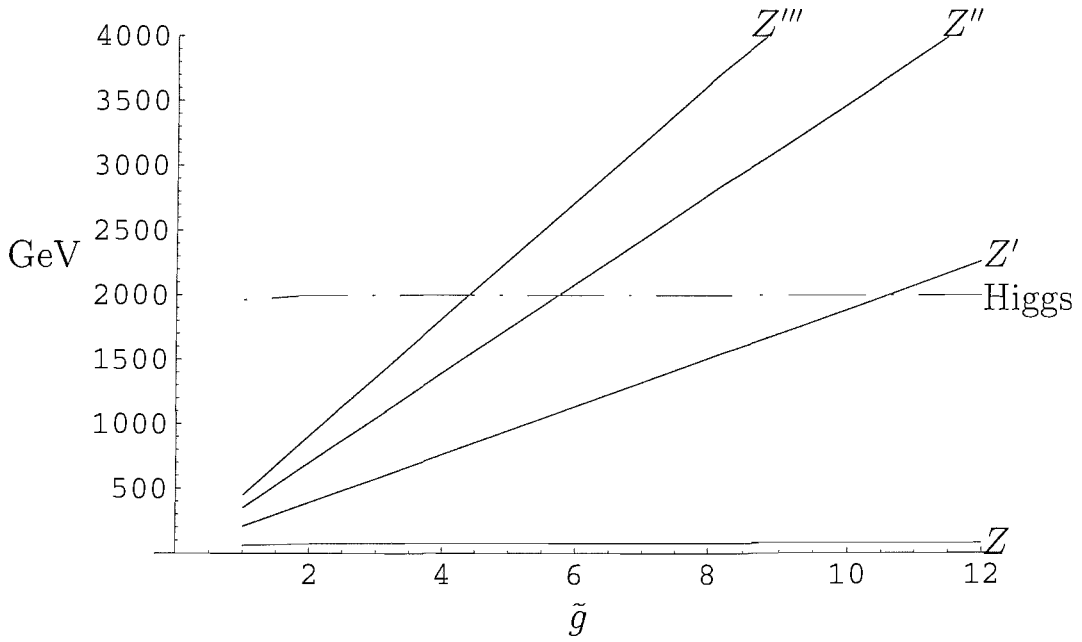

Figure 3.18: Plot of the coupling strength of the additional gauge groups ($\tilde{g}$), against Z' boson masses and Higgs mass for a Deconstructed model with three additional SU(2) gauge groups and one U(1) group

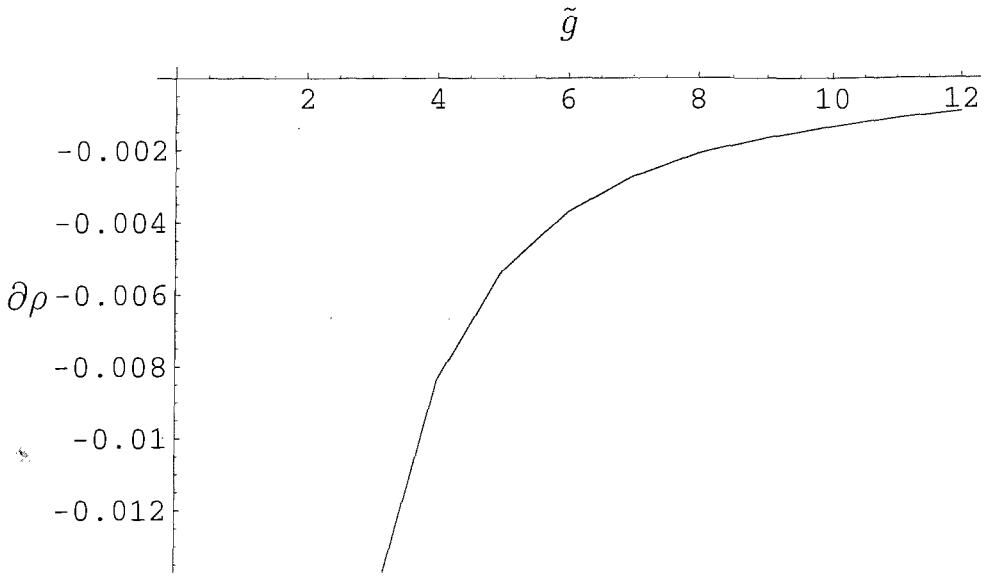

Figure 3.19: Plot of the coupling strength of the additional gauge groups ($\tilde{g}$), against the ρ parameter for a Deconstructed model with three additional SU(2) gauge groups and one U(1) group

3.9 Deconstructed Models with One Variable Higgs Vev.

3.9.1 N=10

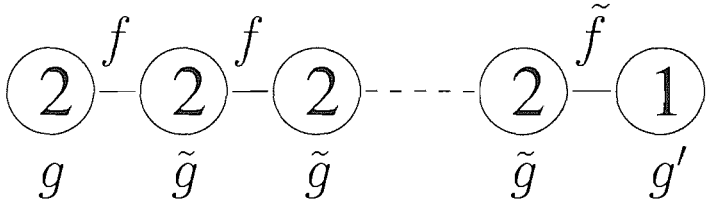

On the basis of the promising results of subsection 3.8.2, we continue to explore the phenomenology achievable by varying further parameters. The last major unexplored set of parameters for these models first introduced by Schmidt et al [24], are the Higgs vevs. We would be interested to see if the variation of these Higgs vevs can be used to strengthen the results of subsection 3.8.2, and whether they might make it possible to revive large N moose models without losing experimental consistency with the W mass bounds.

Following the pattern of the previous sections we first calculate an N=10 moose

model. We set the coupling strength of the additional gauge bosons $\tilde{g}$ to 4π in order to explore the best case scenario at the strict bound of perturbativity. Having found in section 3.4 that the variation of Higgs vevs, other than the Higgs vev between the first SU(2) and the U(1) group, provided little improvement to justify the increased complexity, we explore only variation of that end Higgs vev.

We plot in Figures 3.20-3.23 the effect of decreasing the value of the last Higgs vev relative to the remaining Higgs vevs (which are all equal). Specifically we plot f divided by $\tilde{f}$ against the masses of the W boson, W' bosons and the Higgs. For this choice of axes the effect of varying the Higgs vev becomes more pronounced as we look from left to right along the plot. It expands the region on the graph in which the additional gauge bosons decouple from physics at the observed scale and the Standard Model is replicated. That is a particularly interesting region so its increased visibility is beneficial.

It can be seen for these models that the Higgs mass reduces toward its standard model limit (accounting for the fact that we are working with the maximal possible Standard Model Higgs mass of 1 TeV) on the right of the graph as the last Higgs vev becomes small. The W' bosons increase quickly in mass as this happens and the W mass approaches its Standard Model value. (These two properties are more obvious at Higgs vev ratios larger than the $f/\tilde{f} = 5$, that the plot extends to). As should be expected the results do match those of the Standard Model in this limit.

The presence of a Standard Model limit in these variable Higgs vev models both provides a check on the correctness of our calculation and guarantees a region of parameter space consistent with experiment. We would like to see the matching of the W mass to experimental constraints maintained as far as possible away from the Standard Model limit. If this matching holds while the Higgs mass is increased by the strength-

ened effect of the additional gauge groups we should see an improvement on previous phenomenology.

Unfortunately, as can be seen, the Higgs mass reduces a little sharply as we alter the last Higgs vev. The corresponding W mass results do not begin to move towards their experimental bounds until after the Higgs mass has fallen most of the way toward its Standard Model value. This is perhaps not unexpected as the (lightest) Higgs mass will inevitably be linked strongly to the strength of the lightest Higgs vev. An effect that appears to dominate over the link between Higgs vev and W mass consistency.

Nonetheless, for the sake of completeness having developed the formalism, we should check what effect varying the last Higgs vev has on these models with fewer extra gauge groups.

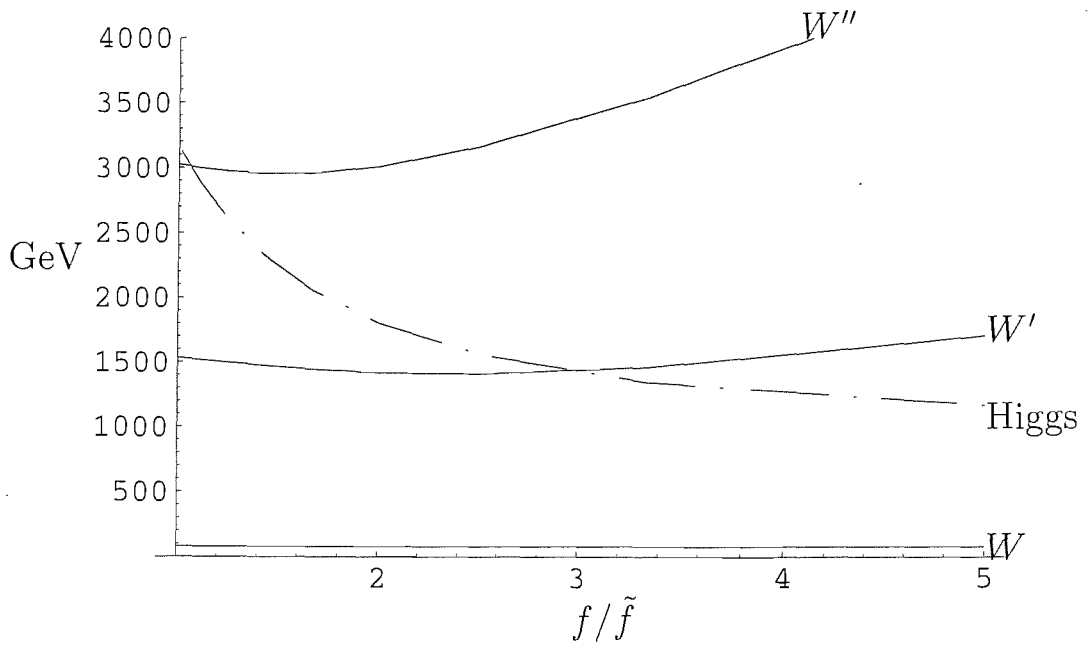

Figure 3.20: Plot of the ratio between the last Higgs vev and its counterparts, against the W' boson masses and Higgs mass for a Deconstructed model with ten additional SU(2) gauge groups and one U(1) group, with additional coupling strengths $\tilde{g} = 4\pi$

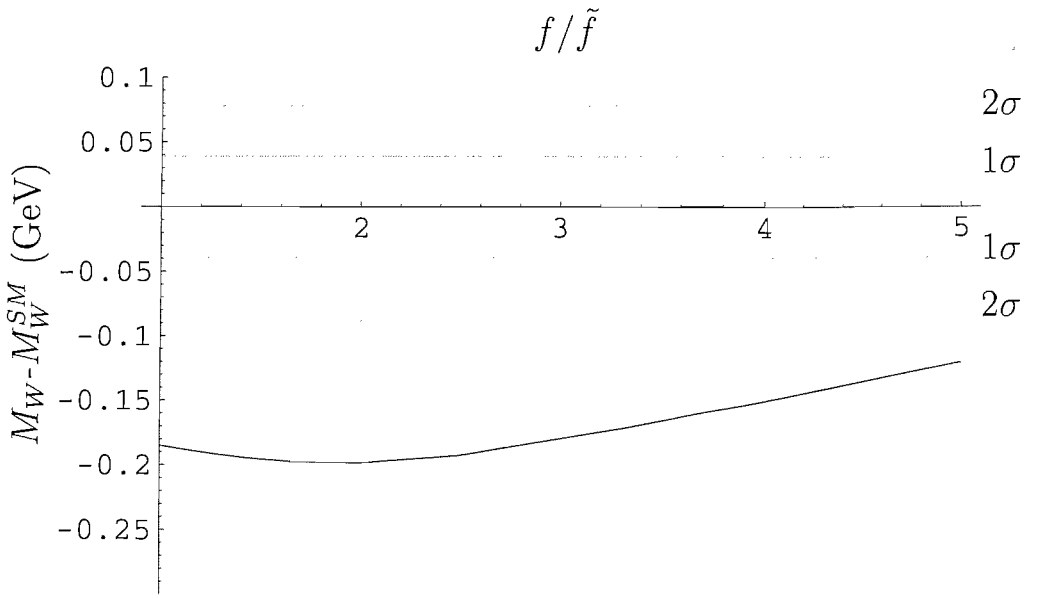

Figure 3.21: Plot of the ratio between the last Higgs vev and its counterparts, against the W boson mass less its Standard Model value for a Deconstructed model with ten additional SU(2) gauge groups and one U(1) group, with additional coupling strengths $\tilde{g} = 4\pi$

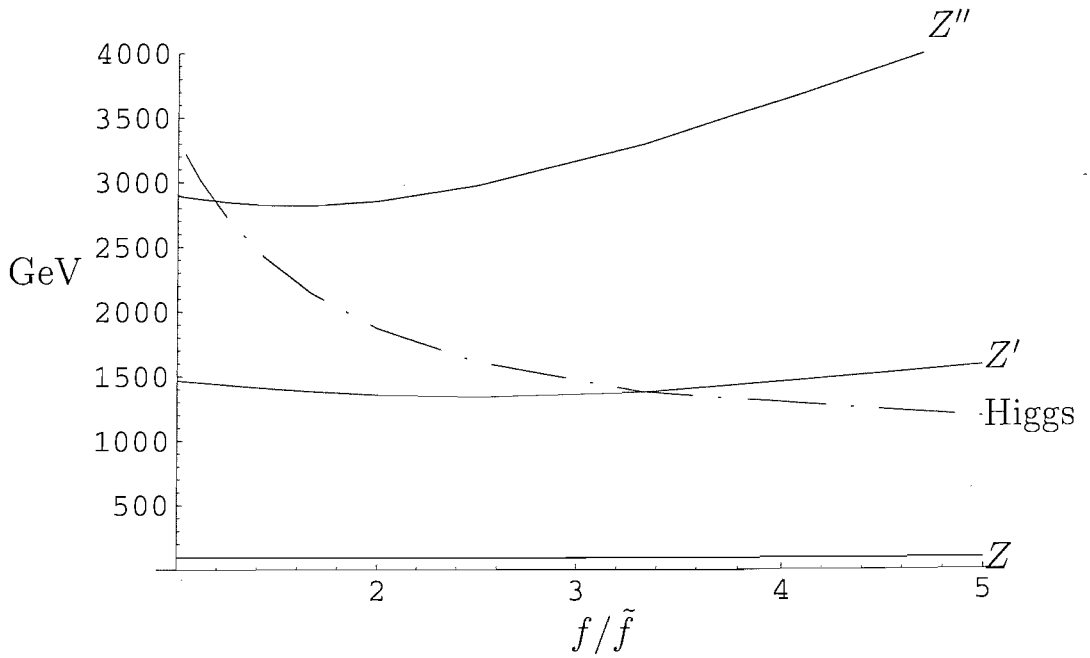

Figure 3.22: Plot of the ratio between the last Higgs vev and its counterparts, against the Z' boson masses and Higgs mass for a Deconstructed model with ten additional SU(2) gauge groups and one U(1) group, with additional coupling strengths $\tilde{g} = 4\pi$

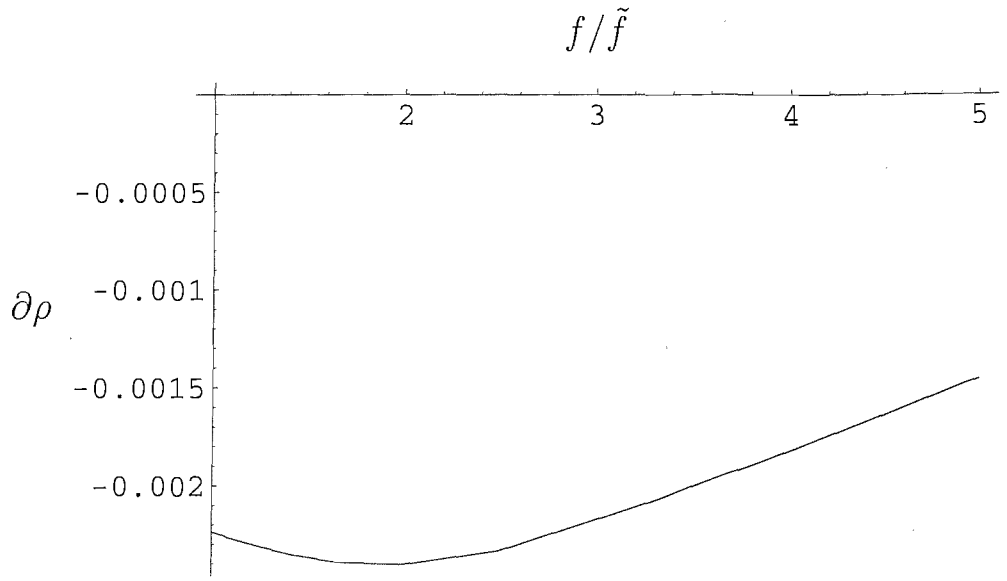

Figure 3.23: Plot of the ratio between the last Higgs vev and its counterparts, against the ρ parameter for a Deconstructed model with ten additional SU(2) gauge groups and one U(1) group, with additional coupling strengths $\tilde{g} = 4\pi$

3.9.2 N=1

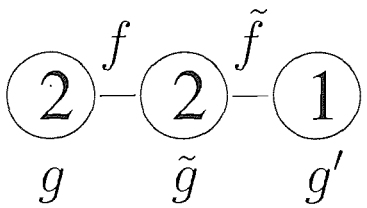

After the disappointing results found in subsection 3.9.1 we press on to see if better phenomenology can be found with minimal additional gauge groups. We start with the smallest moose diagram model of our kind N=1. Again following the pattern of previous sections.

It is more obvious on these plots, Figures 3.24-3.27, that the Standard Model is reproduced as we move further to the right on the graph. The W mass bounds are met easily throughout the range of Higgs vev values. We of course expect this, as the W mass bounds were easily met for N=1 models with strong additional couplings $\tilde{g}$ and we are working at $\tilde{g} = 4\pi$. The reduction of Higgs vev moves us towards a Standard

Model limit, which can only improve the consistency on experimental bounds.

Varying the Higgs vevs for an N=1 model at strong coupling is perhaps a little uninteresting as it serves primarily to improve consistency with experimental constraints that are already easily met.

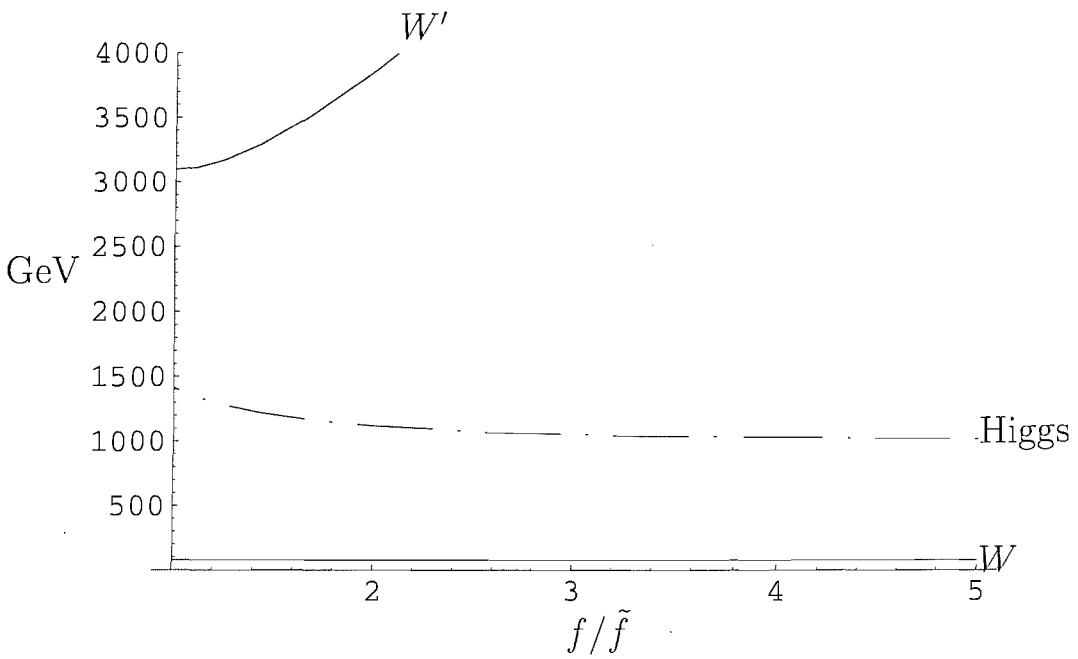

Figure 3.24: Plot of the ratio between the last Higgs vev and its counterparts, against the W' boson masses and Higgs mass for a Deconstructed model with one additional SU(2) gauge groups and one U(1) group, with additional coupling strengths $\tilde{g} = 4\pi$

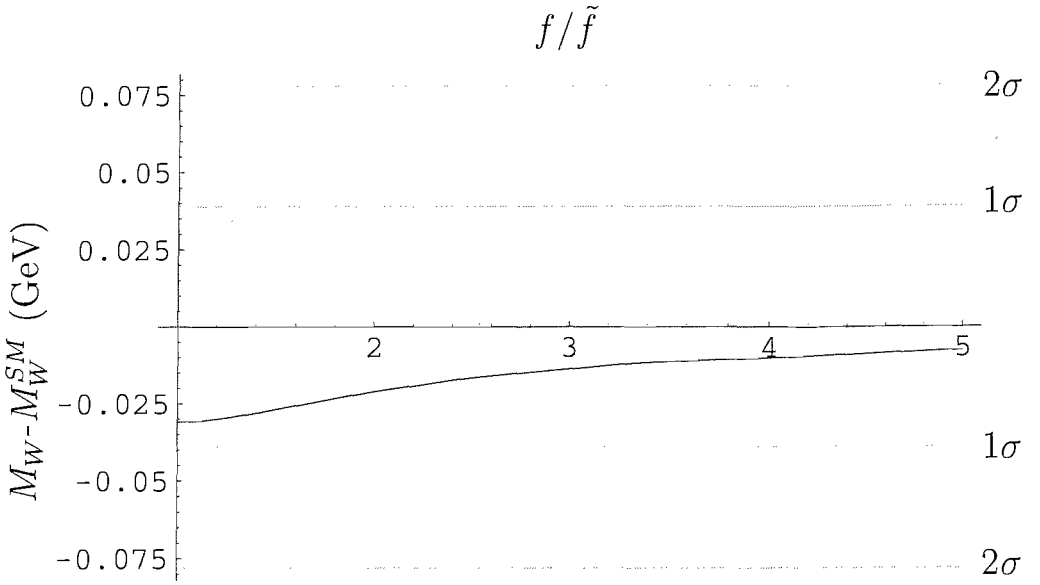

Figure 3.25: Plot of the ratio between the last Higgs vev and its counterparts, against the W boson mass less its Standard Model value for a Deconstructed model with one additional SU(2) gauge groups and one U(1) group, with additional coupling strengths $\tilde{g} = 4\pi$

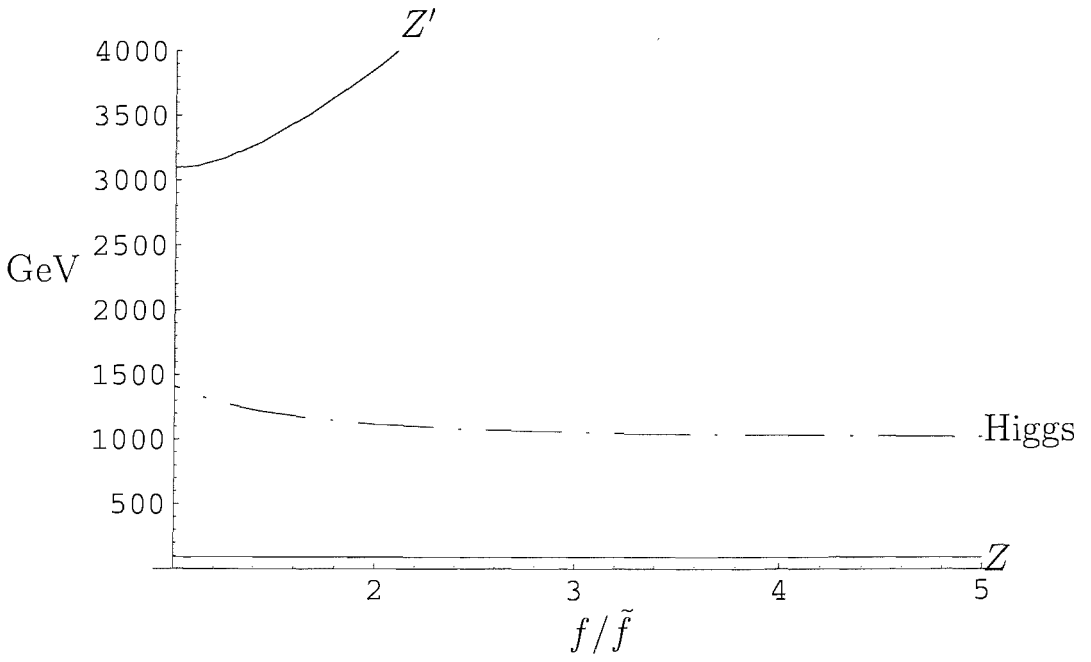

Figure 3.26: Plot of the ratio between the last Higgs vev and its counterparts, against the Z' boson masses and Higgs mass for a Deconstructed model with one additional SU(2) gauge groups and one U(1) group, with additional coupling strengths $\tilde{g} = 4\pi$

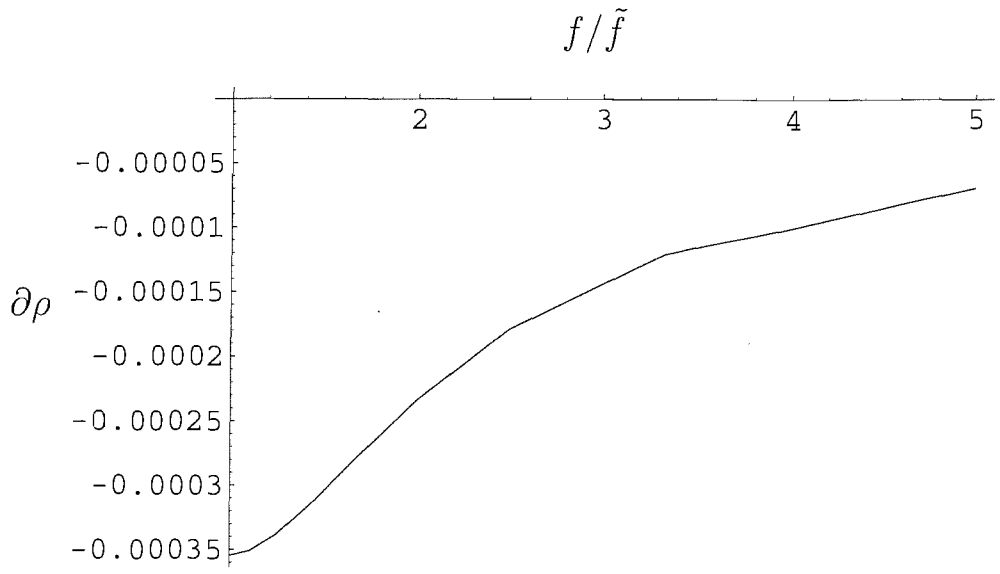

Figure 3.27: Plot of the ratio between the last Higgs vev and its counterparts, against the ρ parameter for a Deconstructed model with one additional SU(2) gauge groups and one U(1) group, with additional coupling strengths $\tilde{g} = 4\pi$

3.9.3 N=3

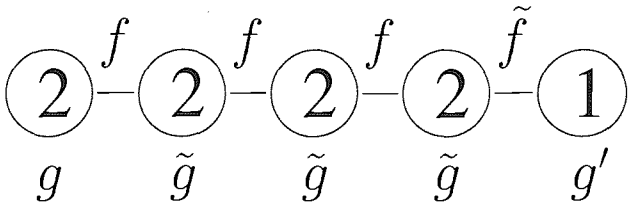

Given that N=3 provided the most interesting phenomenology so far, for variation of the additional coupling strengths in subsection 3.8.2, we will show the results, in Figures 3.28-3.31, for varying the last Higgs vev for that model at $\tilde{g} = 4\pi$.

While varying the Higgs vev does provide us with the power to increase the experimental consistency of our best model so far, we lose too much of the desirable heavy Higgs mass, for the trade off to be useful.

There are however, two ways in which the variation of the Higgs vev could expand our phenomenological options. First it allows us to improve the experimental consistency of larger moose diagram models. We saw this for N=10 in a limited sense, but as

N=3 meets the experimental bounds quite easily there is potential for exploring values of N between these two cases, as we shall in subsection 3.9.4. Secondly we can offset the improvements in experimental consistency from varying the vev against the loss of such consistency for weaker, more perturbative, coupling strengths.

It appears unlikely that we will improve upon the results in subsection 3.8.2 by varying the vevs, but we may well be able to expand the array of models and their parameters that can match experimental constraints.

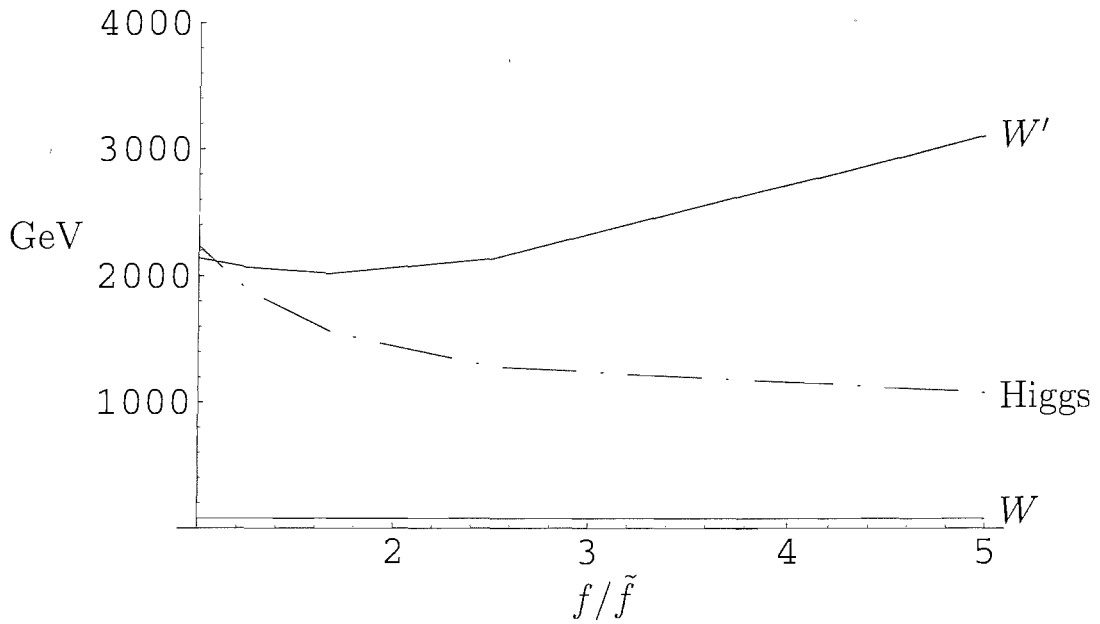

Figure 3.28: Plot of the ratio between the last Higgs vev and its counterparts, against the W' boson masses and Higgs mass for a Deconstructed model with three additional SU(2) gauge groups and one U(1) group, with additional coupling strengths $\tilde{g} = 4\pi$

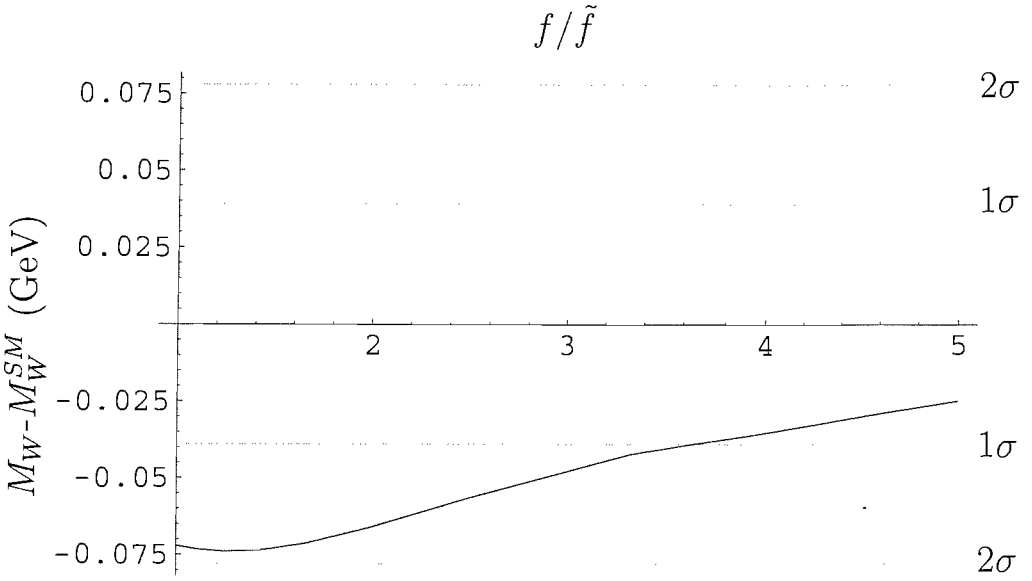

Figure 3.29: Plot of the ratio between the last Higgs vev and its counterparts, against the W boson mass less its Standard Model value for a Deconstructed model with three additional SU(2) gauge groups and one U(1) group, with additional coupling strengths $\tilde{g} = 4\pi$

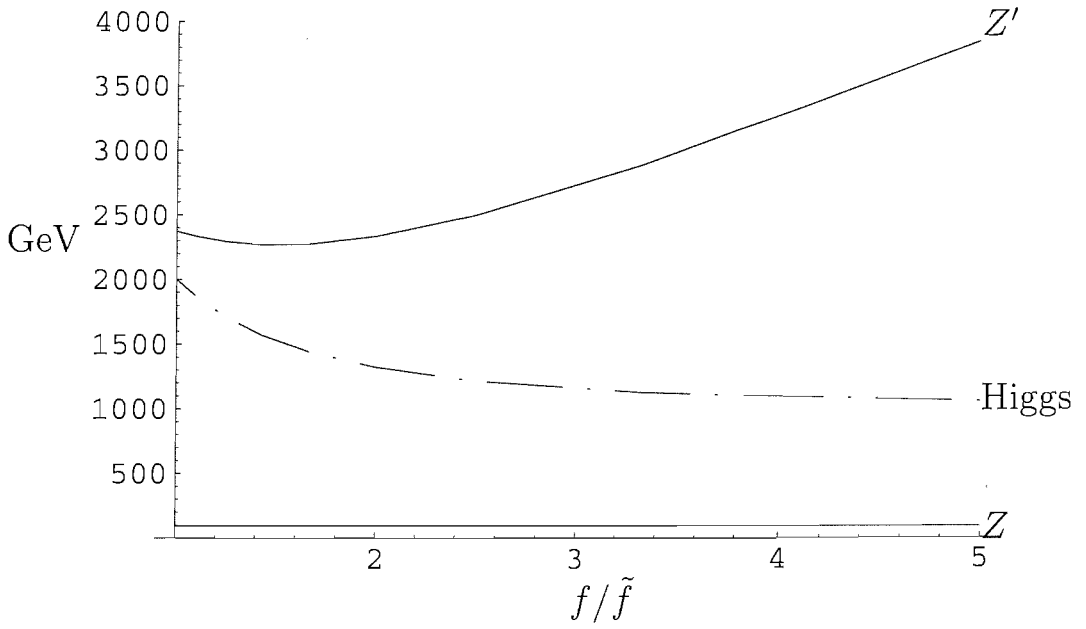

Figure 3.30: Plot of the ratio between the last Higgs vev and its counterparts, against the Z' boson masses and Higgs mass for a Deconstructed model with three additional SU(2) gauge groups and one U(1) group, with additional coupling strengths $\tilde{g} = 4\pi$

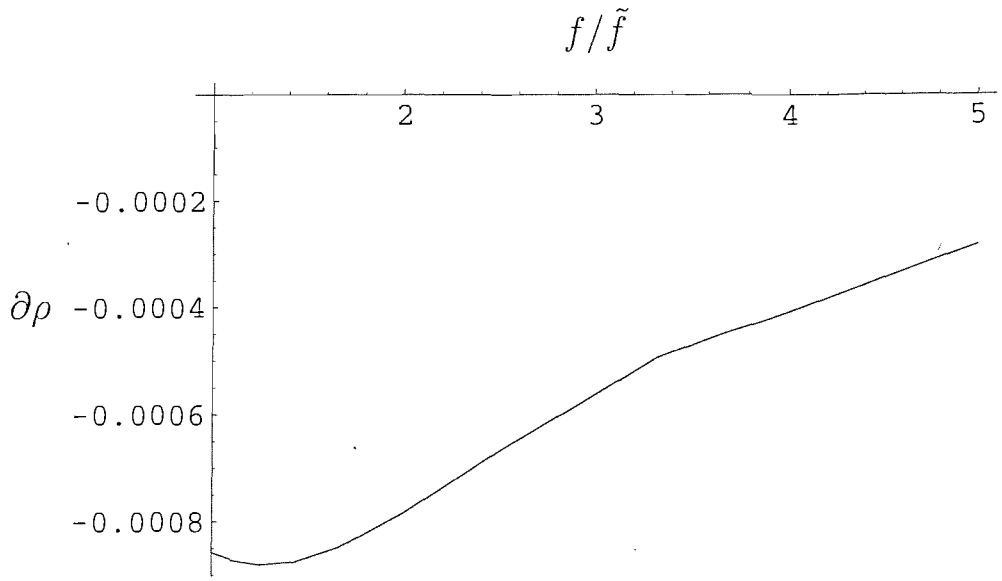

Figure 3.31: Plot of the ratio between the last Higgs vev and its counterparts, against the ρ parameter for a Deconstructed model with three additional SU(2) gauge groups and one U(1) group, with additional coupling strengths $\tilde{g} = 4\pi$

3.9.4 N=7

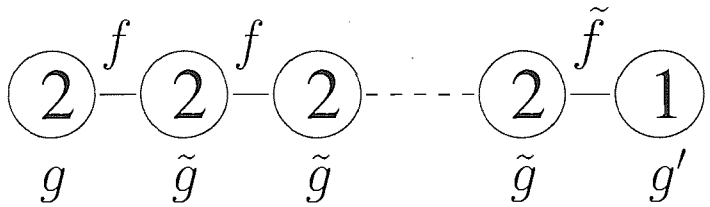

In Figures 3.32-3.35 we display the effects of varying the Higgs vev for a moose diagram with seven additional gauge groups at $\tilde{g} = 4\pi$. What we can observe is that there is a significant region of Higgs vev variation in which the experimental bounds on the W mass are met. While the phenomenology of this region is not of especially great interest, we have managed to get experimental consistency for a quite large moose diagram with a W' boson mass detectable at the LHC and a Higgs mass larger than that observable in the Standard Model (in the sense described on page).

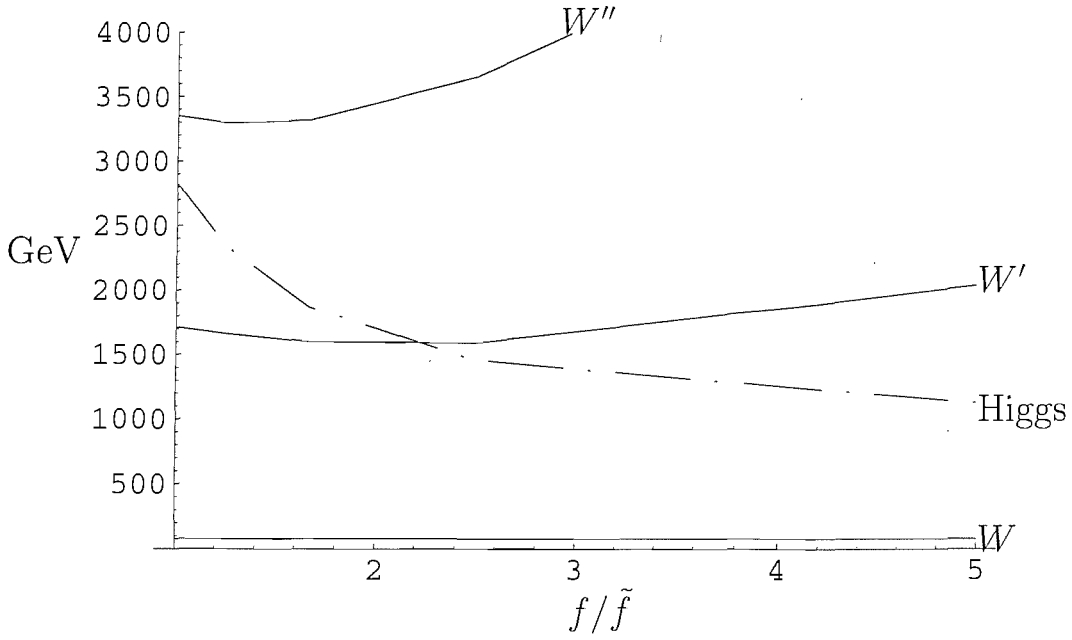

Figure 3.32: Plot of the ratio between the last Higgs vev and its counterparts, against the W' boson masses and Higgs mass for a Deconstructed model with seven additional SU(2) gauge groups and one U(1) group, with additional coupling strengths $\tilde{g} = 4\pi$

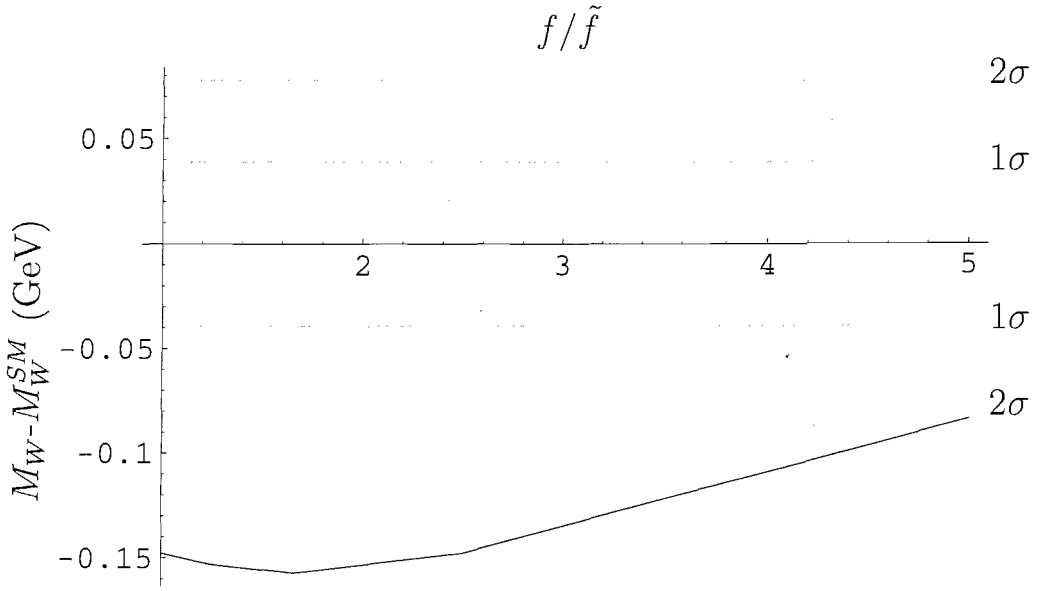

Figure 3.33: Plot of the ratio between the last Higgs vev and its counterparts, against the W boson mass less its Standard Model value for a Deconstructed model with seven additional SU(2) gauge groups and one U(1) group, with additional coupling strengths $\tilde{g} = 4\pi$

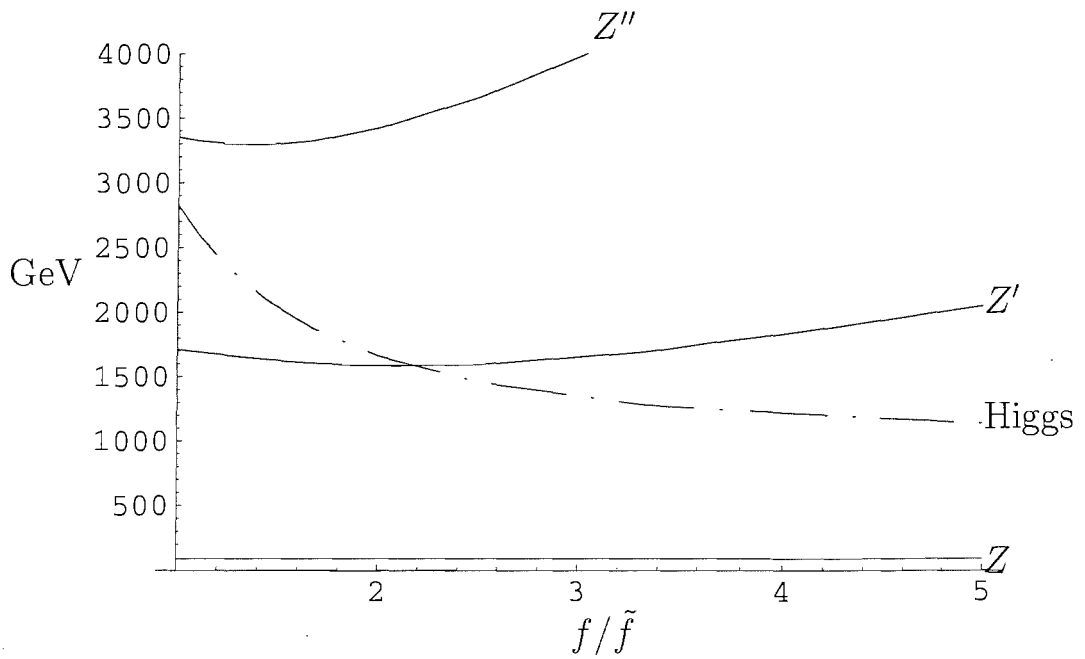

Figure 3.34: Plot of the ratio between the last Higgs vev and its counterparts, against the Z' boson masses and Higgs mass for a Deconstructed model with seven additional SU(2) gauge groups and one U(1) group, with additional coupling strengths $\tilde{g} = 4\pi$

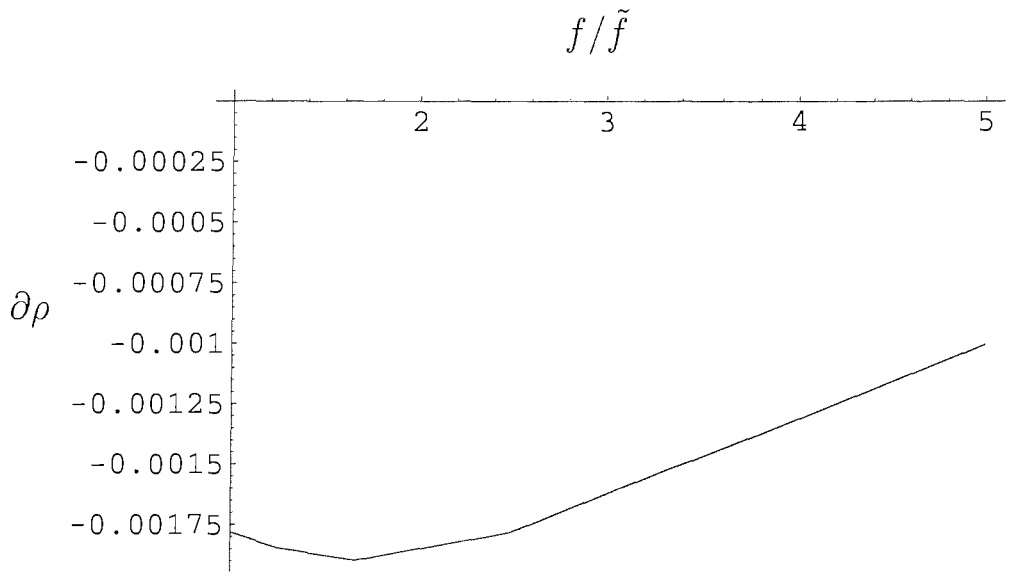

Figure 3.35: Plot of the ratio between the last Higgs vev and its counterparts, against the ρ parameter for a Deconstructed model with seven additional SU(2) gauge groups and one U(1) group, with additional coupling strengths $\tilde{g} = 4\pi$

3.9.5 N=3 - Weaker Couplings with Variable Higgs Vevs

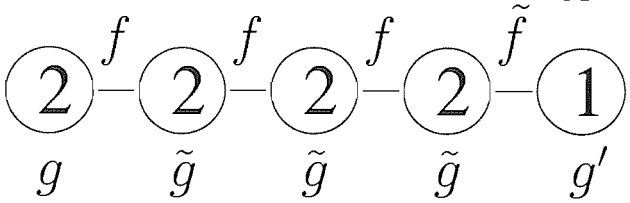

In the following plots, Figures 3.36-3.39, we attempt to use variation in the Higgs vev to find experimental consistency at tree level for more perturbative values of the additional couplings. We do this for an N=3 moose diagram model with additional couplings $\tilde{g}$ set to 6. Approximately half the perturbative limit of 4π, and as such, meaningfully perturbative. Sadly although this reduction in coupling strength does represent perturbativity in principle, it is not a strong enough improvement for the tree level results to be reliable or for the calculation to be accurate within a tractable number of loops. Nonetheless, it represents movement in the correct direction, and establishes such movement is possible.

The graphs show that the W mass experimental bounds can be met at more perturbative coupling strengths for a certain region of Higgs vev scale. They also display that at this scale the W' boson would be within the observable range at the LHC. Unfortunately no pleasing progress is made towards increasing the Higgs mass, which has been our primary goal. In effect we have created a Deconstructed Model at tree level here that is approaching experimental consistency, but for the anticipated effect of larger than desirable loop level corrections, and provides us with LHC phenomenology distinct from the Standard Model.

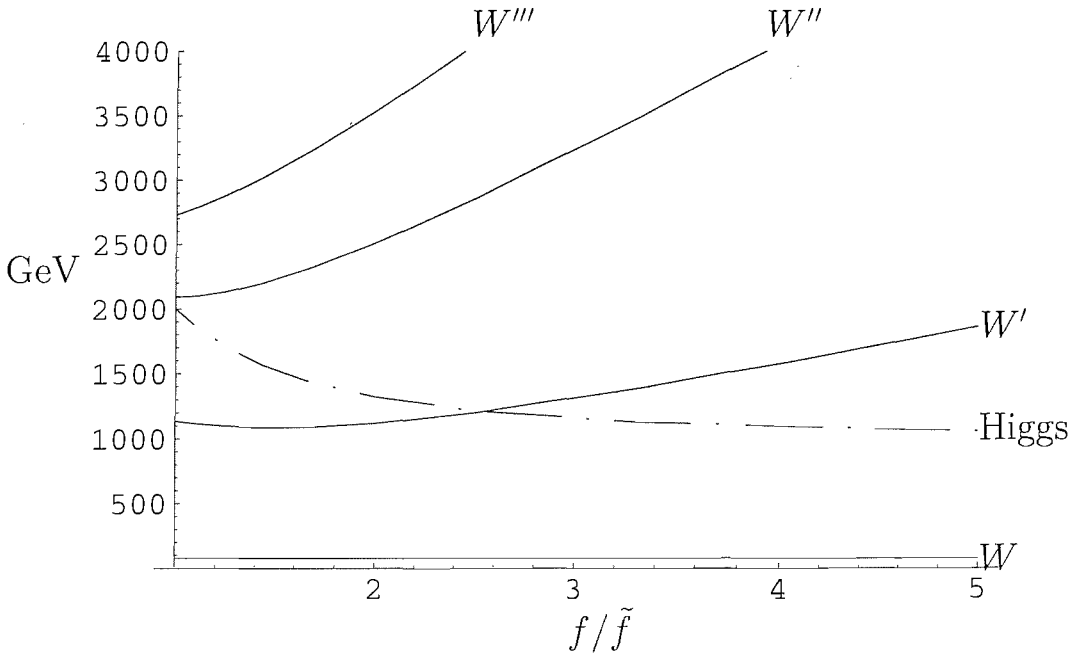

Figure 3.36: Plot of the ratio between the last Higgs vev and its counterparts, against the W' boson masses and Higgs mass for a Deconstructed model with three additional SU(2) gauge groups and one U(1) group, with additional coupling strengths $\tilde{g} = 6$

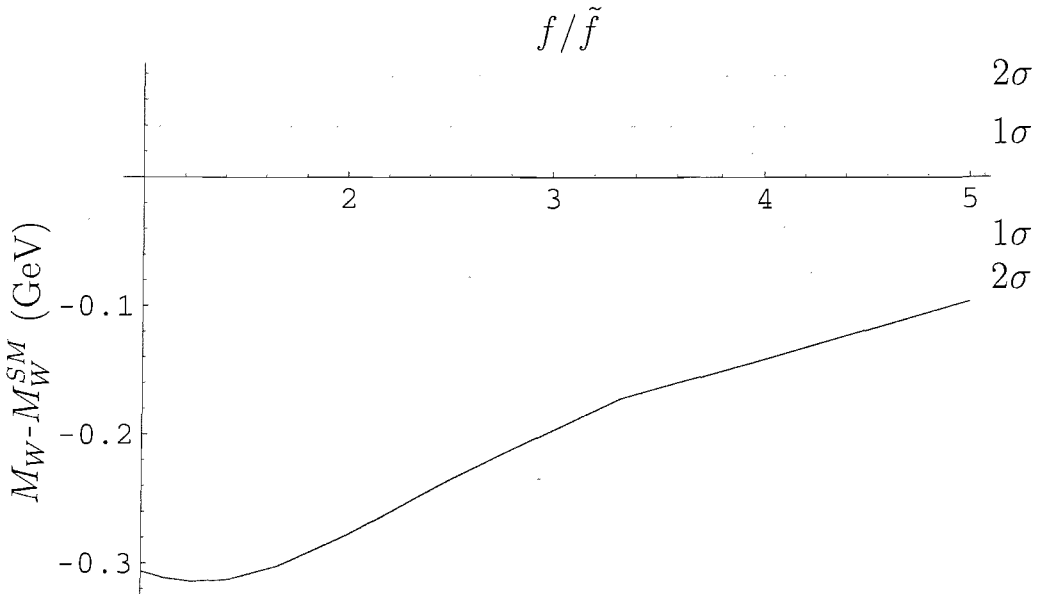

Figure 3.37: Plot of the ratio between the last Higgs vev and its counterparts, against the W boson mass less its Standard Model value for a Deconstructed model with three additional SU(2) gauge groups and one U(1) group, with additional coupling strengths $\tilde{g} = 6$

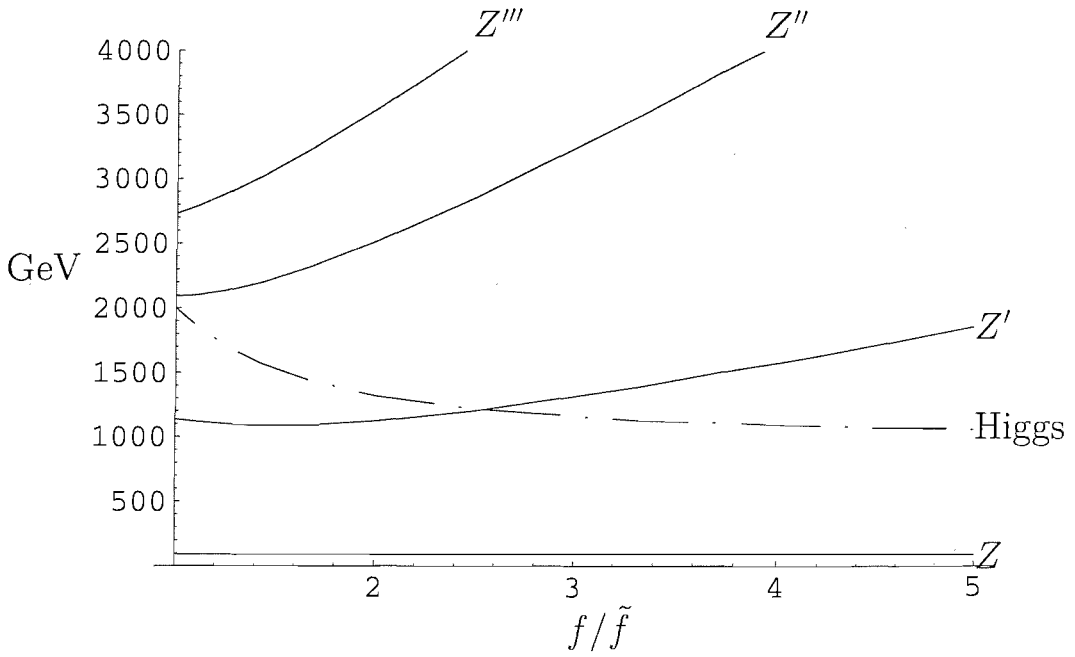

Figure 3.38: Plot of the ratio between the last Higgs vev and its counterparts, against the Z' boson masses and Higgs mass for a Deconstructed model with three additional SU(2) gauge groups and one U(1) group, with additional coupling strengths $\tilde{g} = 6$

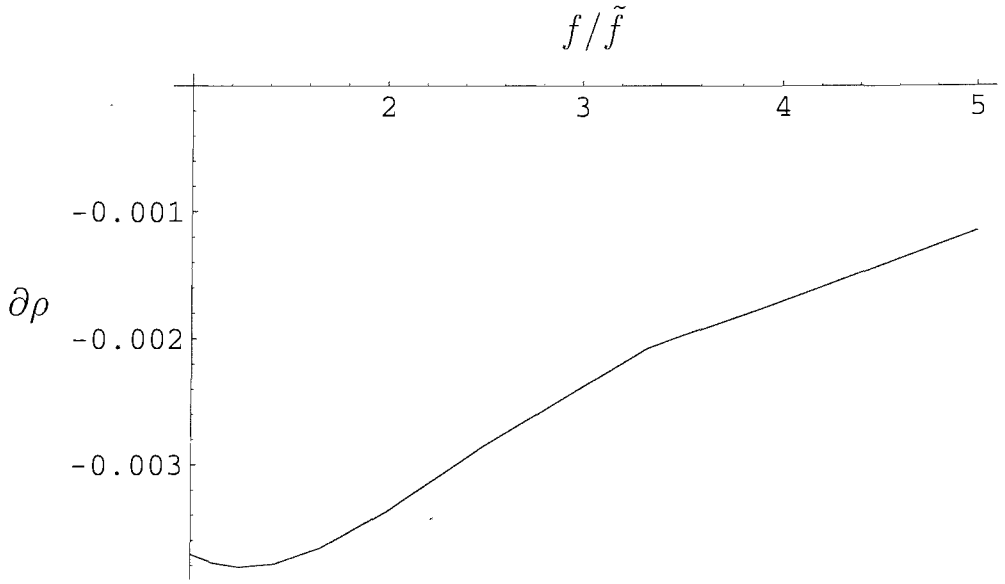

Figure 3.39: Plot of the ratio between the last Higgs vev and its counterparts, against the ρ parameter for a Deconstructed model with three additional SU(2) gauge groups and one U(1) group, with additional coupling strengths $\tilde{g} = 6$

3.10 Conclusions from the Phenomenological Exploration of Tree Level Numerical Analysis in Deconstructed Models

In conclusion to our numerical analysis of tree level Deconstructed moose models we have achieved three areas of promising results.

Firstly an array of models was explored that present diversely new phenomenology from the, as yet unobserved, Standard Model Higgs predictions. While the most interesting results belonged to models that failed to meet current experimental constraint, and as such must be discounted, they did provide precisely the phenomenology we sought to find. On the basis of this analysis we have established that a range of Deconstructed models do indeed predict Higgsless phenomenology and an abundance of new gauge bosons at energies the LHC can probe. Regrettably the most vivid examples of these models fail to accurately conform to the precise experimental constraint set by experiments such as LEP2.

Secondly, we successfully developed a model, consistent with current experimental constraint, which did achieved our goal of an existence proof for a tree level model without a Higgs boson at the LHC with the possibility of the observation of a signature W' boson. The N=3 Deconstructed moose model displayed in subsections 3.8.2 and 3.9.3 met the objective of this existence proof only narrowly and, given that it met experimental constraint only in the strong coupling limit, this result is only naively perturbative and would most likely break down at the loop level.

Finally the model presented in subsection 3.9.5 came close to providing perturbative results for an experimentally consistent model with observably distinct phenomenology from that of the Standard Model. Sadly the presence of a relatively light Higgs meant

that this model fails to meet the stated goal of an effectively Higgsless model at LHC energy scales. Nonetheless, scientific preferences aside, it does represent experimentally valid unitarity corrected new physics which could be both verified or disproved at experiments in the near future. We believe the results of our tree level numerical analysis from a raft of Deconstructed models, presented in this chapter, appreciably better informs consideration of the merits of using Deconstruction to predict fresh LHC-level phenomenology. Our results might well have ruled out attempting Higgsless phenomenology using standard Deconstructed models. They might equally have established that such models easily achieve new Higgsless predictions at LHC energies. Instead we have found data that suggests that it is challenging, but perhaps possible, to develop models that use Deconstruction to present experimentally valid Higgsless predictions at high energy. Certainly we have verified that new physics can be predicted by these theories without violating existing experimental constraint.

Chapter 4

Calculating Electroweak Oblique Corrections in the Standard Model at the One Loop Level

4.1 Loop Level Calculations and the Oblique Electroweak Parameters.

Throughout Chapter 3 we worked exclusively at the tree level in Deconstructed models looking for interesting phenomenology. Having found useful results at the tree level, it becomes important to find out if these models remain consistent with data at the loop level.

As far as we are aware, at time of performing these computations no loop level calculations had been performed for Deconstructed models. Whilst writing up ref [72] was released - we have explicitly checked our results against those as we will explain. We here set about performing a one loop calculation to test models of the form used

in Chapter 3, and perhaps to gain insight into the validity of Deconstructed models in general beyond tree level.

Most of the experimental bounds on beyond the Standard Model physics were established at LEP [62, 63], an electron positron collider, and other similar experiments. We will be interested in corrections to the self-energies of gauge bosons formed through electron positron annihilation as shown in Figure 4.2. These corrections to the standard model gauge boson propagators are called "oblique corrections". There are also possible non-oblique corrections, for example due to the exchange of a new particle between the external fermion lines. Higgs physics of this sort is suppressed because the electron's Yukawa coupling is so small. We will neglect these interactions from the extra gauge bosons in Deconstructed models because we work close to the decoupling limit where the Standard Model fermion interactions return to those of the Standard Model.

In order to establish whether the loop level corrections of our model are large, and whether they are non-perturbative, we adopt a parametrization introduced by Peskin and Takeuchi [60, 61]. The introduced parameters known as the Electroweak Oblique Corrections and denoted S, T and U are used in order to check experimental consistency of Beyond the Standard Model theories. They are defined as

$$\alpha S = 4e^2 \left(\Pi'_{33}(M_Z^2) - \Pi'_{3Q}(0)\right) \tag{4.1}$$

$$\alpha T = \frac{e^2}{s^2 c^2 M_Z^2} \left(\Pi_{11}(0) - \Pi_{33}(0)\right) \tag{4.2}$$

$$\alpha U = 4e^2 \left(\Pi'_{11}(0) - \Pi'_{33}(0)\right) \tag{4.3}$$

where e is the electron charge, s and c are shorthand for $\sin\theta_W$ and $\cos\theta_W$ and the Π are the coefficient of the $g_{\mu\nu}$ piece of the gauge boson self energies. A prime denotes differentiation with respect to the external momentum squared flowing through the diagram.

The majority of experimentally measured parameters, such as the W mass and the ρ-parameter, can be re-expressed as function of the Electroweak Oblique Parameters S, T and U. A table of relations of this kind can be found in Appendix B of the paper by Peskin and Takeuchi [61]. From these inter-relations experimental bounds on S, T and U have been established and can be found in the Particle Data Book [37]. We display the current experimental bounds in Figure 4.1

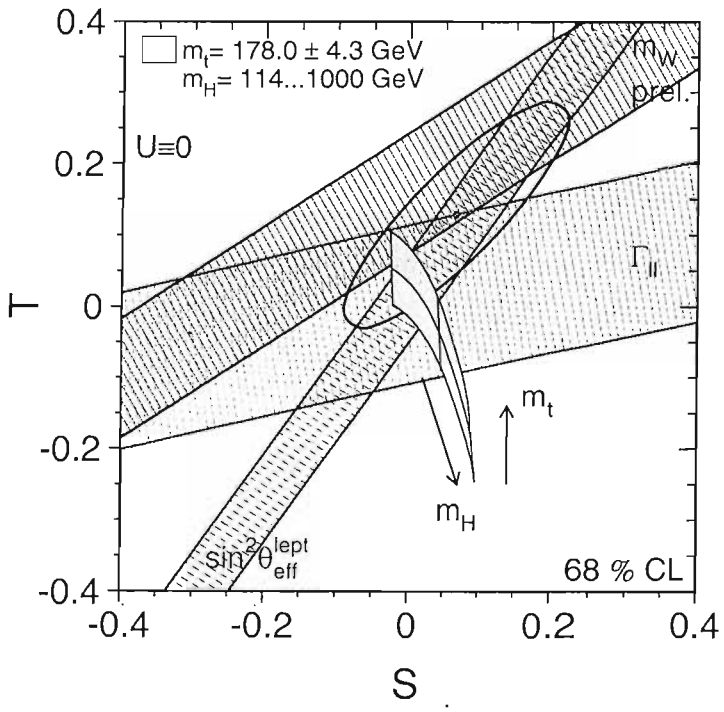

Figure 4.1: Latest electroweak precision measurements taken from [73]. The ellipse is drawn for the reference values: $\delta\alpha^{(5)}_{had}(M_Z^2) = 0.02758$, $\alpha_s(M_Z^2) = 0.118$, $M_Z = 91.1875$ GeV, $m_t = 175$ GeV and $m_h = 150$ GeV and U=0 (see [73] for more details).

In the remainder of this thesis we make use of the experimental bounds set by the Particle Data Book to confirm whether our models are valid at the one loop level. Consequently we concern ourselves only with evaluating at one loop, the S, T and U parameters.

For models of the form introduced in Chapter 3, where the fermions couple only to the end two gauge groups, there is a Custodial Symmetry [24] which fixes the T and U parameters to be zero. As such it is only necessary to calculate the S parameter.

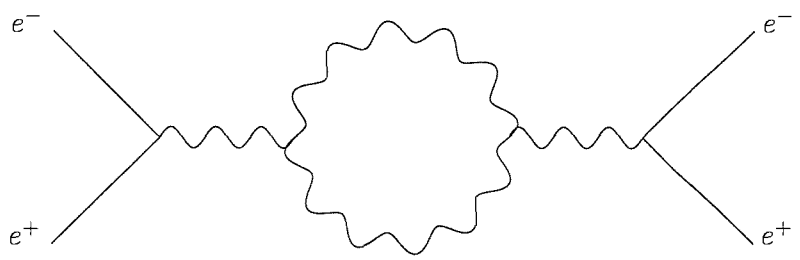

Figure 4.2: A generic diagram for gauge boson production by electron-positron annihilation.

4.2 The Oblique Electroweak Parameter S

The S parameter was defined in the limit where the scale of new physics is much higher than the Z mass as follows, in [60]:

$$\alpha S = 4e^2 \left[\Pi'_{33}(0) - \Pi'_{3Q}(0)\right] \tag{4.4}$$

Here α is the fine-structure constant. $\Pi_{33}(0)$ and $\Pi_{3Q}(0)$ are the self energies for unbroken gauge bosons at zero incoming momentum.

Before we calculate the S parameter in Deconstruction we wish to evaluate it in the Standard Model. This is necessary for two reasons: firstly the S parameter constraints are defined such that the S parameter is zero in the Standard Model. This is achieved by simply subtracting the Standard Model S parameter contribution from any results. The value of the S parameter is dependent on the Higgs mass and so a reference value of the Higgs mass is used to define $S = 0$ (see Figure 4.1). Secondly we will use the computational techniques needed in the Standard Model S parameter computation in performing the analogous calculation in Deconstruction. The form of the S parameter introduced by Peskin and Takeuchi [60] is valid only in the limit where the scale of new physics is much higher than the Z mass. This is clearly no use for any Standard Model calculation and lacks generality, consequently we make use of a more general formula from the paper of Bhattacharyya, Banerjee and Roy [64]. This alternate form of the S parameter is entirely equivalent to that of Peskin and Takeuchi at high scales.

$$S \equiv \frac{16\pi}{M_Z^2}\left[\Pi_{33}(M_Z^2) - \Pi_{33}(0) - \Pi_{3Q}(M_Z^2)\right] \tag{4.5}$$

Here two of the self energies are at the Z mass scale, which would be indistinguishable from zero external momenta for physics at an appreciably higher scale.

It is most useful to work with the mass eigenstate gauge bosons - the Z boson and Photon (A). We thus convert the S parameter into a form which contains the self energies of these fields.

The relations between the gauge and mass eigenstate gauge bosons in the Standard Model are

$$W_\mu^\pm = \frac{1}{\sqrt{2}}\left(W_\mu^1 \mp iW_\mu^2\right), \qquad \begin{pmatrix} Z_\mu \\ A_\mu \end{pmatrix} = \begin{pmatrix} c & -s \\ s & c \end{pmatrix} \begin{pmatrix} W_\mu^3 \\ B_\mu \end{pmatrix} \tag{4.6}$$

from which we can deduce the relations [64],

$$\Pi_{AA} = e^2\Pi_{QQ} \tag{4.7}$$

$$\Pi_{AZ} = \frac{e^2}{cs}(\Pi_{3Q} - s^2\Pi_{QQ}) \tag{4.8}$$

$$\Pi_{ZZ} = \frac{e^2}{c^2s^2}(\Pi_{33} - 2s^2\Pi_{3Q} + s^4\Pi_{QQ}) \tag{4.9}$$

These can be rearranged into the reverse form

$$\Pi_{QQ} = \tfrac{1}{e^2}\Pi_{AA} \tag{4.10}$$

$$\Pi_{3Q} = \tfrac{1}{e^2}(cs\Pi_{ZA} + s^2\Pi_{AA}) \tag{4.11}$$

$$\Pi_{33} = \tfrac{1}{e^2}(c^2s^2\Pi_{ZZ} + 2cs^3\Pi_{ZA} + s^4\Pi_{AA}) \tag{4.12}$$

where e is the coupling of the electron and s and c are shorthand for $\sin\theta_W$ and $\cos\theta_W$ in the Standard Model respectively. It is worth flagging at this point that these relationships differ in Deconstruction. The above relations will have to be re-derived, later in this thesis, from first principles, to accommodate the source of those distinctions. We will begin, however, by performing the calculation in the Standard Model before generalizing.

We can re-express the S parameter, using the above Standard Model relations, in

the following form,

$$S \equiv \frac{16\pi}{e^2 M_Z^2}\left[(c^2 s^2 \Pi_{ZZ}(M_Z^2) + 2cs^3\Pi_{ZA}(M_Z^2) + s^4\Pi_{AA}(M_Z^2))\right.$$
$$-(cs\Pi_{ZA}(M_Z^2) + s^2\Pi_{AA}(M_Z^2)) \tag{4.13}$$
$$\left.-(c^2 s^2 \Pi_{ZZ}(0) + 2cs^3\Pi_{ZA}(0) + s^4\Pi_{AA}(0))\right]$$

In order to calculate the S parameter in the Standard Model we must calculate the three self-energies Z boson to Z boson, Photon to Z boson and Photon to Photon.

4.3 Calculation of the Scalar Two-Point Function B_0

The one loop self energies will be calculated from the sum of all contributing Feynman diagrams formed using Feynman rules, which will be multiplied together and integrated over the undetermined loop momentum. Before we proceed with that calculation it is valuable to establish certain mathematical shorthands that will be useful.

All Feynman diagrams which will be added together to form our self-energies, have certain features in common. Firstly they are one loop diagrams with either one or two internal propagators which contain momentum dependence in their denominators. Secondly they have vertex terms which have momentum dependence only in the numerator. The product of these propagators and vertices will be integrated over all possible values of the loop momentum. The basic template for this is the simplest case, were there are no momenta in the numerator. These are called the Scalar one-point and two point functions A_0 and B_0.

The scalar one-point function has only one propagator, and although simpler will be of less importance in the calculation of our self-energies. Instead we focus on the scalar two-point function. (The method we will follow in the remainder of this section,

for calculating the scalar two-point function, can be found elaborated in Peskin and Schroeder [66].) We define

$$B_0 = \int \frac{d^{4-2\varepsilon}l}{(2\pi)^{4-2\varepsilon}} \frac{g^2(\mu)}{(l^2+m_1^2)((l+p)^2+m_2^2)} \tag{4.14}$$

Here p is the external momentum, l is the loop momentum and m_1 and m_2 are the masses of the gauge bosons to which the respective propagators refer. Using the method of dimensional regularization we are working in $4-2\varepsilon$ dimensions, where ε is, as usual, infinitesimally small. $g(\mu)$ is the coupling which runs according to the momentum scale μ.

Feynman parameterizing as follows

$$\frac{1}{AB} = \int_0^1 dx \frac{1}{[xA+(1-x)B]^2} \tag{4.15}$$

We get

$$\frac{1}{(l^2+m_1^2)((l+p)^2+m_2^2)} = \int_0^1 dx \frac{1}{[x(l+p)^2+xm_2^2+l^2+m_1^2-xl^2-xm_1^2]^2} \tag{4.16}$$

If we now re-parameterize $l \rightarrow l - xp$ we find

$$\int_0^1 dx \frac{1}{[l^2-x^2p^2+xp^2+xm_2^2-xm_1^2+m_1^2]^2} = \int_0^1 dx \frac{1}{(l^2-\Delta)^2} \tag{4.17}$$

where

$$\Delta \equiv x^2p^2 - xp^2 - xm_2^2 + xm_1^2 - m_1^2 \tag{4.18}$$

Now that we have the integral in a simplified form, we can employ a mathematical

identity [66], to perform the integration over loop momentum. In particular we use

$$\int \frac{d^d l}{(2\pi)^d} \frac{1}{(l^2-\Delta)^2} = \frac{i}{(4\pi)^{d/2}} \frac{\Gamma(2-d/2)}{\Gamma(2)} \left(\frac{1}{\Delta}\right)^{2-d/2}, \qquad d \equiv 4-2\varepsilon \tag{4.19}$$

Substituting back into equation 4.14, B_0 becomes

$$B_0 = \int_0^1 dx \frac{ig^2(\mu)}{(4\pi)^{d/2}} \frac{\Gamma(2-d/2)}{\Gamma(2)} \left(\frac{1}{\Delta}\right)^{2-d/2} \tag{4.20}$$

The gamma functions take the following values

$$\Gamma(2) = 2 \tag{4.21}$$

$$\Gamma(2-d/2) = \Gamma(2-2+\varepsilon) = \Gamma(\varepsilon) \tag{4.22}$$

where

$$\Gamma(x) = \frac{1}{x} - \gamma + \mathcal{O}(x)|_{x\to 0} \tag{4.23}$$

We also have

$$\left(\frac{1}{\Delta}\right)^{2-d/2} = \left(\frac{1}{\Delta}\right)^{\varepsilon} \tag{4.24}$$

We thus get B_0 into the following form

$$B_0 = \int_0^1 dx \frac{ig^2(\mu)}{(4\pi)^{2-\varepsilon}} \frac{1}{2} \left(\frac{1}{\varepsilon} - \gamma + \mathcal{O}(\varepsilon)\right) \left(\frac{1}{\Delta}\right)^{\varepsilon} \tag{4.25}$$

We can make use of certain approximations and re-arrangements due to the fact that

ε is infinitesimal:

$$x^{-\varepsilon} = e^{\log x^{-\varepsilon}} \approx 1 - \varepsilon \log x \tag{4.26}$$

$$\left(\frac{1}{\Delta}\right) \approx 1 - \varepsilon \log \Delta \tag{4.27}$$

$$\frac{i}{(4\pi)^{2-\varepsilon}} \approx \frac{i}{(4\pi)^2}(1 + \varepsilon \log 4\pi) \tag{4.28}$$

$$g^2(\mu) = g^2\mu^{2\varepsilon} = g^2(1 + \varepsilon \log \mu^2) \tag{4.29}$$

These can be substituted to simplify B_0, and allow us to separate out terms of order ε. These terms can then be set to zero.We are left with

$$B_0 = \frac{i}{2}\frac{g^2}{(4\pi)^2}\int_0^1 dx \left(\frac{1}{\varepsilon} - \gamma + \log(4\pi) + \log\mu^2 - \log\Delta\right) \tag{4.30}$$

Using the $\overline{MS}$ subtraction scheme this takes the form

$$B_0 = \frac{i}{2}\frac{g^2}{(4\pi)^2}\int_0^1 dx \log\left(\frac{\mu^2}{\Delta}\right) \tag{4.31}$$

where once again Δ is defined by

$$\Delta \equiv x^2p^2 - xp^2 - xm_2^2 + xm_1^2 - m_1^2 \tag{4.32}$$

We are now in a position to evaluate the scalar two-point function explicitly for any given set of values for momenta and masses. In practise we will use the package LoopTools [67] to perform these evaluations.

This expression is the basic template for the loop momenta integrals performed on our Feynman rules.

4.4 Evaluation of Feynman Rule Coefficients

The Feynman rules we will require are derived from the Electroweak Lagrangian (shown in equation 4.33). In this section we will explicitly calculate the coefficients for a couple of examples of vertices, in order to indicate the principles. In Chapter 5 we will need these methods in order to generalize to our Deconstructed models. The momentum dependent parts of the Feynman rules (shown in section 4.5) generalize trivially to Deconstruction, so we will extract them and concentrate on the numerical coefficients. The Lagrangian Density is,

$$\mathcal{L} = -\tfrac{1}{4}F^{\mu\nu}F_{\mu\nu} + \frac{v^2}{4}tr\left[D^{\mu}\Sigma(D_{\mu}\Sigma)^{\dagger}\right] \tag{4.33}$$

where Σ is the Higgs doublet containing the Goldstone bosons, Higgs boson and Higgs vacuum expectation value

$$\Sigma = \begin{pmatrix} \Phi^{+} - i\Phi^{-} \ , \ v + (h + i\chi) \end{pmatrix} \tag{4.34}$$

The covariant derivative takes the form

$$D_{\mu}\Sigma = \partial_{\mu}\Sigma - ig'IB_{\mu}\Sigma + ig\Sigma T^{a}W_{\mu}^{a} \tag{4.35}$$

Our first example will be the calculation of the coefficient of the vertex containing a Z boson coupling to two Goldstone fields. This vertex comes out of the covariant

derivative part of the Electroweak Lagrangian, expanded as follows

$$\mathcal{L} = \begin{pmatrix} \Phi^+ - i\Phi^- \ , \ v \end{pmatrix} \left(\partial_\mu + \tfrac{1}{2}igW^3 \begin{pmatrix} 1 & 0 \\ 0 & -1 \end{pmatrix} - \tfrac{1}{2}ig'B \begin{pmatrix} 1 & 0 \\ 0 & 1 \end{pmatrix} \right) \times \left(\partial_\mu - \tfrac{1}{2}igW^3 \begin{pmatrix} 1 & 0 \\ 0 & -1 \end{pmatrix} + \tfrac{1}{2}ig'B \begin{pmatrix} 1 & 0 \\ 0 & 1 \end{pmatrix} \right) \begin{pmatrix} \Phi^+ + i\Phi^- \\ v \end{pmatrix} \tag{4.36}$$

Contracting the matrices and suppressing terms that will not contribute to the vertex of interest we find

$$\mathcal{L} = \left[\begin{pmatrix} \tfrac{1}{2}igW^3(\Phi^+ - i\Phi^-) - \tfrac{1}{2}ig'B(\Phi^+ - i\Phi^-) \ , \ -\tfrac{1}{2}igW^3 v - \tfrac{1}{2}ig'Bv \end{pmatrix} + \begin{pmatrix} \partial_\mu(\Phi^+ - i\Phi^-) \ , \ \partial_\mu v \end{pmatrix} \right] \times \begin{bmatrix} (-\tfrac{1}{2}igW^3 + \tfrac{1}{2}ig'B)(\Phi^+ + i\Phi^-) + \partial_\mu(\Phi^+ + i\Phi^-) \\ \text{independent of } \Phi \end{bmatrix} \tag{4.37}$$

We now want to re-express the gauge eigenstate gauge bosons in terms of the mass eigenstates using (4.6). The coefficient of the $Z\Phi^+\Phi^-$ vertex is then

$$\mathcal{L} = \partial_\mu \left(\tfrac{1}{2}g \cos\theta_W - \tfrac{1}{2}g' \sin\theta_W \right) \Phi^+\Phi^- Z \tag{4.38}$$

We can write this with the couplings expressed in terms of the electron-photon coupling, by employing the following relations

$$e = g \sin\theta_W \tag{4.39}$$

$$e = g' \cos\theta_W \tag{4.40}$$

We find

$$\mathcal{L} = \partial_\mu \left(\tfrac{1}{2} e \frac{\cos\theta_W}{\sin\theta_W} - \tfrac{1}{2} e \frac{\sin\theta_W}{\cos\theta_W} \right) \Phi^+ \Phi^- Z \tag{4.41}$$

The numerical coefficient (neglecting the standard momentum dependence) of the vertex between a Z boson and two Goldstone bosons is therefore

$$e \frac{c^2 - s^2}{2sc} \tag{4.42}$$

Our second example will be the calculation of the numerical coefficient of the vertex containing a Z boson coupling to a Goldstone field and a W boson. This vertex comes out of the covariant derivative part of the Electroweak Lagrangian, expanded as follows

$$\mathcal{L} = \left(\begin{array}{cc} \Phi^+ - i\Phi^- & , v \end{array} \right) \left(\tfrac{1}{2} i g W^3 \begin{pmatrix} 1 & 0 \\ 0 & -1 \end{pmatrix} - \tfrac{1}{2} i g' B \begin{pmatrix} 1 & 0 \\ 0 & 1 \end{pmatrix} + \tfrac{1}{2} i g W^- \begin{pmatrix} 0 & 0 \\ 1 & 0 \end{pmatrix} \right)$$
$$\times \left(\partial_\mu - \tfrac{1}{2} i g W^3 \begin{pmatrix} 1 & 0 \\ 0 & -1 \end{pmatrix} + \tfrac{1}{2} i g' B \begin{pmatrix} 1 & 0 \\ 0 & 1 \end{pmatrix} - \tfrac{1}{2} i g W^- \begin{pmatrix} 0 & 1 \\ 0 & 0 \end{pmatrix} \right) \begin{pmatrix} \Phi^+ + i\Phi^- \\ v \end{pmatrix} \tag{4.43}$$

Contracting the matrices and suppressing terms that will not contribute to the vertex of interest we have

$$\mathcal{L} = \left(\begin{array}{cc} \tfrac{1}{2} i g W^3 (\Phi^+ - i\Phi^-) - \tfrac{1}{2} i g' B (\Phi^+ - i\Phi^-) & , -\tfrac{1}{2} i g W^3 v - \tfrac{1}{2} i g' B v \end{array} \right) \begin{pmatrix} -\tfrac{1}{2} i g W^- v \\ 0 \end{pmatrix}$$
$$+ h.c. \tag{4.44}$$

Re-expressing this in terms of the mass eigenstate gauge fields gives

$$\mathcal{L} = \tfrac{1}{4}gv(g\cos\theta_W - g'\sin\theta_W)Z\phi^+W^- + h.c. \tag{4.45}$$

Where the hermitian conjugate is,

$$h.c. = \tfrac{1}{4}gv(-g\cos\theta_W - g'\sin\theta_W)Z\phi^+W^- \tag{4.46}$$

Therefore the numerical coefficient of the vertex for a Z boson to a Goldstone boson and W boson is

$$-\tfrac{1}{2}sg'gv \;=\; -sg'M_W \;=\; -e\tfrac{s}{c}M_W \tag{4.47}$$

where we have used the fact $M_W = \frac{1}{2}gv$.

4.5 Feynman Rules.

In order to calculate the gauge boson self energies, and therefore the S parameter, we will require the full set of Feynman rules for all the relevant propagators and vertices. In the conventions used above, the Feynman rules are as follows, with the momenta in all the vertices considered to be incoming.

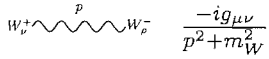

$$\frac{-ig_{\mu\nu}}{p^2+m_W^2}$$

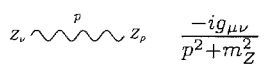

$$\frac{-ig_{\mu\nu}}{p^2+m_Z^2}$$

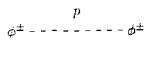

$$\frac{-i}{p^2+m_W^2}$$

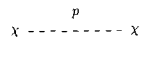

$$\frac{-i}{p^2+m_Z^2}$$

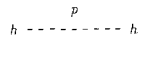

$$\frac{-i}{p^2+m_h^2}$$

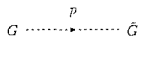

$$\frac{-i}{p^2+m_h^2}$$

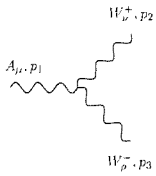

$$ie\left[g_{\mu\nu}(p_2-p_1)_\rho + g_{\nu\rho}(p_3-p_2)_\mu + g_{\rho\mu}(p_1-p_3)_\nu\right]$$

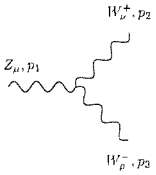

$$-ie\frac{c}{s}\left[g_{\mu\nu}(p_2-p_1)_\rho + g_{\nu\rho}(p_3-p_2)_\mu + g_{\rho\mu}(p_1-p_3)_\nu\right]$$

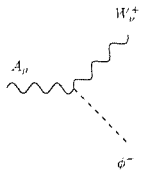

$$ieg_{\mu\nu}m_W$$

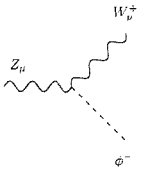

$$-ie\frac{s}{c}g_{\mu\nu}m_W$$

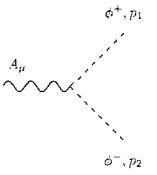

$$-ie(p_1-p_2)_\mu$$

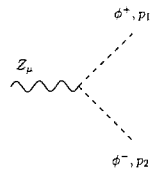

$$-ie\frac{(s^2-c^2)}{2cs}(p_1-p_2)_\mu$$

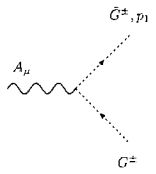

$$\pm iep_{1,\mu}$$

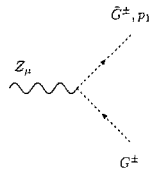

$$\mp ie\frac{c}{s}p_{1,\mu}$$

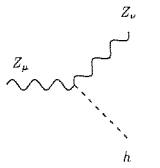

$$ie\frac{1}{c^2 s}g_{\mu\nu}m_W$$

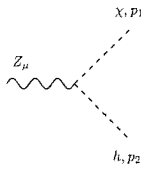

$$-ie\frac{i}{2cs}(p_1-p_2)_\mu$$

4.6 Evaluation of Feynman Diagrams for Photon-Photon Loops

Now that we know the Feynman rules that will be required, we can construct and evaluate the Feynman diagrams which will be require to generate the self-energies. To begin with we will describe how the Photon-Photon Feynman diagrams are formed.

At this stage we won't concern ourselves with 'tadpole diagrams' - ie. diagrams with a single four-point vertex. They are momentum independent and will cancel from

the S parameter. The remainder of the Feynman diagrams that can contribute to the one loop self-energies, have the generic form of figure 4.3.

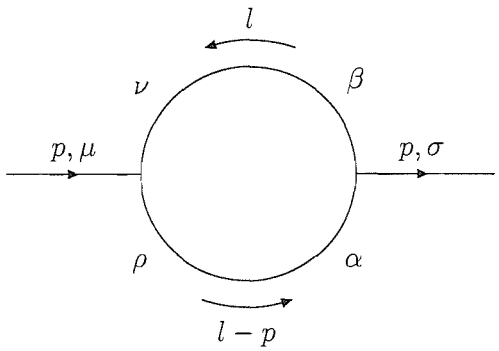

Figure 4.3: Generic form of Feynman diagrams that contribute to the S parameter; showing the routing of the loop momentum and Lorentz indices

Figure 4.3 displays the Lorentz indices which will need to be contracted, as well as the routing of the loop momentum.

We'll begin by calculating the Feynman diagram with two external photons and a Goldstone boson loop.

4.6.1 Photon-Photon One Loop Correction from $\phi^+\phi^-$ Goldstone Boson Loops

Using the Feynman rules from section 4.5, we evaluate the Goldstone loop diagram to be the following

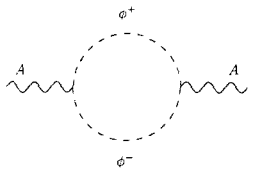

$$= S \int \frac{d^d p}{(2\pi)^d} (-)ies(l + (l+p))_\mu \frac{-i}{l^2 + m_W^2} \times (-)ies(-l - (l+p))_\sigma \frac{-i}{(l+p)^2 + m_W^2} \tag{4.48}$$

Where S stands for the symmetry factor, which is 2 for this Goldstone loop.

First we'll deal with the momentum parts in the numerator as these determine which B-relations apply. We extract these out separately below and expand the brackets.

$$(l+(l+p))_\mu(-l-(l+p))_\sigma = -p_\mu p_\sigma - 4l_\mu p_\sigma - 4l_\mu l_\sigma \tag{4.49}$$

Note the following two point integrals are defined as [68]

$$B_0; B_\mu; B_{\mu\sigma}(p, m_1, m_2) = \int \frac{d^d p}{(2\pi)^d} \frac{1; l_\mu; l_\mu l_\sigma}{(l^2+m_1^2)((l+p)^2+m_2^2)} \tag{4.50}$$

$$B_\mu(p, m_1, m_2) = p_\mu B_1(p, m_1, m_2) \tag{4.51}$$

$$B_{\mu\sigma} = p_\mu p_\sigma B_{21} + g_{\mu\sigma} B_{22} \tag{4.52}$$

Therefore the diagram (4.48) can be rewritten

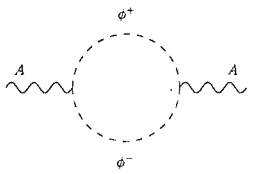

$$= s^2(-p_\mu p_\sigma B_0 - 4p_\sigma B_\mu - 4B_{\mu\sigma}) \tag{4.53}$$

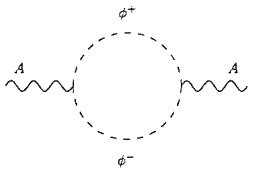

$$= s^2(-p_\mu p_\sigma B_0 - 4p_\mu p_\sigma B_1 - 4p_\mu p_\sigma B_{21} - 4g_{\mu\sigma} B_{22}) \tag{4.54}$$

We suppress keeping track of the momentum scale and the masses of the two-point functions $B_0(p^2, m_W, m_W)$, down to B_0, B_1, B_{22} and so forth, for brevity.

Given that the Ward Identity imposes that

$$p_\mu \left(\quad \right) = 0 \tag{4.55}$$

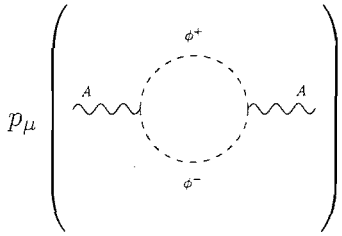

The following relation holds for self-energy diagrams,

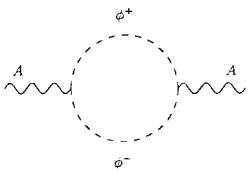

$$= i\left(g_{\mu\sigma} - \frac{p_\mu p_\sigma}{p^2}\right)\Pi(p^2) \tag{4.56}$$

As such we may simply take the $g_{\mu\sigma}$ coefficient to determine the self-energy, since the coefficients of $p_\mu p_\sigma$ must sum to an identical value. Therefore,

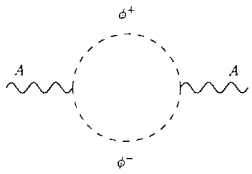

$$= 4s^2 B_{22} \tag{4.57}$$

4.6.2 Photon-Photon One Loop Correction from G^+G^- Faddeev-Popov Ghost Loops

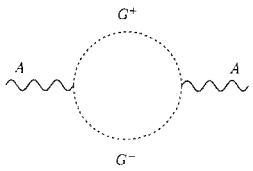

$$= S\int \frac{d^dp}{(2\pi)^d}(-ie)sl_\mu \frac{-i}{l^2+m_W^2}(+ie)s(l+p)_\sigma \frac{-i}{(l+p)^2+m_W^2} \tag{4.58}$$

The symmetry factor S here is one, However there is a factor of -1 because the ghost fields are Grassmann variables which anticommute, analogous to the factor of -1 in

fermion loops.

The momentum parts are

$$l_\mu(l+p)_\sigma = l_\mu p_\sigma + l_\mu l_\sigma \tag{4.59}$$

Therefore

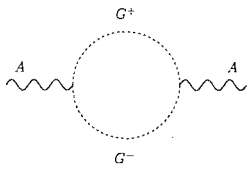

$$= s^2(p_\sigma B_\mu + B_{\mu\sigma}) \tag{4.60}$$

Now using the definitions

$$B_\mu(p, m_1, m_2) = p_\mu B_1(p, m_1, m_2) \tag{4.61}$$

$$B_{\mu\sigma} = p_\mu p_\sigma B_{21} + g_{\mu\sigma} B_{22} \tag{4.62}$$

we find

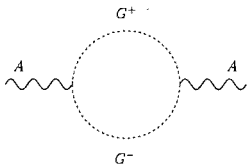

$$= s^2(p_\mu p_\sigma B_1 + p_\mu p_\sigma B_{21} + g_{\mu\sigma} B_{22}) \tag{4.63}$$

Once again using the relationship that follows from the Ward Identity

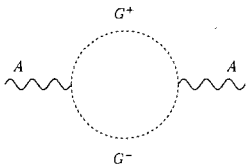

$$= -2s^2 B_{22} \tag{4.64}$$

4.6.3 Photon-Photon One Loop Correction from $W^+\phi^-$ Loops

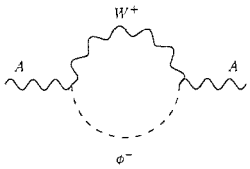

$$= S \int \frac{d^d p}{(2\pi)^d} ies m_W g_{\mu\nu} \frac{-ig_{\nu\beta}}{l^2 + m_W^2} ies m_W g_{\beta\sigma} \frac{-i}{(l+p)^2 + m_W^2} \quad (4.65)$$

The symmetry factor S here is one. Here the metric tensors contract, and the result is quite trivial

4.6.4 Photon-Photon One Loop Correction from W^+W^- Loops

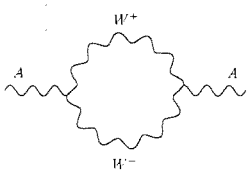

$$\begin{aligned} = S \int \frac{d^d p}{(2\pi)^d} ies \left[g_{\mu\nu}(p_2 - p_1)_\rho + g_{\nu\rho}(p_3 - p_2)_\mu + g_{\rho\mu}(p_1 - p_3)_\nu \right] \\ \frac{-ig_{\nu\beta}}{l^2 + m_W^2} ies \left[g_{\sigma\beta}(p_2 - p_1)_\alpha + g_{\beta\alpha}(p_3 - p_2)_\sigma \right. \\ \left. + g_{\alpha\sigma}(p_1 - p_3)_\beta \right] \frac{-ig_{\rho\alpha}}{(l+p)^2 + m_W^2} \end{aligned} \quad (4.66)$$

The symmetry factor S here has value 2. The momentum factors after contraction are

$$= 6[p_\mu p_\sigma + p_\mu l_\sigma + l_\mu l_\sigma] + 4[-p_\mu p_\sigma - 4p_\mu l_\sigma - 4l_\mu l_\sigma] + g_{\mu\sigma}[-5p^2 - 2pl - 2l^2] \quad (4.67)$$

Using the relations in equation 4.61 we can re-express the diagram as follows

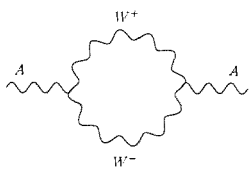

$$\begin{aligned} = s^2[2p_\mu p_\sigma B_0 - 10p_\mu p_\sigma B_1 - 10p_\mu p_\sigma B_{21} - 10g_{\mu\sigma} B_{22} \\ -5g_{\mu\sigma} p^2 B_0 - 2p^2 B_{21} - 8g_{\mu\sigma} B_{22}] \end{aligned} \quad (4.68)$$

Using the relations from Passarino and Veltman's paper [68]:

$$p^2 B_{21} + B_{22} = -1/2 p^2 B_1 \tag{4.69}$$

$$-m^2 B_0 = p^2 B_{21} + 4B_{22} + 1/2(2m^2 + 1/3p^2) \tag{4.70}$$

$$p^2 B_1 = -1/2 p^2 B_0 \tag{4.71}$$

and employing the Ward Identity, we find the W^+W^- loop gives,

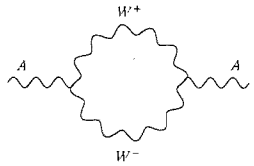

$$= s^2 \left(\left(-2m_W^2 + 4p^2 \right) B_0 + 10 B_{22} + 2 \left(2m_W^2 + 1/3p^2 \right) \right) \tag{4.72}$$

4.7 Corrections from Loops

Collecting the evaluated diagrams from section 4.6 for the photon-photon corrections we find

W^+W^-

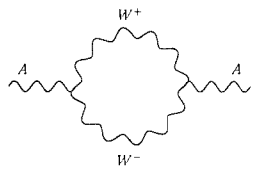

$$s^2 \left(\left(-2m_W^2 + 4p^2 \right) B_0 + 10 B_{22} + 2 \left(2m_W^2 + 1/3p^2 \right) \right)$$

$W^+\phi^-$

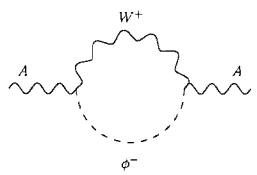

$$2s^2 m_W^2 B_0$$

$\phi^+\phi^-$

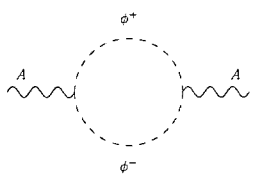

$$4s^2 B_{22}$$

G^+G^-

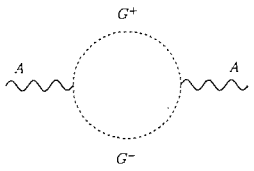

$$-2s^2B_{22}$$

Included in the above diagrams are symmetry factors of 2 for W^+W^- and $\phi^+\phi^-$. There are no symmetry factors for G^+G^- or $W^+\phi^-$. However there is a factor of -1 in G^+G^- because the ghost fields are Grassmann variables which anticommute, analogous to the factor of -1 in fermion loops.

The summation of these photon-photon one loop corrections yields the photon-photon self energy Π_{AA}. We use $\Delta\Pi_{AA}$ to signify the suppression of momentum independent contributions to the self energy, which will not be required to calculate the S parameter

$$\Delta\Pi_{AA} = s^2[4p^2B_0 + 12B_{22} + 2(2m^2 + 1/3p^2)] \tag{4.73}$$

Using the formulae in (4.69) we may solve for B_{22} [69]

$$B_{22} = 1/6\left\{(-2m^2 - 1/2p^2)B_0 - 2m^2 - 1/3p^2\right\} \tag{4.74}$$

Substituting for B_{22} into equation (4.73) we find the photon self-energy;

$$\Delta\Pi_{AA} = -\frac{\alpha}{4\pi}\left\{\left[3p^2 - 4m_W^2\right]B_0(p^2, m_W, m_W)\right\} \tag{4.75}$$

The Feynman diagrams for the Z boson to photon self energy are:

W^+W^-

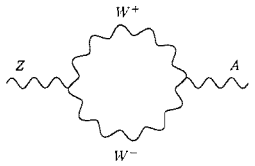

$$sc\left(\left(-2m_W^2+4p^2\right)B_0+10B_{22}+2\left(2m_W^2+1/3p^2\right)\right)$$

$W^+\phi^-$

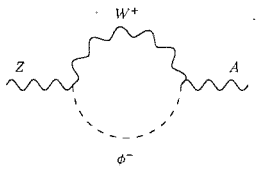

$$-2\tfrac{s^3}{c}m_W^2B_0$$

$\phi^+\phi^-$

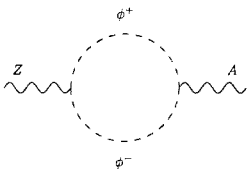

$$2\tfrac{s}{c}(c^2-s^2)B_{22}$$

G^+G^-

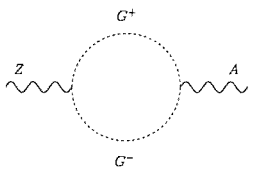

$$-2scB_{22}$$

The summation of the these diagrams yields the Z boson-photon self energy.

$$\Delta\Pi_{ZA}=sc\left(\left(-2m_W^2+4p^2\right)B_0+10B_{22}+2\left(2m_W^2+1/3p^2\right)\right)-2\frac{s^3}{c}(m_W^2B_0+B_{22}) \tag{4.76}$$

Substituting with (4.74) this becomes

$$\Delta\Pi_{ZA}=-\frac{\alpha}{4\pi}\left\{\frac{1}{3sc}\left\{\left[(9c^2+\tfrac{1}{2})p^2-(12c^2+4)m_W^2\right]B_0(p^2,m_W,m_W)+\frac{1}{3}p^2\right\}\right\} \tag{4.77}$$

The Feynman diagrams for the Z boson to Z boson self energy are:

W^+W^-

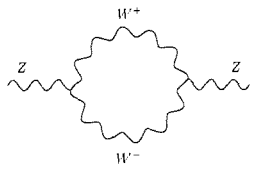

$$c^2\left(\left(-2m_W^2+4p^2\right)B_0+10B_{22}+2\left(2m_W^2+1/3p^2\right)\right)$$

$W^+\phi^-$

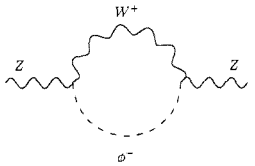

$$2\tfrac{s^4}{c^2}m_W^2B_0$$

$\phi^+\phi^-$

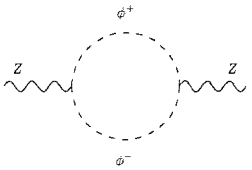

$$\tfrac{(c^2-s^2)^2}{c^2}B_{22}$$

G^+G^-

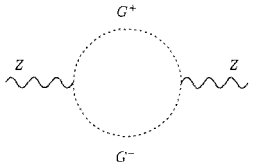

$$-2c^2B_{22}$$

These diagrams can be calculated analogously to Π_{AA} and Π_{ZA}, to give

$$\Delta\Pi_{ZZ}=-\frac{\alpha}{4\pi}\left\{\frac{1}{6s^2c^2}\left\{\left[(18c^4+2c^2-\tfrac{1}{2})p^2-(24c^4+16c^2-10)m_W^2\right]B_0(p^2,m_W,m_W)\right.\right.$$
$$\left.\left.+(4c^2-1)\frac{1}{3}p^2\right\}\right\} \tag{4.78}$$

However there are additional contributions from the following two diagrams:

Zh

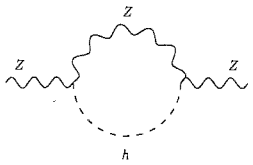

$$\frac{m_W^2}{c^4} B_0(p^2, m_Z, m_h)$$

χh

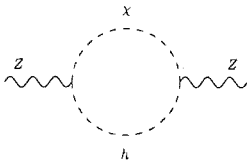

$$\frac{1}{c^2} B_{22}(p^2, m_Z, m_h)$$

Using the more general relations for B_0, B_{21}, B_{22}, which apply when the masses in the two-point function are not equal

$$p^2 B_{21} + B_{22} = \tfrac{1}{2} A_0(m_1) - \tfrac{1}{2}(p^2 - m_0^2 + m_1^2) B_1 \tag{4.79}$$

$$A_0(m_1) - m_0^2 B_0 = p^2 B_{21} + 4B_{22} + \frac{1}{2}(m_1^2 + m_0^2 + \tfrac{1}{3}p^2) \tag{4.80}$$

$$B_1(p^2, m_0, m_1) = \frac{1}{2p^2}\left[A_0(m_0) - A_0(m_1) - (p^2 - m_0^2 + m_1^2) B_0(p^2, m_0, m_1)\right] \tag{4.81}$$

Which have the following solution for B_{22}:

$$\begin{aligned} B_{22}(p^2, m_0, m_1) = \frac{1}{6}\Big\{ & \tfrac{1}{2}\left[A(m_0) + A(m_1)\right] + (-\tfrac{1}{2}p^2 - m_0^2 - m_1^2) B_0 \\ & + \tfrac{m_1^2 - m_0^2}{2p^2}\left[A(m_0) - A(m_1) - (m_1^2 - m_0^2) B_0\right] \\ & - m_0^2 - m_1^2 - \tfrac{1}{3}p^2 \Big\} \end{aligned} \tag{4.82}$$

These extra diagrams contribute the following additional term to Π_{ZZ},

$$\begin{aligned} \Delta\Pi_{ZZ} = -\frac{\alpha}{4\pi}\Bigg\{ & \frac{1}{12 s^2 c^2}\Big\{\left[2m_h^2 - m_Z^2 - p^2\right] B_0(p^2, m_Z, m_h) \\ & - \frac{(m_Z^2 - m_h^2)^2}{p^2}\left(B_0(p^2, m_Z, m_h) - B_0(0, m_Z, m_h)\right) - \frac{2}{3}p^2 \Big\}\Bigg\} \end{aligned} \tag{4.83}$$

We keep one factor here of $B_0(0, m_Z, m_h)$ as a lone momentum independent term, as it is convenient in performing the cancellation of the divergences in section 4.8.

Collecting together results, we get the Electroweak self energies below. Noting that the momentum independent terms are suppressed as they don't contribute to the S parameter, which is the objective we've set out to calculate.

$$\Pi_{AA} = -\frac{\alpha}{4\pi}\left\{\left[3p^2 - 4m_W^2\right] B_0(p^2, m_W, m_W)\right\} \tag{4.84}$$

$$\Pi_{ZA} = -\frac{\alpha}{4\pi}\left\{\frac{1}{3sc}\left\{\left[(9c^2 + \tfrac{1}{2})p^2 - (12c^2 + 4)m_W^2\right] B_0(p^2, m_W, m_W) + \frac{1}{3}p^2\right\}\right\} \tag{4.85}$$

$$\begin{aligned}\Pi_{ZZ} = -\frac{\alpha}{4\pi}\Bigg\{\frac{1}{6s^2c^2}\Bigg\{\Bigg[(18c^4 + 2c^2 - \frac{1}{2})p^2 - (24c^4 + 16c^2 - 10)m_W^2\Bigg] B_0(p^2, m_W, m_W) \\ +(4c^2 - 1)\frac{1}{3}p^2\Bigg\} + \frac{1}{12s^2c^2}\Big\{\left[2m_h^2 - m_Z^2 - p^2\right] B_0(p^2, m_Z, m_h) \\ -\frac{(m_Z^2 - m_h^2)^2}{p^2}\left(B_0(p^2, m_Z, m_h) - B_0(0, m_Z, m_h)\right) - \frac{2}{3}p^2\Big\}\Bigg\}\end{aligned} \tag{4.86}$$

We now have the self energy contributions which we require in order to calculate the Electroweak oblique parameters, of which the S parameter will be of specific interest.

4.8 Cancelation of Divergences in the Standard Model at One Loop

From section 4.2 we know that the S parameter expands to equation 4.2.

$$\begin{aligned} S \equiv \frac{16\pi}{e^2 M_Z^2} \big[& (c^2 s^2 \Pi_{ZZ}(M_Z^2) + 2cs^3 \Pi_{ZA}(M_Z^2) + s^4 \Pi_{AA}(M_Z^2)) \\ & -(cs\Pi_{ZA}(M_Z^2) + s^2 \Pi_{AA}(M_Z^2)) \\ & -(c^2 s^2 \Pi_{ZZ}(0) + 2cs^3 \Pi_{ZA}(0) + s^4 \Pi_{AA}(0))\big] \end{aligned} \tag{4.87}$$

Electromagnetic gauge invariance implies $\Pi_{AA}(0) = \Pi_{ZA}(0) = 0$ [64, 63] consequently only the terms with momentum dependent coefficients in the these self energies will contribute to the S parameter. Equally an observation that the Z-Z self energy appears twice in the S parameter, with a difference of a sign and a differing momentum scale, makes it apparent that all but the terms with momentum dependent coefficients must cancel here too. Therefore, the S parameter is formed only from the terms with momentum dependent coefficients from the gauge boson self energies.

The momentum dependent terms in the neutral current gauge boson self energies from chapter 4 are as follows,

$$\Delta\Pi_{AA} = -\frac{\alpha}{4\pi}\left\{3p^2 B_0(p^2, m_W, m_W)\right\} \tag{4.88}$$

$$\Delta\Pi_{ZA} = -\frac{\alpha}{4\pi}\left\{\frac{1}{3sc}\left\{(9c^2 + \tfrac{1}{2})p^2 B_0(p^2, m_W, m_W) + \frac{1}{3}p^2\right\}\right\} \tag{4.89}$$

$$\Delta\Pi_{ZZ} = -\frac{\alpha}{4\pi}\left\{\frac{1}{6s^2c^2}\{(18c^4+2c^2-\frac{1}{2})p^2B_0(p^2,m_W,m_W) \right.$$
$$+(4c^2-1)\frac{1}{3}p^2\Big\} + \frac{1}{12s^2c^2}\left\{-p^2B_0(p^2,m_Z,m_h)\right.$$
$$\left.\left.-\frac{(m_Z^2-m_h^2)^2}{p^2}\left(B_0(p^2,m_Z,m_h)-B_0(0,m_Z,m_h)\right)-\frac{2}{3}p^2\right\}\right\} \tag{4.90}$$

The divergences must cancel within the S parameter, as it is a physical observable. Divergences are present in the scalar two-point functions through B_0. Denoting the divergences in B_0 as Δ, the insertion of the abbreviated self energy relations below into equation 4.2, must equal zero.

$$\Delta\Pi_{AA} = -\frac{\alpha}{4\pi}\left\{3p^2\Delta\right\} \tag{4.91}$$

$$\Delta\Pi_{ZA} = -\frac{\alpha}{4\pi}\left\{\frac{1}{3sc}\left\{(9c^2+\tfrac{1}{2})p^2\Delta\right\}\right\} \tag{4.92}$$

$$\Delta\Pi_{ZZ} = -\frac{\alpha}{4\pi}\left\{\frac{1}{6s^2c^2}\left\{(18c^4+2c^2-\tfrac{1}{2})p^2\Delta\right\}+\frac{1}{12s^2c^2}\left\{-p^2\Delta\right\}\right\} \tag{4.93}$$

The substitution and cancellation of divergences is shown explicitly below,

$$S(divergences) = c^2s^2\left\{\frac{1}{6s^2c^2}\left\{(18c^4+2c^2-\tfrac{1}{2})M_Z^2\Delta\right\}+\frac{1}{12s^2c^2}\left\{-M_Z^2\Delta\right\}\right\}$$
$$+2cs^3\left\{\frac{1}{3sc}\left\{(9c^2+\tfrac{1}{2})M_Z^2\Delta\right\}\right\}+s^4\left\{3M_Z^2\Delta\right\}$$
$$-cs\left\{\frac{1}{3sc}\left\{(9c^2+\tfrac{1}{2})M_Z^2\Delta\right\}\right\}-s^2\left\{3M_Z^2\Delta\right\} \tag{4.94}$$

$$S(divergences) = \left\{ \frac{1}{6} \left\{ (18c^4 + 2c^2 - \tfrac{1}{2}) M_Z^2 \Delta \right\} + \frac{1}{12} \left\{ -M_Z^2 \Delta \right\} \right\}$$
$$+ 2s^2 \left\{ \frac{1}{3} \left\{ (9c^2 + \tfrac{1}{2}) M_Z^2 \Delta \right\} \right\} + s^4 \left\{ 3M_Z^2 \Delta \right\}$$
$$- \left\{ \frac{1}{3} \left\{ (9c^2 + \tfrac{1}{2}) M_Z^2 \Delta \right\} \right\} - s^2 \left\{ 3M_Z^2 \Delta \right\} \tag{4.95}$$

$$S(divergences) = \frac{1}{12} \left[\left\{ \left\{ (36c^4 + 4c^2 - 1) M_Z^2 \Delta \right\} + \left\{ -M_Z^2 \Delta \right\} \right\} \right.$$
$$+ s^2 \left\{ (72c^2 + 4) M_Z^2 \Delta \right\} + s^4 \left\{ 36M_Z^2 \Delta \right\}$$
$$\left. \left\{ -(36c^2 + 2) M_Z^2 \Delta \right\} - s^2 \left\{ 36M_Z^2 \Delta \right\} \right] \tag{4.96}$$

Implementing the relation $s^2 = 1 - c^2$

$$S(divergences) = \frac{1}{12} \left[(36c^4 + 4c^2 - 1) - 1 \right.$$
$$+ (1 - c^2)(72c^2 + 4) + 36(1 - c^2)^2$$
$$\left. - (36c^2 + 2) - 36(1 - c^2) \right] M_Z^2 \Delta \tag{4.97}$$
$$\equiv 0 \tag{4.98}$$

Here we have confirmed that the standard model S parameter, as expected, is free of divergences. A statement which also establishes that the S parameter is momentum scale independent (ie. the running coupling μ in equation 4.14 has no bearing on the observable S parameter.).

In the leading log approximation one sets

$$B_0 = \frac{g^2}{(4\pi)^2} \mathrm{Log} \left(\frac{\Lambda^2}{m^2} \right) \tag{4.99}$$

where Λ is a UV cut off on the integration and m the largest mass in the loop. The

UV cut off dependence cancels as we have just shown explicitly. The largest mass in the loops will be either M_W or m_h. Explicitly in this approximation one finds

$$S = \frac{1}{12\pi}\mathrm{Log}\left(\frac{m_h^2}{M_W^2}\right) \tag{4.100}$$

This is the familiar result from refs [68, 70, 71].

We can of course now substitute the full values of the self energies into the S parameter definition, in the knowledge that they are divergence free. Doing so with the W/Z boson masses from experimental data and a Higgs mass set to 100GeV the S parameter has the value $S = 0.140$.

Chapter 5

Calculating Electroweak Oblique Corrections in Deconstruction at the One Loop Level

In the previous chapter we computed the contributions to the S parameter from the gauge sector of the Standard Model. That analysis developed the techniques we need to calculate the additional contributions to S in deconstructed models. We will concentrate on the special case of a deconstructed model with just a single additional SU(2) gauge group beyond the Standard Model here. As we saw in Chapter 3 to obtain deconstructed models that are compatible at tree level with the electroweak constraints one must concentrate on the decoupling limit where the gauge coupling of the new gauge groups is large ($\tilde{g} \to \infty$). For this reason we will pay special attention to that limit of our computations. We also make use of [72] in which a parallel analysis of the S contribution in that limit is made in the low energy effective theory of Deconstruction. Our computations extend that analysis beyond the leading log approximation and pro-

vide an explicitly renormalizable model of the symmetry breaking dynamics through the inclusion of Higgs fields.

5.1 Evaluation of Mixing Angles in N=1 Deconstruction

We explore the simplest form of a Deconstructed model, that with an N=1 $U(1) \times SU(2)_1 \times SU(2)_2$ gauge group. [24]

The Lagrangian Density for an N=1 Deconstructed model is

$$\mathcal{L} = -\tfrac{1}{4}B^{\mu\nu}B_{\mu\nu} - \tfrac{1}{4}W_1^{a\ \mu\nu}W_{1\ \mu\nu}^{a} - \tfrac{1}{4}W_2^{a\ \mu\nu}W_{2\ \mu\nu}^{a} + \tfrac{1}{4}tr\left[D^{\mu}\Sigma_1(D_{\mu}\Sigma_1)^{\dagger}\right] + \tfrac{1}{4}tr\left[D^{\mu}\Sigma_2(D_{\mu}\Sigma_2)^{\dagger}\right] \quad (5.1)$$

Where Σ_1, Σ_2 are the two Higgs doublets within the N=1 Deconstructed model.

$$\Sigma_1 = \begin{pmatrix} \Phi_1^+ - i\Phi_1^- \ , \ v_1 + (h_1 + i\chi_1) \end{pmatrix} \quad (5.2)$$

$$\Sigma_2 = \begin{pmatrix} \Phi_2^+ - i\Phi_2^- \ , \ v_2 + (h_2 + i\chi_2) \end{pmatrix} \quad (5.3)$$

We will restrict to the case where $v_1 = v_2 = v$ for simplicity (we will also assume the two Higgs bosons have the same mass). The two covariant derivatives in the $(N, \tilde{N})$ representation are as follows,

$$D_{\mu}\Sigma_1 = \partial_{\mu}\Sigma_1 - ig'IB_{\mu}\Sigma_1 + i\tilde{g}\Sigma_1 T^a W_{1\mu}^a \quad (5.4)$$

$$D_{\mu}\Sigma_2 = \partial_{\mu}\Sigma_2 - i\tilde{g}T^a W_{1\mu}^a \Sigma_2 + ig\Sigma_2 T^a W_{2\mu}^a \quad (5.5)$$

The Feynman rules for three point vertices in such an N=1 Deconstructed moose model can be found by extracting out the relevant terms from this Lagrangian. To get the

Feynman rules in terms of the mass eigenstate gauge bosons of the spontaneously broken symmetry, we employ the following mixing angle matrix expansions (obtained in practice by diagonalizing the mass matrices in section 2.7).

$$W = a_{12}W_1 + a_{22}W_2 \tag{5.6}$$

$$W' = a_{11}W_1 + a_{21}W_2 \tag{5.7}$$

$$A = b_{00}B + b_{10}W_1^3 + b_{20}W_2^3 \tag{5.8}$$

$$Z' = b_{01}B + b_{11}W_1^3 + b_{21}W_2^3 \tag{5.9}$$

$$Z = b_{02}B + b_{12}W_1^3 + b_{22}W_2^3 \tag{5.10}$$

In addition we must find the Goldstone boson eigenvector components. The mass matrices are given via the gauge fixing terms discussed in section 2.1 and in this case are

$$M_\phi^2 = v^2 \begin{pmatrix} g^2 + \tilde{g}^2 & -\tilde{g}^2 \\ -\tilde{g}^2 & \tilde{g}^2 \end{pmatrix} \tag{5.11}$$

$$M_\chi^2 = v^2 \begin{pmatrix} g^2 + \tilde{g}^2 & -\tilde{g}^2 \\ -\tilde{g}^2 & \tilde{g}^2 + g'^2 \end{pmatrix} \tag{5.12}$$

We define the mixing angles after diagonalization as

$$\phi = c_{12}\phi_1 + c_{22}\phi_2 \tag{5.13}$$

$$\phi' = c_{11}\phi_1 + c_{21}\phi_2 \tag{5.14}$$

$$\chi = d_{12}\chi_1 + d_{22}\chi_2 \tag{5.15}$$

$$\chi' = d_{11}\chi_1 + d_{21}\chi_2 \tag{5.16}$$

5.2 The Large $\tilde{g}$ Limit

Phenomenologically compatible models all live at large values of the additional SU(2) group's coupling, $\tilde{g}$. One can explicitly find the leading terms in the expansion of the above couplings in this limit. This was mostly done in [24] and we reproduce those results here extended to the c and d coefficients. Firstly the QED coupling is given by

$$e = \frac{g'\tilde{g}g}{\sqrt{g^2\tilde{g}^2 + g'^2g^2 + g'^2\tilde{g}^2}} \tag{5.17}$$

The a coefficients are then

$$a_{22} = 1 - \frac{1}{8}\lambda^2 \tag{5.18}$$

$$a_{12} = \frac{\lambda}{2} \tag{5.19}$$

$$a_{21} = -\frac{\lambda}{2} \tag{5.20}$$

$$a_{11} = 1 - \frac{1}{8}\lambda^2 \tag{5.21}$$

where $\lambda = g/\tilde{g}$ (and we will similarly use $\lambda' = g'/\tilde{g}$). Both λ and λ' are zero in the formal $\tilde{g} \to \infty$ limit.

The b coefficients are

$$b_{00} = \frac{e}{g'} \tag{5.22}$$

$$b_{10} = \frac{e}{\tilde{g}} \tag{5.23}$$

$$b_{20} = \frac{e}{g} \tag{5.24}$$

$$b_{01} = -\frac{\lambda'}{2} \tag{5.25}$$

$$b_{11} = 1 - \frac{1}{8}(\lambda^2 + \lambda'^2) \tag{5.26}$$

$$b_{21} = -\frac{\lambda}{2} \tag{5.27}$$

$$b_{02} = \frac{-g'}{\sqrt{g^2 + g'^2}} \left(1 - \frac{1}{8}(\lambda^2 + \lambda'^2) + \frac{1}{2}\frac{\lambda^4}{(\lambda^2 + \lambda'^2)}\right) \tag{5.28}$$

$$b_{12} = \frac{1}{2}\frac{1}{\tilde{g}} \left(\frac{g^2 - g'^2}{\sqrt{g^2 + g'^2}}\right) \tag{5.29}$$

$$b_{22} = \frac{g}{\sqrt{g^2 + g'^2}} \left(1 - \frac{1}{8}(\lambda^2 + \lambda'^2) + \frac{1}{2}\frac{\lambda'^4}{(\lambda^2 + \lambda'^2)}\right) \tag{5.30}$$

Finally the cs and ds are given by

$$c_{22} = -\frac{1}{\sqrt{2}} \left(1 - \frac{1}{4}\lambda^2\right) \tag{5.31}$$

$$c_{12} = \frac{1}{\sqrt{2}} \left(1 + \frac{1}{4}\lambda^2\right) \tag{5.32}$$

$$c_{21} = \frac{1}{\sqrt{2}} \left(1 + \frac{1}{4}\lambda^2\right) \tag{5.33}$$

$$c_{11} = \frac{1}{\sqrt{2}} \left(1 - \frac{1}{4}\lambda^2\right) \tag{5.34}$$

$$d_{22} = -\frac{1}{\sqrt{2}}\left(1 - \frac{1}{4}\lambda^2 + \frac{1}{4}\lambda'^2\right) \tag{5.35}$$

$$d_{12} = \frac{1}{\sqrt{2}}\left(1 + \frac{1}{4}\lambda^2 - \frac{1}{4}\lambda'^2\right) \tag{5.36}$$

$$d_{21} = \frac{1}{\sqrt{2}}\left(1 + \frac{1}{4}\lambda^2 - \frac{1}{4}\lambda'^2\right) \tag{5.37}$$

$$d_{11} = \frac{1}{\sqrt{2}}\left(1 - \frac{1}{4}\lambda^2 + \frac{1}{4}\lambda'^2\right) \tag{5.38}$$

5.3 Tree Level S Parameter in Deconstruction

Before reviewing the calculation of the S parameter in Deconstruction at the loop level, which is our main interest, we will present the calculation at tree level. The tree level calculation follows the work of Schmidt et al. in their paper [24].

The S parameter can be defined in the limit where the scale of new physics is much higher than the Z mass as follows [61]

$$\alpha S = 4e^2\left[\Pi'_{33}(0) - \Pi'_{3Q}(0)\right] \tag{5.39}$$

$$= 4e^2\left[\Pi'_{3Y}(0)\right] \tag{5.40}$$

The mass matrix for a Deconstructed model with generic N is

$$M_Z^2 = \frac{v^2}{4}\begin{pmatrix} g^2 & -g\tilde{g} & & & \\ -g\tilde{g} & 2\tilde{g}^2 & & & \\ & & \ddots & & \\ & & & 2\tilde{g}^2 & -\tilde{g}g' \\ & & & -\tilde{g}g' & g'^2 \end{pmatrix}\begin{pmatrix} W^3_{N+1} \\ W^3_N \\ \vdots \\ W^3_1 \\ B \end{pmatrix}$$

For this tree level calculation we work in the limit where the additional couplings $\tilde{g}$ are set to be very large compared to the Standard Model couplings g and g'. In this limit the central gauge groups decouple from the end two groups as their coupling strengths to each other of order $\tilde{g}^2$ are much greater than their couplings to the end groups of order $g\tilde{g}, \tilde{g}g'$. By diagonalizing groups 1 to N we determine how much each mass eigenstate gauge boson couples to the end two unbroken gauge groups.

Diagrammatically Π_{3Y}, in the strong coupling $\tilde{g}$ limit, at tree level is as follows;

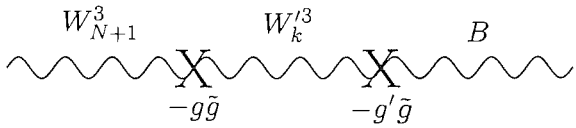

The central propagator is made up of a mixture of all the gauge groups. We are specifically interested in the contributions from the beyond the Standard Model bosons.

Note here that only W^3_1 and W^3_N can couple through the end two Higgs fields to B and W^3_{N+1}. Therefore the relevant mixing angles are b_{1k} and b_{Nk} where k runs from 1 to N. We can then evaluate the Feynman diagram for Π_{3Y}.

$$\Pi_{3Y}(p^2) = \sum_{k=1}^{N} \left(\frac{-i\tilde{g}f^2}{4}\right)\left(\frac{-b_{Nk}b^*_{1k}}{p^2 - m^2_{Z'_k}}\right)\left(\frac{-i\tilde{g}f^2}{4}\right) \tag{5.41}$$

$$\Pi'_{3Y}(0) = \sum_{k=1}^{N} \left(\frac{-i\tilde{g}f^2}{4}\right)\left(\frac{b_{Nk}b^*_{1k}}{m^4_{Z'_k}}\right)\left(\frac{-i\tilde{g}f^2}{4}\right) \tag{5.42}$$

Using equation 5.40 we therefore have a relation for the tree level value of the S parameter

$$\alpha S = 4e^2\left[\sum_{k=1}^{N}\left(\frac{\tilde{g}^2f^4}{16}\right)\left(\frac{b_{Nk}b^*_{1k}}{m^4_{Z'_k}}\right)\right] \tag{5.43}$$

Equations for the Z' masses and the mixing angles b_{Nk} and b^*_{1k}, for these models can

be found from relations in the appendix of [24]. Note $\lambda \equiv g/\tilde{g}$, $\lambda' \equiv g'/\tilde{g}$.

$$m_{Z'_n}^2 = \tilde{g}^2 f^2 \left(\sin \frac{n\pi}{2(N+1)}\right)^2 + 2m_Z^2 \left(\cos \frac{n\pi}{2(N+1)}\right)^2 (1 + \mathcal{O}(\lambda^2)) \tag{5.44}$$

$$b_{nm} = \sqrt{\frac{2}{N+1}} \sin \frac{\pi nm}{N+1} + \mathcal{O}(\lambda^2) \tag{5.45}$$

We are calculating the S parameter in the limit where the scale of new physics is much greater than the Z mass. Consequently the second term in the expression for the Z' mass may be suppressed. By substituting for n and m in the generic relation for the central mixing angles we extract b_{Nk} and b^*_{1k}.

$$m_{Z'_n}^2 = \tilde{g}^2 f^2 \left(\sin \frac{n\pi}{2(N+1)}\right)^2 \tag{5.46}$$

$$b^*_{1k} = \sqrt{\frac{2}{N+1}} \sin \frac{\pi k}{N+1} + \mathcal{O}(\lambda^2) \tag{5.47}$$

$$b_{Nk} = \sqrt{\frac{2}{N+1}} \sin \frac{\pi Nk}{N+1} + \mathcal{O}(\lambda^2) \tag{5.48}$$

Substituting into equation 5.43 we get

$$\alpha S = 4e^2 \left[\sum_{k=1}^{N} \frac{2}{16(N+1)} \left(\frac{\sin \frac{\pi k}{N+1} \sin \frac{\pi Nk}{N+1}}{\sin^4 \frac{n\pi}{2(N+1)}}\right)\right] \tag{5.49}$$

which can be simplified into the form

$$\alpha S = \frac{2N(N+2)}{3(N+1)} \frac{\lambda^2 \lambda'^2}{\lambda^2 + \lambda'^2} \tag{5.50}$$

We have made use of the fact that in the large $\tilde{g}$ limit e^2 reduces to the form (as in the Standard Model)

$$e^2 = \frac{g^2 g'^2}{g^2 + g'^2} \tag{5.51}$$

The result can be expressed in terms of the gauge boson masses. For the $N = 1$ model one finds for example

$$\alpha S = 4\frac{M_W^2}{M_W'^2}\sin^2\theta_w \tag{5.52}$$

To be compatible with the electroweak data one needs $S < 0.2$ (see figure 4.1) which implies $M_{W'} \sim 2$ TeV which is broadly in line with our findings in chapter 3.

5.4 Non-Limiting Scenario S Parameter in Deconstruction

When we extend the S-parameter computation beyond the large $\tilde{g}$ limit we must be careful about how we define the S parameter itself. Quantities such as $\sin\theta_W$ and $\cos\theta_W$ are specific to the Standard Model and become more complicated in Deconstructed models. In particular we must define S in terms of measured quantities.

Let us work backwards in the Standard Model from the usual definition of S

$$S \equiv \frac{16\pi}{M_Z^2}\left[\Pi_{33}(M_Z^2) - \Pi_{33}(0) - \Pi_{3Q}(M_Z^2)\right] \tag{5.53}$$

The relations between the broken and unbroken gauge bosons are

$$\Pi_{AA} = e^2\Pi_{QQ} \tag{5.54}$$

$$\Pi_{AZ} = \frac{e^2}{g_Z}(\Pi_{3Q} - s^2\Pi_{QQ}) \tag{5.55}$$

$$\Pi_{ZZ} = \frac{e^2}{g_Z^2}(\Pi_{33} - 2s^2\Pi_{3Q} + s^4\Pi_{QQ}) \tag{5.56}$$

Here the Z coupling has been parameterized as $g_Z(T^3 - s^2Q)$ - in the Standard Model $g_Z = g/c$. These can be rearranged into the reverse format

$$\Pi_{QQ} = \tfrac{1}{e^2}\Pi_{AA} \tag{5.57}$$

$$\Pi_{3Q} = \tfrac{s^2}{e^2}\Pi_{AA} + \tfrac{1}{g_Z e}\Pi_{ZA} \tag{5.58}$$

$$\Pi_{33} = \tfrac{s^4}{e^2}\Pi_{AA} + \tfrac{2s^2}{g_Z e}\Pi_{ZA} + \tfrac{1}{g_Z^2}\Pi_{ZZ} \tag{5.59}$$

so that

$$\begin{aligned} S \equiv \frac{16\pi}{e^2 M_Z^2}\Big[&(\tfrac{e^2}{g_Z^2}\Pi_{ZZ}(M_Z^2) + \tfrac{2es^2}{g_Z}\Pi_{ZA}(M_Z^2) + s^4\Pi_{AA}(M_Z^2)) \\ &-(\tfrac{2e}{g_Z}\Pi_{ZA}(M_Z^2) + s^2\Pi_{AA}(M_Z^2)) \\ &-(\tfrac{e^2}{g_Z^2}\Pi_{ZZ}(0) + \tfrac{2es^2}{g_Z}\Pi_{ZA}(0) + s^4\Pi_{AA}(0))\Big] \end{aligned} \tag{5.60}$$

The quantities g_Z, s^2 and e are all experimentally measured quantities so we will use this as our definition of S. We now turn to understanding what values these quantities take in the N=1 deconstructed model. As in the Standard Model they are extracted from the coupling of the Z boson and photon to fermions. The model has been defined such that the fermions only couple to the end two gauge groups of the moose chain; consequently the neutral boson coupling breaks down into two pairs of unbroken sub-diagrams.

The Z boson vertex contributions are:

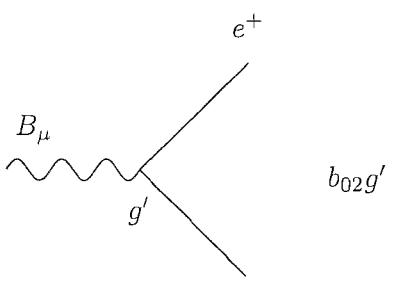

summed with

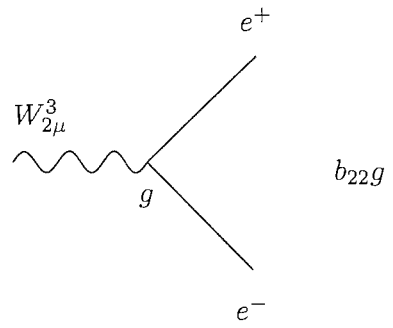

Similarly the photon vertex contributions are:

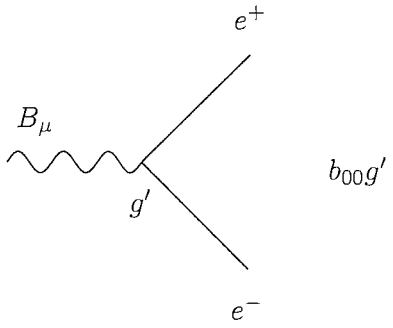

summed with

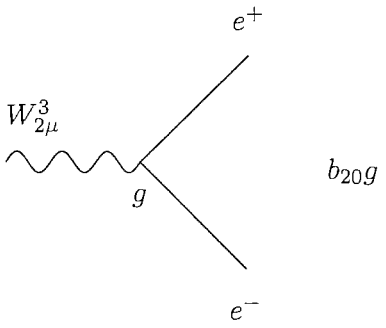

From which we obtain the neutral current parts of the covariant derivative

$$D^{NC}_\mu = Z_\mu(b_{22}gT^3 + b_{02}g'Y) + A_\mu(b_{20}gT^3 + b_{00}g'Y) \tag{5.61}$$

We define the charge Q to be the coupling between photons and electrons. By inserting

the values for the mixing angles from [24] into the photon part of the covariant derivative we establish the relation $Q = T^3 + Y$ as in the Standard Model

$$b_{00} = \frac{e}{g'}, b_{20} = \frac{e}{g} \tag{5.62}$$

Therefore

$$D_\mu^{NC} = Z_\mu(b_{22}gT^3 + b_{02}g'Y) + A_\mu(eT^3 + eY) \tag{5.63}$$

$$= Z_\mu(b_{22}gT^3 + b_{02}g'Y) + A_\mu eQ \tag{5.64}$$

Here it is obvious that [24] have chosen to describe the mixing angles to the photon in terms of an arbitrary parameter e in the knowledge that the above relation defines that parameter to be the charge on the electron.

Analogously to the standard model, we reparameterise the Z boson charge using the simple relation below [72]

$$b_{22}gT^3 + b_{02}g'Y = (b_{22}g - b_{02}g')T^3 + b_{02}g'Q \tag{5.65}$$

The covariant derivative can then be written in the simplified form we want to establish g_Z and s^2.

$$\begin{aligned} D_\mu^{NC} &= Z_\mu((b_{22}g - b_{02}g')T^3 + b_{02}g'Q) + A_\mu eQ \\ &= Z_\mu(b_{22}g - b_{02}g')\left(T^3 + \frac{b_{02}g'}{b_{22}g - b_{02}g'}Q\right) + A_\mu eQ \\ &= Z_\mu g_Z\left(T^3 - s^2Q\right) + A_\mu eQ \end{aligned} \tag{5.66}$$

Consequently

$$g_Z \equiv b_{22}g - b_{02}g' \tag{5.67}$$

and

$$s^2 \equiv \frac{b_{02}g'}{b_{22}g - b_{02}g'} \tag{5.68}$$

We can now compute (5.60) explicitly in this deconstructed model.

5.5 Vertex Coefficients

We have just worked through the photon and Z to electron couplings in the deconstructed model. We will need the full set of vertices in the gauge sector to compute S parameter contributions. As an example let us compute the photon W W vertex explicitly. There are two contributing diagrams in terms of the undiagonalized gauge states - the $W^3W^1W^2$ vertices for each of the two SU(2) groups. We must then re-write each of the three fields in terms of the mass eigenstates using the eigenstate expansions given in section 5.1. The two diagrams contribute (stripping off the momentum dependence)

$$C_{AWW} = \tilde{g}b_{10}a_{12}^2 - gb_{20}a_{22}^2 \tag{5.69}$$

One then proceeds throughout the model in this fashion and we find for the vertex coefficients (with the standard momentum factor stripped)

$$C_{AWW} = \tilde{g}b_{10}a_{12}^2 - gb_{20}a_{22}^2 \tag{5.70}$$

$$C_{AW'W} = \tilde{g}b_{10}a_{12}a_{11} - gb_{20}a_{22}a_{21} \tag{5.71}$$

$$C_{AW'W'} = \tilde{g}b_{10}a_{11}^2 - gb_{20}a_{21}^2 \tag{5.72}$$

$$C_{A\phi\phi} = g'c_{12}^2 b_{00} - gc_{22}^2 b_{20} \tag{5.73}$$

$$C_{A\phi'\phi} = g'c_{12}c_{11}b_{00} - gc_{22}c_{21}b_{20} \tag{5.74}$$

$$C_{A\phi'\phi'} = g'c_{11}^2 b_{00} - gc_{21}^2 b_{20} \tag{5.75}$$

$$C_{AGG} = \tilde{g}b_{10}a_{12}^2 - gb_{20}a_{22}^2 \tag{5.76}$$

$$C_{AG'G} = \tilde{g}b_{10}a_{12}a_{11} - gb_{20}a_{22}a_{21} \tag{5.77}$$

$$C_{AG'G'} = \tilde{g}b_{10}a_{11}^2 - gb_{20}a_{21}^2 \tag{5.78}$$

$$C_{ZWW} = g'b_{12}a_{12}^2 - gb_{22}a_{22}^2 \tag{5.79}$$

$$C_{ZW'W} = g'b_{12}a_{12}a_{11} - gb_{22}a_{22}a_{21} \tag{5.80}$$

$$C_{ZW'W'} = \tilde{g}b_{12}a_{11}^2 + gb_{22}a_{21}^2 \tag{5.81}$$

$$C_{Z\phi\phi} = g'c_{12}^2 b_{02} - gc_{22}^2 b_{22} \tag{5.82}$$

$$C_{Z\phi'\phi} = g'c_{12}c_{11}b_{02} - gc_{22}c_{21}b_{22} \tag{5.83}$$

$$C_{Z\phi'\phi'} = g'c_{11}^2 b_{02} - gc_{21}^2 b_{22} \tag{5.84}$$

$$C_{ZGG} = g'b_{12}a_{12}^2 - gb_{22}a_{22}^2 \tag{5.85}$$

$$C_{ZG'G} = g'b_{12}a_{12}a_{11} - gb_{22}a_{22}a_{21} \tag{5.86}$$

$$C_{ZG'G'} = \tilde{g}b_{12}a_{11}^2 + gb_{22}a_{21}^2 \tag{5.87}$$

$$C_{Z\chi h} = g'b_{02}d_{12} + gb_{22}d_{22} \tag{5.88}$$

$$C_{Z\chi' h} = g'b_{02}d_{12} + gb_{22}d_{22} \tag{5.89}$$

$$C_{Z\chi h'} = g'b_{02}d_{11} + gb_{22}d_{21} \tag{5.90}$$

$$C_{Z\chi' h'} = g'b_{02}d_{11} + gb_{22}d_{21} + \tilde{g}b_{12}d_{11} + \tilde{g}b_{12}d_{12} \tag{5.91}$$

5.6 Feynman Diagrams in Deconstruction

The self energies required to calculate the S parameter are formed from the Feynman diagrams shown in this section. The Feynman diagrams are displayed with the momentum independent vertex coefficients written in abbreviated form, such as C_{AWW}. The values of these factors are shown in section 5.5.

In this section we suppress the $W-\phi$ loops and $Z-\chi$ loop diagrams as they cancel out of the S parameter calculation. Their presence in Chapter 4 was for completeness and to make consistency with references [70, 71, 68] clearer.

For the diagrams below containing Standard Model like gauge bosons in the loops, B_0 and B_{22} are defined as $B_0 \equiv B_0(p^2, m_W^2, m_W^2)$, $B_{22} \equiv B_{22}(p^2, m_W^2, m_W^2)$.

Photon-Photon corrections

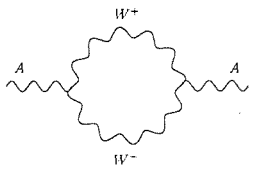

$$= C_{AWW}^2 \left(\left(-2m_W^2 + 4p^2 \right) B_0 + 10 B_{22} + 2 \left(2m_W^2 + 1/3p^2 \right) \right)$$

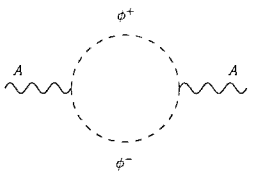

$$= C_{A\phi\phi}^2 4 B_{22}$$

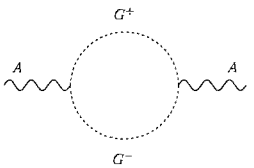

$$= C_{AGG}^2 (-) 2 B_{22}$$

Z boson-Photon corrections

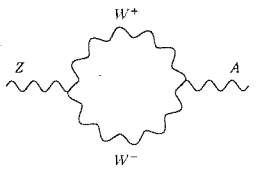

$$= C_{ZWW} C_{AWW} \left(\left(-2m_W^2 + 4p^2 \right) B_0 + 10 B_{22} + 2 \left(2m_W^2 + 1/3p^2 \right) \right)$$

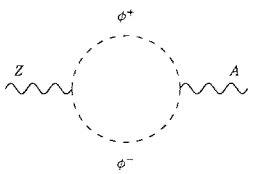

$$= C_{Z\phi\phi} C_{A\phi\phi} 4 B_{22}$$

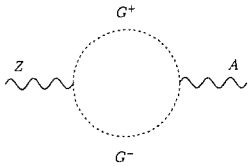

$$= C_{ZGG}C_{AGG}(-)2B_{22}$$

Z boson-Z boson corrections

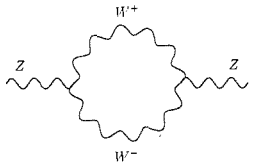

$$= C^2_{ZWW}\left(\left(-2m_W^2 + 4p^2\right)B_0 + 10B_{22} + 2\left(2m_W^2 + 1/3p^2\right)\right)$$

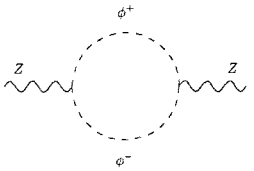

$$= C^2_{Z\phi\phi}4B_{22}$$

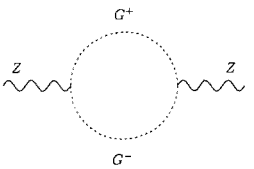

$$= C^2_{ZGG}(-)2B_{22}$$

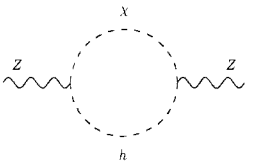

$$= C^2_{Z\chi h}4B_{22}(p^2, m_Z^2, m_h^2)$$

For the diagrams below containing heavy gauge bosons and Standard Model like bosons in the loops, B_0 and B_{22} are defined as $B_0 \equiv B_0(p^2, m^2_{W'}, m^2_W)$, $B_{22} \equiv B_{22}(p^2, m^2_{W'}, m^2_W)$.

Photon-Photon corrections

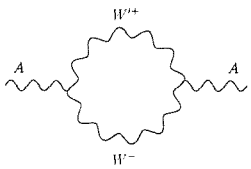

$$= C^2_{AW'W}\left(\left(-2m_W'^2 + 4p^2\right)B_0 + 10B_{22} + 2\left(m_W'^2 + m_W^2 + 1/3p^2\right)\right)$$

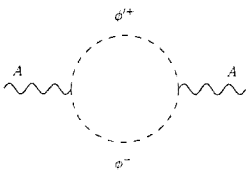

$$= C^2_{A\phi'\phi}4B_{22}$$

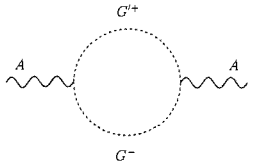

$$= C^2_{AG'G}(-)2B_{22}$$

Z boson-Photon corrections

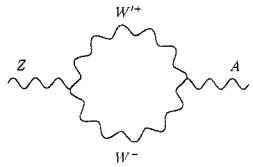

$$= C_{ZW'W}C_{AW'W}\left(\left(-2m'^2_W + 4p^2\right)B_0 + 10B_{22} + 2\left(m'^2_W + m^2_W + 1/3p^2\right)\right)$$

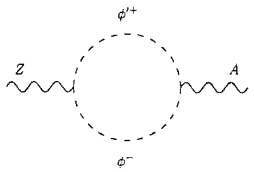

$$= C_{Z\phi'\phi}C_{A\phi'\phi}4B_{22}$$

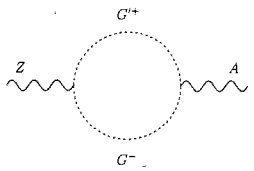

$$= C_{ZG'G}C_{AG'G}(-)2B_{22}$$

Z boson-Z boson corrections

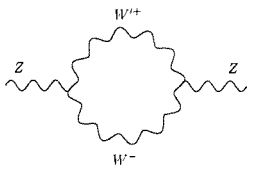

$$= C^2_{ZW'W}\left(\left(-2m'^2_W + 4p^2\right)B_0 + 10B_{22} + 2\left(m'^2_W + m^2_W + 1/3p^2\right)\right)$$

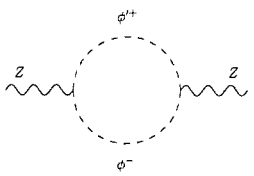

$$= C^2_{Z\phi'\phi}4B_{22}$$

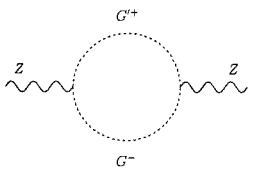

$$= C^2_{ZG'G}(-)2B_{22}$$

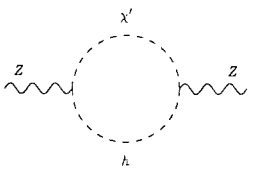

$$= C^2_{Z\chi'h}4B_{22}(p^2, m^2_{Z'}, m^2_h)$$

Photon-Photon corrections

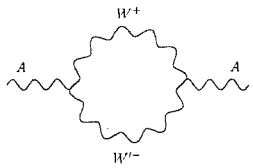

$$= C_{AWW'}^2 \left(\left(-2m_W^2 + 4p^2 \right) B_0 + 10B_{22} + 2\left(m_W^2 + m_W'^2 + 1/3p^2 \right) \right)$$

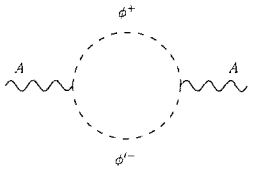

$$= C_{A\phi\phi'}^2 4B_{22}$$

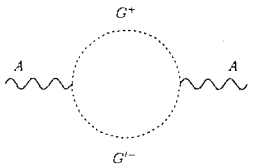

$$= C_{AGG'}^2 (-)2B_{22}$$

Z boson-Photon corrections

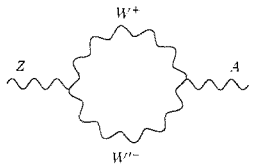

$$= C_{ZWW'} C_{AWW'} \left(\left(-2m_W^2 + 4p^2 \right) B_0 + 10B_{22} + 2\left(m_W^2 + m_W'^2 + 1/3p^2 \right) \right)$$

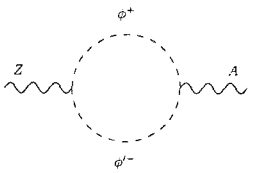

$$= C_{Z\phi\phi'} C_{A\phi\phi'} 4B_{22}$$

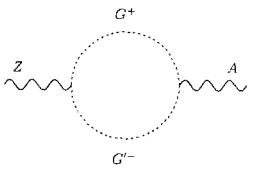

$$= C_{ZGG'} C_{AGG'} (-)2B_{22}$$

Z boson-Z boson corrections

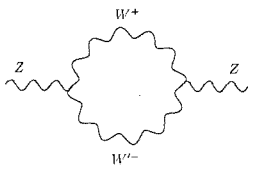

$$= C_{ZWW'}^2 \left(\left(-2m_W^2 + 4p^2 \right) B_0 + 10B_{22} + 2\left(m_W^2 + m_W'^2 + 1/3p^2 \right) \right)$$

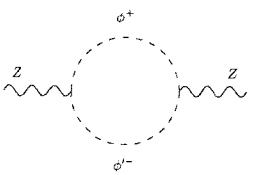

$$= C_{Z\phi\phi'}^2 4B_{22}$$

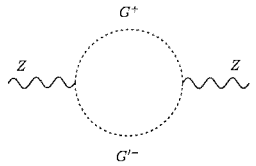

$$= C^2_{ZGG'}(-)2B_{22}$$

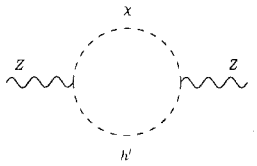

$$= C^2_{Z\chi h'} 4B_{22}(p^2, m_Z^2, m_{h'}^2)$$

For the diagrams below containing only heavy gauge bosons in the loops B_0 and B_{22} are defined as $B_0 \equiv B_0(p^2, m^2_{W'}, m^2_{W'})$, $B_{22} \equiv B_{22}(p^2, m^2_{W'}, m^2_{W'})$.

Photon-Photon corrections

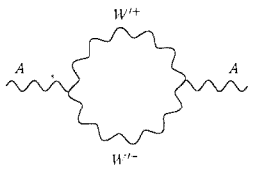

$$= C^2_{AW'W'}\left(\left(-2m'^2_W + 4p^2\right)B_0 + 10B_{22} + 2\left(2m'^2_W + 1/3p^2\right)\right)$$

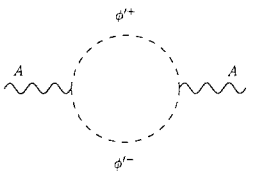

$$= C^2_{A\phi'\phi'} 4B_{22}$$

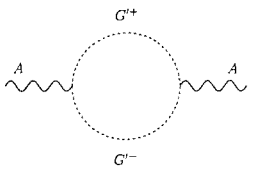

$$= C^2_{AG'G'}(-)2B_{22}$$

Z boson-Photon corrections

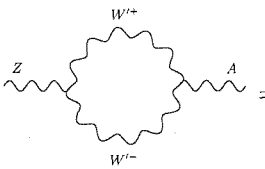

$$= C_{ZW'W'}C_{AW'W'}\left(\left(-2m'^2_W + 4p^2\right)B_0 + 10B_{22} + 2\left(2m'^2_W + 1/3p^2\right)\right)$$

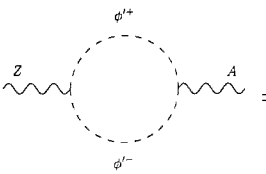

$$= C_{Z\phi'\phi'}C_{A\phi'\phi'} 4B_{22}$$

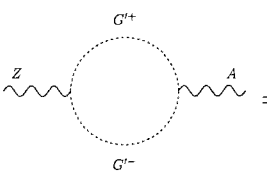

$$= C_{ZG'G'}C_{AG'G'}(-)2B_{22}$$

Z boson-Z boson corrections

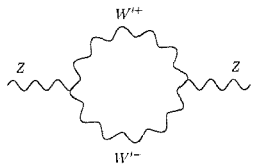

$$= C^2_{ZW'W'}\left(\left(-2m'^2_W + 4p^2\right)B_0 + 10B_{22} + 2\left(2m'^2_W + 1/3p^2\right)\right)$$

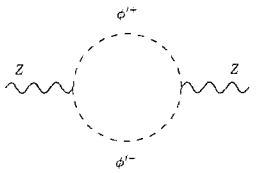

$$= C^2_{Z\phi'\phi'}4B_{22}$$

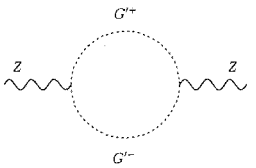

$$= C^2_{ZG'G'}(-)2B_{22}$$

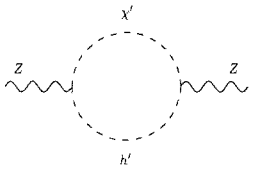

$$= C^2_{Z\chi'h'}4B_{22}(p^2, m^2_{Z'}, m^2_{h'})$$

The self-energies $\Delta\Pi_{AA}, \Delta\Pi_{ZA}$ and $\Delta\Pi_{ZZ}$ form from these diagrams in an analogous way to that shown in sections 4.6 and 4.7 in the Standard Model.

5.7 Comparison To The Work Of [72]

A parallel analysis of the contributions to the S parameter has been performed in [72]. There they work in the effective low energy theory of the deconstruction model without an explicit Higgs boson - we can just drop our Higgs diagrams to make a comparison.

They also work only in the $\tilde{g} \to \infty$ limit. In this limit as we have discussed in section 5.2 the gauge and mass eigenstates for the end two groups are the same and become the Standard Model gauge bosons. The central group's gauge bosons become the heavy W' and Z'. We can see this explicitly by using the large $\tilde{g}$ expansions in section 5.2 on the loop diagrams with just the "non-prime" gauge bosons in section 5.6 they become the Standard Model diagrams of chapter 4.

As an explicit example consider the photon self energy contribution with two Ws in the loop. The diagram in section 5.6 and the Standard Model diagram in section 4.7 only differ in the momentum independent coefficient. Taking the leading large $\tilde{g}$ limit on the result in section 5.6 gives

$$\begin{aligned} C_{AWW}^2 &= (\tilde{g} b_{10} a_{12}^2 - g b_{20} a_{22}^2)^2 \\ &= (\tilde{g} \frac{e}{\tilde{g}} \frac{g}{2\tilde{g}} - g \frac{e}{g} (1)^2)^2 \\ &= e^2 \end{aligned} \tag{5.92}$$

The remaining diagrams with the lightest mass eigenstates just reproduce the results of Chapter 4 in this limit.

The new contributions to S therefore come from the diagrams with the the heavy "primed" particles in the loops. In fact [72] work only in the leading log approximation. This means that their S parameter result depends on just the diagrams which have a result of the form $g_{\mu\nu} p^2 \log \frac{M_{W'}^2}{\Lambda^2}$. There are three such diagrams for each of the AA and ZA self-energies - those with internal W's, primed charged Goldstones and finally primed ghosts. We have explicitly checked our results against those diagrams.

As an example consider the photon self energy diagram with two W' bosons in the loop. From section 5.6 and taking the leading log approximation we have the momentum dependence

$$\left(\left(-2m_W'^2 + 4p^2 \right) B_0 + 10 B_{22} + 2 \left(2m_W'^2 + 1/3 p^2 \right) \right) = \frac{1}{(4\pi)^2} \frac{19}{6} g_{\mu\nu} p^2 \log \left(\frac{\Lambda^2}{M_{W'}^2} \right) \tag{5.93}$$

where Λ is the UV cut off on the diagrams (remember that without the Higgs the theory is non-renormalizable).

The additional Feynman rule factor, taking the large $\tilde{g}$ limit gives

$$\begin{aligned} C^2_{AW'W'} &= (\tilde{g}b_{10}a^2_{11} - gb_{20}a^2_{21})^2 \\ &= (\tilde{g}\frac{e}{\tilde{g}}(1)^2 - g\frac{e}{g}(0)^2)^2 \\ &= e^2 \end{aligned} \tag{5.94}$$

This is the result of [72].

In this way one finds the full results from the three diagrams of [72]

$$\Pi_{AA} = g_{\mu\nu}\frac{e^2}{(4\pi)^2}3p^2\log\left(\frac{\Lambda^2}{M^2_{W'}}\right) \tag{5.95}$$

$$\Pi_{ZA} = g_{\mu\nu}\frac{e^2}{(4\pi)^2}\frac{3}{2}\left(\frac{c}{s}-\frac{s}{c}\right)p^2\log\left(\frac{\Lambda^2}{M^2_{W'}}\right) \tag{5.96}$$

For Π_{ZZ} there is a fourth diagram in which a primed and an unprimed Goldstone live in the loop. This can be found in section 5.6 and we have again checked it's contribution is that found in [72]. One has

$$\Pi_{ZZ} = g_{\mu\nu}\frac{e^2}{(4\pi)^2}\left[\frac{3}{4}\left(\frac{c}{s}-\frac{s}{c}\right)^2 - \frac{1}{24s^2c^2}\right]p^2\log\left(\frac{\Lambda^2}{M^2_{W'}}\right) \tag{5.97}$$

It is easy then to compute the loop contributions to the S parameter from the heavy gauge sector in the large $\tilde{g}$ limit since the light sector is just that of the Standard model and we may use the usual definition for S in equation 5.40. Substituting in we find

$$S = -\frac{19}{24\pi}\log\frac{\Lambda^2}{M^2_{W'}} \tag{5.98}$$

5.7.1 An Alternative Derivation

The calculation in the paper by Chivukula et al [72] is calculated by making use of the Feynman diagrams that we have independently derived in section 5.6 in the strong coupling limit. We have however discovered a very brief way of replicating these results by employing the method of Schmidt et al [24] presented in section 5.3 but at the loop level instead of the tree level.

Naively in the large $\tilde{g}$ limit the gauge boson mass matrices decouple into two sectors - the light Standard Model fields and a heavy sector of additional W bosons. One can immediately see there are the one loop S parameter contributions from Figure 5.1. The first is just the Standard Model loop diagram and the second a diagram containing loops of the diagonalised additional gauge groups (as used in tree level form in section 5.3).

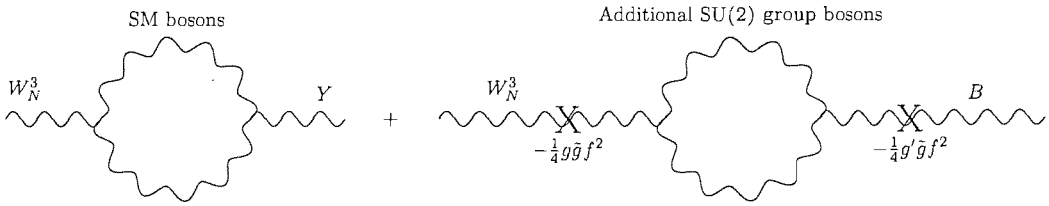

Figure 5.1: One loop S parameter contribution diagrams

In addition to the diagrams in Figure 5.1, we have the equivalent diagrams but with W_N^3 at both ends and hypercharge Y at both ends. Also to be consistent with reference [72] we will reparameterise in terms of the photon field A and the Z boson field Z, were

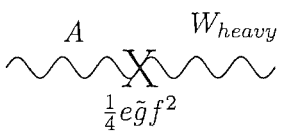

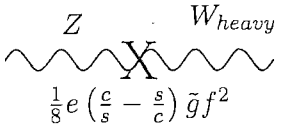

The beyond the Standard Model contribution diagrams in full then look like

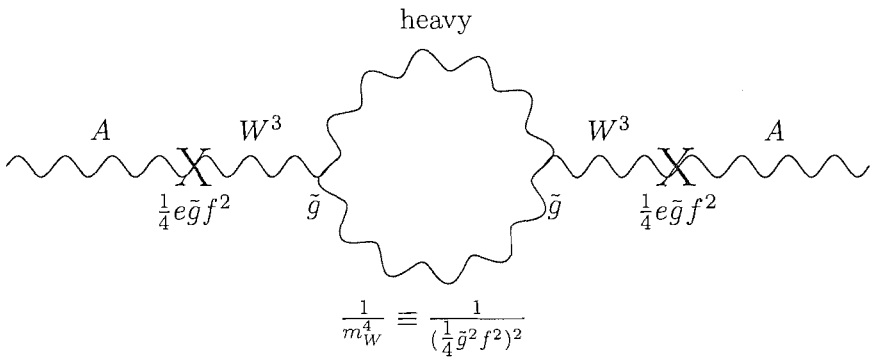

And similarly for Z boson to photon and Z boson to Z boson. The factor of $1/M_{W'}^4$ comes from the two internal propagators not in the loop. Note the factors of $\tilde{g}$ cancel.

Let us compute just the $p^2 g_{\mu\nu}$ contributions from the loops of heavy Ws in the N=1 moose model - as in [72] we will refer to the heavy W as the ρ. For the photon self-energy we obtain, in the leading log approximation

$$\Pi_{AA}^{\mu\nu}(p) = ip^2 g^{\mu\nu}\left[3\log\frac{\Lambda^2}{M_{\rho^\pm}^2}\right] \tag{5.99}$$

The W self energy is easily obtained from the results we have given previously but is in fact just equal to the photon self energy. This term is precisely the extra term beyond the Standard Model contribution in [72]. The ZA mixing self-energy gives

$$\Pi_{ZA}^{\mu\nu}(p) = \frac{ie^2}{(4\pi)^2}\, p^2 g^{\mu\nu}\left(\frac{3}{2}\left\{\frac{c}{s}-\frac{s}{c}\right\}\log\frac{\Lambda^2}{M_{\rho^\pm}^2}\right) \tag{5.100}$$

Again this matches the term in [72] and here clearly differs from the photon self energy by replacing the photon W' mixing by the ZW' mixing.

Finally we predict the Z-boson self-energy to be the same but with a further vertex replacement to give,

$$\Pi^{\mu\nu}_{ZZ}(p) = \frac{ie^2}{(4\pi)^2} p^2 g^{\mu\nu} \left(\frac{3(c^2 - s^2)^2}{4s^2c^2} \right) \log \frac{\Lambda^2}{M^2_{\rho^\pm}} \tag{5.101}$$

This term is again present in [72].

This analysis is slightly over simplified so far. In addition to the mass mixings between the light Standard Model fields and the heavy sector there are also three point vertices that become important at one loop. These are vertices which couple a light gauge boson to one Goldstone from the light sector and one from the heavy sector. In the large $\tilde{g}$ limit as shown in [72] only the Z vertices are present. At leading log approximation there is just a single extra diagram shown

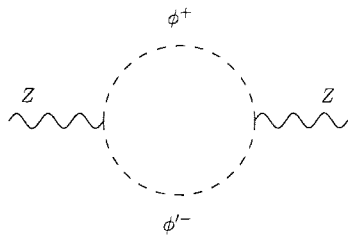

There is therefore one extra diagram contribution

$$\Pi^{\mu\nu}_{ZZ}(p) = \frac{ie^2}{(4\pi)^2} p^2 g^{\mu\nu} \left(-\frac{1}{24s^2c^2} \right) \log \frac{\Lambda^2}{M^2_{\rho^\pm}} \tag{5.102}$$

We have now reproduced the final results in [72]. We can also easily obtain their S parameter result. The diagrams in the light gauge sector are just the well known Standard Model contributions to the S parameter but one must set $m_h = \Lambda$

$$S = \frac{1}{12\pi}\mathrm{Log}\left(\frac{\Lambda^2}{M_W^2}\right) \tag{5.103}$$

Then inserting the above self energy contributions into the formulae for the S parameter in section 4.2 one finds their final result,

$$S = \frac{1}{12\pi}\mathrm{Log}\left(\frac{M_\rho^2}{M_W^2}\right) - \frac{17}{24\pi}\mathrm{Log}\left(\frac{\Lambda^2}{M_\rho^2}\right) \tag{5.104}$$

Note the result grows as M_ρ grows at large $\tilde{g}$. Reproducing this result using the results of our previous analysis provides support for the numerical results discussed before in this thesis. This simple method for computing in the large $\tilde{g}$ limit may also make models with $N > 1$ accessible to computation which has not so far been done either here or in the literature.

5.8 Inclusion of the Higgs

The addition of the Higgs diagram contributions to the result of Sekhar et. al. shown in equation 5.104 must cancel the $m_h = \Lambda$ divergences, in order that result be renormalisable. There are four diagrams that contribute shown below.

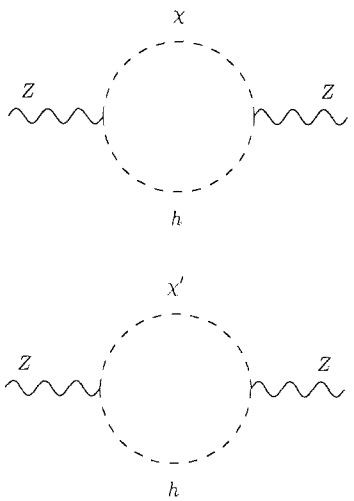

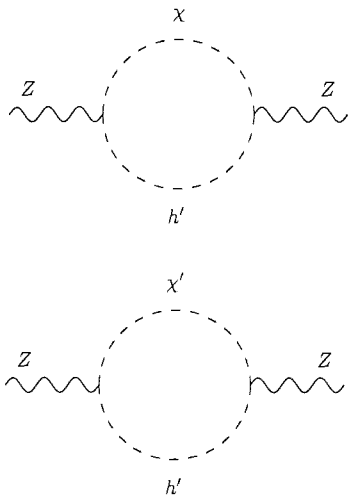

Here we will look at the Higgs-χ loop in detail, substituting for the mixing angles in the $\tilde{g} \to \infty$ limit. The diagram takes the form

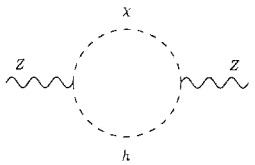

$= C^2_{Z\chi h} 4B_{22}(p^2, m_Z^2, m_h^2)$ The C-factor for a Z to Higgs-χ vertex in the $\tilde{g} \to \infty$ limit is

$$C_{Z\chi h} = \left(g' b_{02} d_{12} + g b_{22} d_{22}\right) \tag{5.105}$$

and we will use the large $\tilde{g}$ relations

$$b_{02} = \frac{-g'}{\sqrt{g^2 + g'^2}} \left(1 - \frac{1}{8}(\lambda^2 + \lambda'^2) + \frac{1}{2}\frac{\lambda^4}{(\lambda^2 + \lambda'^2)}\right) \tag{5.106}$$

$$b_{12} = \frac{1}{2}\frac{1}{\tilde{g}} \left(\frac{g^2 - g'^2}{\sqrt{g^2 + g'^2}}\right) \tag{5.107}$$

$$b_{22} = \frac{g}{\sqrt{g^2 + g'^2}} \left(1 - \frac{1}{8}(\lambda^2 + \lambda'^2) + \frac{1}{2}\frac{\lambda'^4}{(\lambda^2 + \lambda'^2)}\right) \tag{5.108}$$

$$d_{22} = -\frac{1}{\sqrt{2}} \left(1 - \frac{1}{4}\lambda^2 + \frac{1}{4}\lambda^2\right) \tag{5.109}$$

$$d_{12} = \frac{1}{\sqrt{2}}\left(1 + \frac{1}{4}\lambda^2 - \frac{1}{4}\lambda^2\right) \tag{5.110}$$

$$d_{21} = \frac{1}{\sqrt{2}}\left(1 + \frac{1}{4}\lambda^2 - \frac{1}{4}\lambda'^2\right) \tag{5.111}$$

$$d_{11} = \frac{1}{\sqrt{2}}\left(1 - \frac{1}{4}\lambda^2 + \frac{1}{4}\lambda'^2\right) \tag{5.112}$$

We find in this limit

$$C_{Z\chi h} = \frac{i}{2\sqrt{2}\sqrt{g^2+g'^2}}\left(g^2 - g'^2\right)|_{\tilde{g}\to\infty} \tag{5.113}$$

We therefore have

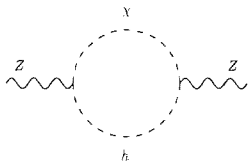

$$= \frac{1}{2(g^2+g'^2)}(g^2 - g'^2)^2 B_{22}(p^2, m_Z^2, m_h^2)|_{\tilde{g}\to\infty}$$

From equation 4.74 we can see that the momentum dependent part of $B_{22}(p^2, m_Z^2, m_h^2)$ is $-\frac{1}{12}B_0(p^2, m_Z^2, m_h^2)$ which is a divergent contribution of $-\frac{1}{12}\mathrm{Log}\left(\Lambda^2\right)$. Consequently

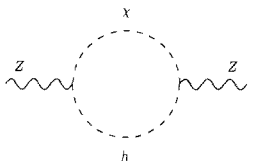

$$= -\frac{1}{24(g^2+g'^2)}(g^2 - g'^2)^2 \mathrm{Log}\left(\Lambda^2/m_h^2\right)|_{\tilde{g}\to\infty}$$

Substituting for the Z-Z self energy part of the S parameter (equation 5.60) that contributes to the divergences through the Higgs diagrams, shown in equation 5.114 we find

$$\Delta S \equiv \frac{16\pi}{e^2 M_Z^2}\frac{e^2}{g_Z^2}\Pi_{ZZ}(M_Z^2) \tag{5.114}$$

The Higgs-χ diagram contribution is

$$S_{h\chi} = \frac{4}{24\pi}\mathrm{Log}\left(\Lambda^2/m_h^2\right) \tag{5.115}$$

On summation with the Higgs'-χ, Higgs-χ' and Higgs'-χ' loops the contribution to the divergences from the Higgs diagrams is,

$$S = \frac{17}{24\pi}\mathrm{Log}\left(\Lambda^2/m_h^2\right) \tag{5.116}$$

which cancels the divergences from the non-Higgs diagrams shown in equation 5.104. The result is finite as required.

5.9 Beyond Leading Log Approximation

We have so far explicitly computed the leading log approximation for S but we have sufficient information to compute the full answer. It is therefore interesting to test the leading log approximation. As an example we will study the sub-leading contributions to the Higgs Z gauge loops (or equally Higgs Z' loops). The generic form of the momentum dependence of these loops is given by

$$\begin{aligned}\Pi(p^2) = \; & (2m_h^2 - M_Z^2 - p^2)B_0(p^2, m_h, M_z) \\ & -\tfrac{(M_Z^2-m_h^2)^2}{p^2}(B_0(p^2, m_h, M_z) - B_0(0, m_h, M_z)) - \tfrac{2}{3}p^2\end{aligned} \tag{5.117}$$

where

$$B_0(p^2, m_h, M_Z) = \int \frac{d^4k}{\pi^2}\frac{1}{(k^2+m_h^2)}\frac{1}{((k+p)^2+M_Z^2)} \tag{5.118}$$

Since m_h is large relative to the energy scale at which precision measurements have

been taken we will Taylor expand B_0

$$B_0(p^2, m_h, M_z) = B_0(0, m_h, M_z) + p^2 B_0'(0, m_h, M_z) + p^4 B_0''(0, m_h, M_z) + ... \quad (5.119)$$

The coefficients are

$$B_0(0, m_h, M_z) = \int \frac{d^4k}{\pi^2} \frac{1}{(k^2 + m_h^2)} \frac{1}{(k^2 + M_Z^2)}$$
$$B_0'(0, m_h, M_z) = \int \frac{d^4k}{\pi^2} \frac{1}{(k^2 + m_h^2)} \frac{1}{(k^2 + M_Z^2)} \left[\frac{4c_\phi^2 k^2}{(k^2 + M_Z^2)^2} - \frac{1}{(k^2 + M_Z^2)} \right]$$
$$B_0''(0, m_h, M_z) = \int \frac{d^4k}{\pi^2} \frac{1}{(k^2 + m_h^2)} \frac{1}{(k^2 + M_Z^2)} \left[\frac{16c_\phi^4 k^4}{(k^2 + M_Z^2)^4} - \frac{12c_\phi^2 k^2}{(k^2 + M_Z^2)^3} + \frac{1}{(k^2 + M_Z^2)^2} \right]$$

Performing the angular integration over the angle ϕ between p and k gives forms that can be numerically integrated (these can be checked by their invariance to the interchange of M_Z and m_h)

$$B_0(0, m_h, M_z) = \int \frac{d^4k}{\pi^2} \frac{1}{(k^2 + m_h^2)} \frac{1}{(k^2 + M_Z^2)}$$
$$B_0'(0, m_h, M_z) = \int \frac{d^4k}{\pi^2} \frac{1}{(k^2 + m_h^2)} \frac{1}{(k^2 + M_Z^2)} \left[\frac{k^2}{(k^2 + M_Z^2)^2} - \frac{1}{(k^2 + M_Z^2)} \right]$$
$$B_0''(0, m_h, M_z) = \int \frac{d^4k}{\pi^2} \frac{1}{(k^2 + m_h^2)} \frac{1}{(k^2 + M_Z^2)} \left[\frac{2k^4}{(k^2 + M_Z^2)^4} - \frac{3k^2}{(k^2 + M_Z^2)^3} + \frac{1}{(k^2 + M_Z^2)^2} \right]$$

Note the leading log approximation is to set $B_0(0) = \mathrm{Log}\frac{\Lambda^2}{m_h^2}$ and drop everything else.

The S parameter depends on the derivatives of Π so we are most interested in evaluating

$$\Pi'(0) = -B_0(0, m_h, M_z) + (2m_h^2 - M_Z^2) B_0'(0, m_h, M_z) - (M_Z^2 - m_h^2)^2 B_0''(0, m_h, M_z) - \frac{2}{3} \quad (5.120)$$

To simulate the effect of this term in S we subtract the logarithmic divergence through a suitably normalized term $\mathrm{Log}(\Lambda^2/M_\rho^2)$ with M_ρ the appropriate W boson mass. We plot the full value of this difference as a function of m_h/M_ρ in Figure 5.2 and compare to the leading log result. For large m_h there is a constant shift in the Π' contribution of about a factor of 3 relative to the pure log term. For very large m_h/M_ρ this is a small effect but if that ratio falls to as low as 10 then the error is of order the logarithmic term. We conclude that provided the Higgs and W' masses do not accidentally become degenerate then the leading log approximation will be valid. If they do come too close though the sub-leading terms can contribute significantly.

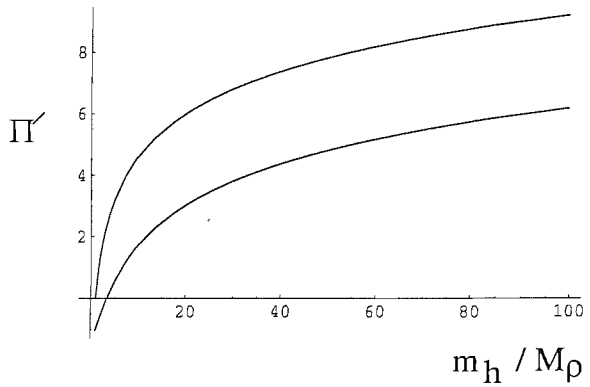

Figure 5.2: A plot of the quantity Π' (with the divergence subtracted by a term Log m_h^2/M_ρ^2 term) from the Higgs diagrams as a function of m_h/M_ρ. The top curve that goes through zero at $m_h/M_\rho = 1$ is the leading log approximation, the lower curve the full result.

5.10 Phenomenology

We saw in Chapter 3 that the only Deconstruction models even close to compatible with experimental constraints were those with large $\tilde{g}$ (see for example section 3.8.2) so we will continue to use the results above from that limit. We found in leading log approximation

$$S = \frac{1}{12\pi}\mathrm{Log}\left(\frac{m_h^2}{M_W^2}\right) - \frac{19}{24\pi}\mathrm{Log}\left(\frac{m_h^2}{M_{W'}^2}\right) \tag{5.121}$$

This should be compared with the value at one loop in the Standard Model

$$S = \frac{1}{12\pi}\mathrm{Log}\left(\frac{m_h^2}{M_W^2}\right) \tag{5.122}$$

The first two terms are identical reflecting the fact that the loop diagrams involving the Standard Model particles are precisely as in the Standard Model in this limit.

For comparison to experiment, the S parameter is defined as zero in the Standard Model for some fixed reference Higgs mass - 150 GeV for the data we will use from [73]. The deviations in the deconstructed models are therefore

$$S_{\mathrm{decon}} = \frac{1}{12\pi}\mathrm{Log}\left(\frac{m_h^2}{(150\ \mathrm{GeV})^2}\right) - \frac{19}{24\pi}\mathrm{Log}\left(\frac{m_h^2}{M_{W'}^2}\right) \tag{5.123}$$

To claim any success in a deconstructed model one would want to have pushed the Higgs mass beyond 1 TeV by the presence of the extra W' boson. We therefore plot this contribution for $m_h = 1000$ GeV as a function of $M_{W'}$ in Fig 5.3.

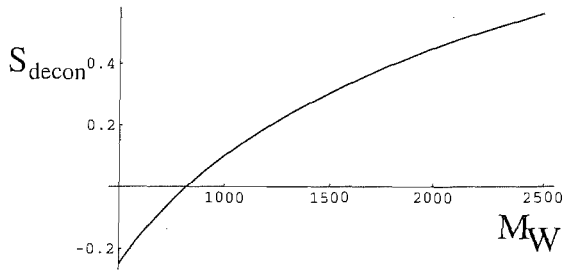

Figure 5.3: A plot of the contribution to the S parameter in the Deconstruction model for a Higgs mass of 1 TeV for varying mass of the extra W boson.

If the model were compatible with the data at tree level and the Higgs mass was of order 800GeV then the model predicts that S is roughly zero which is consistent

with the data shown in Figure 4.1. In fact we found in Chapter 3 that at tree level we could at best bring such models to the upper bounds on experimental limits and then only when the extra Ws had masses in excess of 2 TeV - for these parameters we find values of S that are a little too large (0.4 or so) even at loop level. It's worth noting that to accommodate such a large value of S one would also need a source of positive T which we have not addressed at all. We must conclude that finding such deconstructed models that truly fit the data remains a challenge.

Chapter 6

Conclusions

Over recent years there has been a great deal of interest in methods for resolving the unitarity problem in W scattering presented in section 2.2. The conventional method for resolving this problem is through the Higgs Mechanism. Next year a new particle accelerator called the Large Hadron Collider (LHC) will come online which will probe the energies at which the unitarity problem becomes explicit. If this new accelerator does not find the Higgs boson, a particle required if the Higgs Mechanism is correct, then the question of how unitarity is resolved will be wide open.

Anticipating the need for alternative theories to the Higgs Mechanism, for resolving unitarity if the LHC fails to find the Higgs boson, many theorists have proposed Higgsless models to tackle this pressing question. Kaluza Klein theory and Deconstruction are two of the leading candidates for addressing the issue of maintaining unitarity without a low energy Higgs boson. In this thesis we have studied a range of models within the framework of Deconstruction, at tree level in Chapter 3 and at the one loop level in Chapter 5.

Our analysis has demonstrated that at tree level models can be generated that do not have a Higgs boson at the energies that will be probed at the LHC (section 3.8.2).

These models have additional gauge boson which could be detected at the LHC as a signature verifying the model.

At the time that the write up of this thesis commenced no research had been published exploring Deconstruction at the loop level. In Chapter 5 we have calculated the S parameter for the purposes of confirming or disproving the validity at the one loop level, within perturbation theory, of our tree level calculations. Recently a parallel analysis has been published, as presented in section 5.7, that also explores loop level physics in Deconstruction (and proves consistent with our own findings).

We have found that the loop level contributions to S are of order the experimental constraints or larger. Combining both the difficulty of a producing a tree level successful model of this type and the sizable loop contributions we conclude that producing such a model that is fully compatible with constraints is at best hard.

Deconstruction does though still present interesting implications for LHC phenomenology, that would resolve the unitarity problem without recourse to a Higgs boson at the LHC energy scale. It is apparent, through the results of this thesis, that these Deconstructed models face appreciable problems and that subtle exotic models may be required to address these issues.

Bibliography

[1] D. Ivanenko and G. Sardanashvily, Phys. Rept. **94**, 1 (1983).

[2] A. Salam, "Weak And Electromagnetic Interactions," Svartholm: Elementary Particle Theory, Proceedings Of The Nobel Symposium Held 1968 At Lerum, Sweden*, Stockholm 1968, 367-377, Reprinted in *Lichtenberg, D. B. (ed.), Rosen, S. P. (ed.): Developments In The Quark Theory Of Hadrons, Vol. 1*, 160-170, and in *Lai, C. H. (ed.): Gauge Theory Of Weak and Electromagnetic Interactions*, 188-198, Also in *Rosner, J.L. (ed.): New particles* 29-39, Also in *Ali, A. (ed.) et al.; Selected pape.

[3] S. Weinberg, Phys. Rev. Lett. **19**, 1264 (1967).

[4] C. N. Yang and R. L. Mills, Phys. Rev. **96**, 191 (1954).

[5] R. P. Feynman, "QED. The Strange Theory Of Light And Matter," Penguin Books, ISBN 0 14 01.2505 1.

[6] M. Gell-Mann, Phys. Lett. **8**, 214 (1964).

[7] H. Fritzsch, M. Gell-Mann and H. Leutwyler, Phys. Lett. B **47**, 365 (1973).

[8] H. D. Politzer, Phys. Rept. **14** (1974) 129.

[9] E. Reya, Phys. Rept. **69**, 195 (1981).

[10] D. J. Gross and F. Wilczek, Phys. Rev. D **8**, 3633 (1973).

[11] S. Weinberg, Physica A **96**, 327 (1979).

[12] A. Pich, Rept. Prog. Phys. **58**, 563 (1995) [arXiv:hep-ph/9502366].

[13] E. S. Abers and B. W. Lee, Phys. Rept. **9**, 1 (1973).

[14] C. H. Llewellyn Smith, Phys. Lett. B **46**, 233 (1973).

[15] S. Weinberg, Phys. Rev. D **19** (1979) 1277; L. Susskind, Phys. Rev. D **20** (1979) 2619.

[16] W. A. Bardeen, C. T. Hill and M. Lindner, Phys. Rev. D **41** (1990) 1647.

[17] L. F. Abbott and E. Farhi, Phys. Lett. B **101** (1981) 69.

[18] T. Kaluza, Sitzungsber. Preuss. Akad. Wiss. Berlin. (*Math Phys*)pp. 966-972 (1921); O. Klein, *Z. Phys.* **37** 895 (1926).

[19] R. S. Chivukula and H. J. He, Phys. Lett. B **532**, 121 (2002) [arXiv:hep-ph/0201164].

[20] R. Sekhar Chivukula, D. A. Dicus and H. J. He, Phys. Lett. B **525**, 175 (2002) [arXiv:hep-ph/0111016].

[21] C. Csaki, C. Grojean, H. Murayama, L. Pilo and J. Terning, Phys. Rev. D **69**, 055006 (2004) [arXiv:hep-ph/0305237].

[22] C. Csaki, C. Grojean, L. Pilo and J. Terning, Phys. Rev. Lett. **92**, 101802 (2004) [arXiv:hep-ph/0308038].

[23] T. Nagasawa and M. Sakamoto, Prog. Theor. Phys. **112**, 629 (2004) [arXiv:hep-ph/0406024].

[24] R. Foadi, S. Gopalakrishna and C. Schmidt, JHEP **0403**, 042 (2004) [arXiv:hep-ph/0312324].

[25] N. Arkani-Hamed, A. G. Cohen and H. Georgi, Phys. Rev. Lett. **86**, 4757 (2001) [arXiv:hep-th/0104005].

[26] C. T. Hill, S. Pokorski and J. Wang, Phys. Rev. D **64**, 105005 (2001) [arXiv:hep-th/0104035].

[27] R. S. Chivukula, M. Kurachi and M. Tanabashi, JHEP **0406**, 004 (2004) [arXiv:hep-ph/0403112].

[28] R. S. Chivukula, H. J. He, J. Howard and E. H. Simmons, Phys. Rev. D **69**, 015009 (2004) [arXiv:hep-ph/0307209].

[29] J. Hirn and J. Stern, Eur. Phys. J. C **34**, 447 (2004) [arXiv:hep-ph/0401032].

[30] R. S. Chivukula and H. Georgi, Phys. Lett. B **188**, 99 (1987).

[31] R. S. Chivukula, H. Georgi and L. Randall, Nucl. Phys. B **292**, 93 (1987).

[32] H. Georgi, Front. Phys. **54**, 1 (1982).

[33] K. Sfetsos, Nucl. Phys. B **612**, 191 (2001) [arXiv:hep-th/0106126].

[34] G. 't Hooft, Nucl. Phys. B **33**, 173 (1971).

[35] G. 't Hooft, Nucl. Phys. B **35**, 167 (1971).

[36] D. Bailin and A. Love, "INTRODUCTION TO GAUGE FIELD THEORY," Hilger (1986) 348 P. (Graduate Student Series In Physics).

[37] S. Eidelman *et al.* [Particle Data Group], Phys. Lett. B **592**, 1 (2004).

[38] H. Georgi, "Weak Interactions And Modern Particle Theory," Menlo Park, Usa: Benjamin/cummings (1984) 165p.

[39] S. Weinberg, PhysicaA **96**, 327 (1979).

[40] P. W. Higgs, Phys. Lett. **12**, 132 (1964).

[41] P. W. Higgs, Phys. Rev. Lett. **13**, 508 (1964).

[42] P. W. Higgs, Phys. Rev. **145**, 1156 (1966).

[43] C. H. Llewellyn Smith, Phys. Lett. B **46**, 233 (1973).

[44] D. A. Dicus and V. S. Mathur, Phys. Rev. D **7**, 3111 (1973).

[45] J. M. Cornwall, D. N. Levin and G. Tiktopoulos, Phys. Rev. Lett. **30**, 1268 (1973) [Erratum-ibid. **31**, 572 (1973)].

[46] J. M. Cornwall, D. N. Levin and G. Tiktopoulos, Phys. Rev. D **10**, 1145 (1974) [Erratum-ibid. D **11**, 972 (1975)].

[47] B. W. Lee, C. Quigg and H. B. Thacker, Phys. Rev. Lett. **38**, 883 (1977).

[48] Y. Kawamura, Prog. Theor. Phys. **103**, 613 (2000) [arXiv:hep-ph/9902423].

[49] Y. Kawamura, Prog. Theor. Phys. **105**, 999 (2001) [arXiv:hep-ph/0012125].

[50] L. J. Hall and Y. Nomura, Phys. Rev. D **64**, 055003 (2001) [arXiv:hep-ph/0103125].

[51] A. Hebecker and J. March-Russell, Nucl. Phys. B **613**, 3 (2001) [arXiv:hep-ph/0106166].

[52] A. Hebecker and J. March-Russell, Nucl. Phys. B **625**, 128 (2002) [arXiv:hep-ph/0107039].

[53] C. T. Hill, S. Pokorski and J. Wang, Phys. Rev. D **64**, 105005 (2001) [arXiv:hep-th/0104035].

[54] R. S. Chivukula, D. A. Dicus, H. J. He and S. Nandi, Phys. Lett. B **562**, 109 (2003) [arXiv:hep-ph/0302263].

[55] S. De Curtis, D. Dominici and J. R. Pelaez, Phys. Lett. B **554**, 164 (2003) [arXiv:hep-ph/0211353].

[56] S. De Curtis, D. Dominici and J. R. Pelaez, Phys. Rev. D **67**, 076010 (2003) [arXiv:hep-ph/0301059].

[57] Y. Abe, N. Haba, Y. Higashide, K. Kobayashi and M. Matsunaga, Prog. Theor. Phys. **109**, 831 (2003) [arXiv:hep-th/0302115].

[58] K. G. Wilson, Phys. Rev. B **4**, 3174 (1971).

[59] K. G. Wilson and J. B. Kogut, Phys. Rept. **12**, 75 (1974).

[60] M. E. Peskin and T. Takeuchi, Phys. Rev. Lett. **65**, 964 (1990).

[61] M. E. Peskin and T. Takeuchi, Phys. Rev. D **46**, 381 (1992).

[62] [ALEPH Collaboration], Phys. Rept. **427**, 257 (2006) [arXiv:hep-ex/0509008].

[63] G. . Altarelli, R. . Kleiss and C. . Verzegnassi, "Z PHYSICS AT LEP-1. PROCEEDINGS, WORKSHOP, GENEVA, SWITZERLAND, SEPTEMBER 4-5, 1989. VOL. 1: STANDARD PHYSICS,"

[64] G. Bhattacharyya, S. Banerjee and P. Roy, Phys. Rev. D **45**, 729 (1992) [Erratum-ibid. D **46**, 3215 (1992)].

[65] J. A. Bagger, A. F. Falk and M. Swartz, Phys. Rev. Lett. **84** (2000) 1385 [arXiv:hep-ph/9908327].

[66] M. E. Peskin and D. V. Schroeder, "An Introduction To Quantum Field Theory,"

[67] T. Hahn and M. Perez-Victoria, Comput. Phys. Commun. **118**, 153 (1999) [arXiv:hep-ph/9807565].

[68] G. Passarino and M. J. G. Veltman, Nucl. Phys. B **160**, 151 (1979).

[69] D. M. Pierce, J. A. Bagger, K. T. Matchev and R. j. Zhang, Nucl. Phys. B **491**, 3 (1997) [arXiv:hep-ph/9606211].

[70] D. C. Kennedy and B. W. Lynn, Nucl. Phys. B **322**, 1 (1989).

[71] A. Denner, Fortsch. Phys. **41**, 307 (1993).

[72] S. Matsuzaki, R. S. Chivukula and E. H. Simmons, arXiv:hep-ph/0607191.

[73] [ALEPH Collaboration, DELPHI Collaboration, L3 Collaboration, OPAL Collaboration, SLD Collaboration, LEP Electroweak Working Group, SLD Electroweak Group, and SLD Heavy Flavour Group], arXiv:hep-ex/0509008.